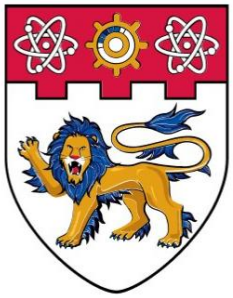

NANYANG TECHNOLOGICAL UNIVERSITY
SINGAPORE

QUANTITATIVE RELIABILITY AND AIRWORTHINESS ANALYSIS OF PROPULSION SYSTEMS OF MULTI-ROTOR UAVS FOR CERTIFICATION IN CIVIL AIRSPACE

SIDDESH GOVIND

SCHOOL OF MECHANICAL AND AEROSPACE ENGINEERING

2024

QUANTITATIVE RELIABILITY AND AIRWORTHINESS ANALYSIS OF PROPULSION SYSTEMS OF MULTI-ROTOR UAVS FOR CERTIFICATION IN CIVIL AIRSPACE

SIDDESH GOVIND

SCHOOL OF MECHANICAL AND AEROSPACE ENGINEERING

A thesis submitted to the Nanyang Technological University
in partial fulfilment of the requirement for the degree of
Master of Engineering

2024

Statement of Originality

I hereby certify that the work embodied in this thesis is the result of original research, is free of plagiarised materials, and has not been submitted for a higher degree to any other University or Institution.

07/08/24

.....
[DD/MM/YY]

.....
Siddesh Govind

Supervisor Declaration Statement

I have reviewed the content and presentation style of this thesis and declare it is free of plagiarism and of sufficient grammatical clarity to be examined. To the best of my knowledge, the research and writing are those of the candidate except as acknowledged in the Author Attribution Statement. I confirm that the investigations were conducted in accord with the ethics policies and integrity standards of Nanyang Technological University and that the research data are presented honestly and without prejudice.

04/12/24

[DD/MM/YY]

Prof Mir Feroskhan

Authorship Attribution Statement

This thesis contains material from 3 papers published in the following peer-reviewed journal(s) /conferences from Chapters accepted at conferences in which I am listed as an author.

Chapter 4 is published in its entirety as T. T., S. Govind, A. Roy, B. F. Ng, and K. H. Low, "A Reliability Framework for Safe Octorotor UAV Flight Operations," 2023 International Conference on Unmanned Aircraft Systems (ICUAS), Warsaw, Poland, 2023, pp. 1013-1020. https://dx.doi.org/10.1109/ICUAS57906.2023.10156536

The contributions of the co-authors are as follows:

- I prepared the initial manuscript drafts and performed the primary data analysis. I reviewed and validated the simplified Markov diagram done by Anurag Roy. I conducted the payload analysis by building upon and modifying the reliability framework. I co-implemented the Markov Modelling on the Octorotor configurations with Thanaraj T.
- Thanaraj T initiated the project direction, designed the reliability framework, and provided critical revisions to the manuscript drafts.
- Anurag Roy Assisted with the simplification of the Markov diagram.
- Prof. Ng Provided overall guidance on the manuscript and contributed to refining the research direction.

Chapter 6 is partially published (Sections 6.1-6.3) as J. Wang, S. Govind, X. Hu and M. Feroskhan, "UAV flight test and its endurance degradation modelling by considering the energy efficiency and flight stability factors," 2023 IEEE/AIAA 42nd Digital Avionics Systems Conference (DASC), Barcelona, Spain, 2023, pp. 1-5, https://dx.doi.org/10.1109/DASC58513.2023.10311139

The contributions of the co-authors are as follows:

- I initiated the project direction and suggested the test methodology and area for testing. I designed and developed the test setup and conducted the test platform selection. I identified root causes of failures encountered while testing in the Vicon room at the School of Mechanical and Aerospace Engineering. I wrote the initial manuscript for the published paper. I Served as one of the pilots who flew the test runs alongside Sivakumar Anush Kumar, Thanaraj T., Dr. John Wang, Dr. Dai Wei, Pang Bizhao, and Deng Chao.
- Dr Wang Jinlong Performed the Exploratory Data Analysis seen in Chapter 6.3.and edited and revised the manuscript.
- Prof Mir Provided guidance on the manuscript.

This thesis also contains material from a paper currently submitted for review to be published in the following peer-reviewed journal:

Chapters 3 and 5 are combined and submitted as a paper titled “Comprehensive Reliability Analysis and Degradation Modelling of Electric UAV Propulsion Systems: An Integrated Qualitative and Quantitative Approach” to the Journal of Reliability Engineering & System Safety.

The contributions of the co-authors are as follows:

- I initiated the project direction and suggested the test methodology and testing area. I conducted the Failure Modes and Effects Analysis (FMEA) of all individual propulsion system components. I designed and developed the testbed setup and component selection. I identified root causes of failures encountered during testing.

I mentored and guided the parameter tuning for Brandon Goh. I performed the initial data analysis presented in Chapter 5.10 and applied the initial algorithms to the testbed data. I implemented the model for degradation failure. I co-analysed the different models for data fitting with Brandon Goh. I wrote and edited the manuscript for the published paper.

- Brandon Goh Initiated the initial algorithm development using the data provided by and conducted parameter tuning on the implemented algorithm.

07/08/24

.....	.....
[DD/MM/YY]	Siddesh Govind

Acknowledgements

Pursuing a Master's Degree in Engineering has been a highly rewarding journey for me. It has given me the chance to delve deeply into a subject I am passionate about, enhance my research skills, and make meaningful contributions to the field of engineering. Along the way, I have faced both challenges and successes, which have not only bolstered my academic and professional capabilities, but also fostered personal growth and resilience. I am grateful for the guidance and support of numerous individuals without whom this journey would not have been possible.

Firstly, I would like to extend my heartfelt gratitude to my supervisor, Assistant Professor Mir Feroskhan, for his unwavering support during challenging times, his guidance during moments of confusion, and his continuous encouragement. His patience, insightful advice, and constructive feedback have consistently motivated me. I am extremely thankful for his commitment to my academic growth and his remarkable ability to both challenge and support me.

I would like to express my sincere gratitude to the Air Traffic Management Research Institute (ATMRI) at Nanyang Technological University (NTU) for providing me with an exceptional research environment and access to state-of-the-art facilities. These resources have been crucial to the successful completion of this thesis.

Additionally, I would like to acknowledge my colleagues-turned-friends at ATMRI and NTU, particularly Dr. Jinlong, Dr. John Wang, Mr. T. Thanaraj, Ms. Chao Deng, Mr. Qingyu Tan, Mr. Mingcheng Zhang, Mr. Anush Kumar, and others. Their encouragement, camaraderie, and valuable discussions have been instrumental to my progress and well-being during this journey.

Lastly, I would like to recognize the support and encouragement from my family and friends, whose understanding and patience have been essential during this process. Their unwavering belief in my potential has provided me with strength and motivation.

Thank you all for being a constant source of support and inspiration throughout this journey.

Abstract

Unmanned Aerial Vehicles (UAVs) have become increasingly integral to a diverse array of industrial applications, including military, civilian, and commercial uses. Ensuring their airworthiness is critical for the safe and effective operation of UAVs. This necessitates advancements in sophisticated urban air traffic management strategies and the implementation of robust evaluation tools. Assessing UAV airworthiness requires a detailed examination of their reliability or health state, utilizing available data and model-based evaluation criteria.

Evaluating the reliability of UAVs involves analysing their capacity to perform designated functions reliably, safely, and efficiently over a specified period. This critical evaluation requires continuous monitoring and analysis of data pertaining to the UAV's operational performance, including indicators such as reliability, maintainability, and availability.

In this context, this thesis explores and establishes diverse methodologies adaptable to various scenarios, considering the format and quantity of available source data. By employing both statistical and data-driven approaches, the research developed models for assessing the reliability and performance degradation of UAVs at both the component and system levels. Through FMEA, critical failure modes in UAV propulsion systems were identified, revealing that motor failures account for approximately 45% of total failures. Weibull analysis predicted motor failures with a 90% confidence interval, highlighting wear-out mechanisms as predominant. Additionally, LSTM-based models for predicting UAV performance degradation achieved an accuracy of 85% in forecasting remaining useful life (RUL). These models demonstrated significant potential in enhancing predictive maintenance strategies, reducing downtime by up to 30%, and improving the overall reliability and safety of UAV operations. This work aims to refine UAV airworthiness evaluation methodologies, ensuring their safe integration and operation in complex airspace systems.

Table of Contents

Table of Figures

Table of Tables

List of Abbreviations

ACAI	Available Control Authority Index
AIC	Akaike’s Information Criterion
Adam	Adaptive Moment Estimation
ANN	Artificial Neural Networks
ATMRI	Air Traffic Management Research Institute
CAAS	Civil Aviation Authorities of Singapore
C-index	Concordance Index
CDF	Cumulative Distribution Function
CNN	Convolutional Neural Networks
EDA	Exploratory Data Analysis
ESC	Electronic speed controller
ESS	Effective Sample Size
FAA	Federal aviation administration
FMEA	Failure mode and effects analysis
FR	Failure rate
FTA	Fault Tree Analysis
HDI	Highest Density Interval
HMC	Hamiltonian Monte Carlo
HITL	Hardware in the Loop
IMU	Inertial measurement unit
KM	Kaplan-Meier
LSTM	Long Short-Term Memory
LiPo	Lithium Polymer

LWMM	Linear Weibull Mixed Model
MAPE	Mean Absolute Percentage Error
MCMC	Monte Carlo Markov Chain
MCSE	Monte Carlo Standard Error
MLE	Maximum Likelihood Estimation
MTBF	Mean time between failure
MTTF	Mean time to failure
MTTR	Mean time to repair
NHPP	Non-Homogeneous Poisson Process
NUTS	No-U-Turn Sampler
NWMM	Nonlinear Weibull Mixed Model
PDF	Probability Density Function
R^2	R-squared
ReLU	Rectified Linear Unit
RMSE	Root Mean Squared Error.
RNN	Recurrent Neural Network
RPM	Revolutions per minute
RUL	Remaining Useful Life
SITL	Software in the Loop
SOC	State-of-Charge
UAM	Urban air mobility
UAS	Unmanned aircraft system
UAV	Unmanned aerial vehicle
UAV-FD	Unmanned aerial vehicle fault detection

Chapter 1 Introduction

Tasks that were previously thought to be impossible or prohibitively expensive are now possible thanks to Unmanned Aerial Vehicles (UAVs), which are transforming a variety of modern applications, including military operations and commercial services. As their role in Urban Air Mobility (UAM) grows, they face more difficulties in maintaining airworthiness and operational safety. The foundation for the thesis is laid out in this chapter, which highlights the urgent need for secure and dependable UAV systems. It draws attention to how important airworthiness certification is becoming as a requirement for integrating UAVs into intricate airspaces. In order to address the dependability and airworthiness of UAV propulsion systems, the chapter also describes the goals, parameters, and difficulties of the research.

1.1 Background

Over the past few decades, the world has witnessed a rapid rise in Unmanned Aerial Vehicles (UAVs) numbers and applications as described by the Federal Aviation Administration and O'Donnell [1], [2]. Due to their affordable pricing and versatile functions, they have become easily accessible and have been favoured by the public to perform complex tasks [3], [4] that would otherwise be nearly impossible or costly. As described by Ahmed et al, UAVs fulfil various possible use cases and combined with their increased usage, they are expected to play a significant role in urban air mobility (UAM) [5], where multi-layer mobility is expected to be established in urban airspace, especially to alleviate ground traffic congestion [6], [7], [8], [9].

1.1.1 UAV Operation Phase Analysis

In a typical commercial UAV operation, there are certain phases involved in planning and executing the flight operation. For recreational flights, the phases are simplified to execute the flights in low-risk airspace. Commercially, when involving a large UAV or an operation in

high-risk airspace, there will be additional phases that consider aspects such as risk assessment, certification of UAV, permits, etc.

To generalize all the phases that are involved in a typical commercial UAV operation, a framework is summarized in Figure 1.1. In the pre-licensing phase, the UAV to be flown is sent for certification and its airworthiness is then assessed by regulators. Upon completion of this phase, the UAV operators will be granted operator permits, and activity permits depending on the proposed airspace to be flown in.

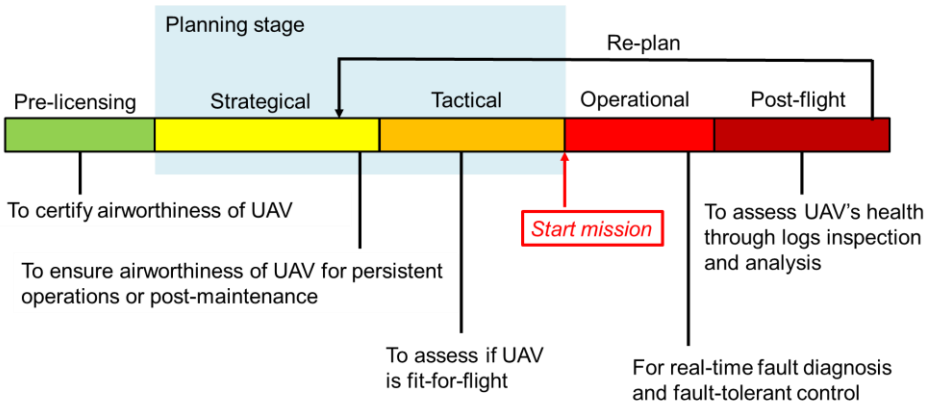

Figure 1.1: Phases illustration of UAV operations.

Next, the planning stage includes strategical and tactical phases as described by Gonçalves et al. [10]. The strategical phase can last anywhere from days to hours before the time of flight. In this phase, the airworthiness of the UAV is checked by performing required maintenance or preparations for flight. The tactical phase is from hours to minutes before a flight, where the operators ensure the UAV is fit-for-flight at the operating location.

Once the mission starts, UAVs can either be piloted by a remote pilot or by autonomous control. During this operational phase, real-time fault diagnosis and fault-tolerant control are implemented to ensure the UAV remains controllable and performs its operation safely. The post-flight phase commences when all the UAV flights and sorties are completed. Here, the UAV operators will inspect the UAV's health using flight data from sensors and fault diagnosis systems. Whether the UAV requires maintenance, repair, or preparation for the next flight

mission, re-planning will commence following the post-flight phase.

1.2 Significance of UAV reliability study

As the number of UAVs being used across various applications continues to rise, there has also been a rise in the number of UAV accidents. Sudden mechanical failures in propulsion systems are the most common cause of such accidents, accounting for about 40% in 2015 and 60% in 2016 [10]. Therefore, it is crucial to evaluate the reliability of the UAV propulsion system and provide reliable support strategies for maintenance or replacement.

1.2.1 Regulatory Landscape and Challenges in UAV Certification

The advent of UAM underscores the necessity of ensuring UAV airworthiness for their safe integration and operation within urban environments. This imperative has spurred a focused stream of research dedicated to the airworthiness assessment of UAVs through the lens of reliability engineering. Central to this discourse is the introduction of reliability modelling-based characterizations, aimed at estimating airworthiness with an emphasis on the resilience and dependability of UAV operations. Concurrently, there has been a significant advancement in the development of sophisticated, data-driven algorithms leveraging machine learning. These innovations offer a nuanced approach to understanding and enhancing UAV reliability, highlighting the critical intersection of traditional engineering principles with cutting-edge computational methodologies in the pursuit of operational excellence in UAV systems.

This project covered the UAV phase analysis as summarised in Figure 1.1 and Section 1.1.1. The actual research roadmap is based on the collected data parameters from the UAV in the Post-flight phase to build up the evaluation model and principle to reflect the drone's health and safety. Then these established criteria could be used in the Pre-licensing phase to certify the airworthiness of the UAV which can be the fundamental input for the following Strategic and Tactical phases. Therefore, the core research work of this project focuses on the effective

modelling ability based on the UAV flight data.

Presently, a standardized regulatory framework specifically designed for the safe operational management of UAVs is absent. Nevertheless, it is posited that there exists a substantial overlap in airworthiness considerations between manned and unmanned aircraft [11], [12]. This assumption suggests a foundational basis for developing UAV-specific regulatory measures.

Despite these considerations, the literature reveals notable deficiencies, particularly in the methodologies for assessing the reliability of various UAV system components as per defined criteria. Compounding this issue is the scarcity of UAV-specific datasets, which are pivotal for comprehensive reliability analysis. In the context of Singapore, the development of a generalized reliability model is advocated as a strategic imperative to facilitate the licensing and regulatory oversight of Unmanned Aerial Systems (UAS). Such a model would not only bridge the existing knowledge gap but also significantly enhance the efficiency of current processes on a quantitative level.

1.3 Research Roadmap

This study follows the reliability analysis framework as presented in Figure 1.2. The framework, which draws from several studies [13], [14], [15], [16], [17], provides a concise overview of two primary ideas for achieving overall system reliability in any given system, which are component level analysis and system level analysis.

A UAV comprises of an array of components that make up different subsystems, introduced in a previous report from ATMRI [18] which include:

- Airframe
- Propulsion
- Power distribution and storage
- Flight control
- Navigation/GPS

Each of these subsystems has its unique set of components, all of which contribute to subsystem-level reliability and, in turn, the overall UAS reliability.

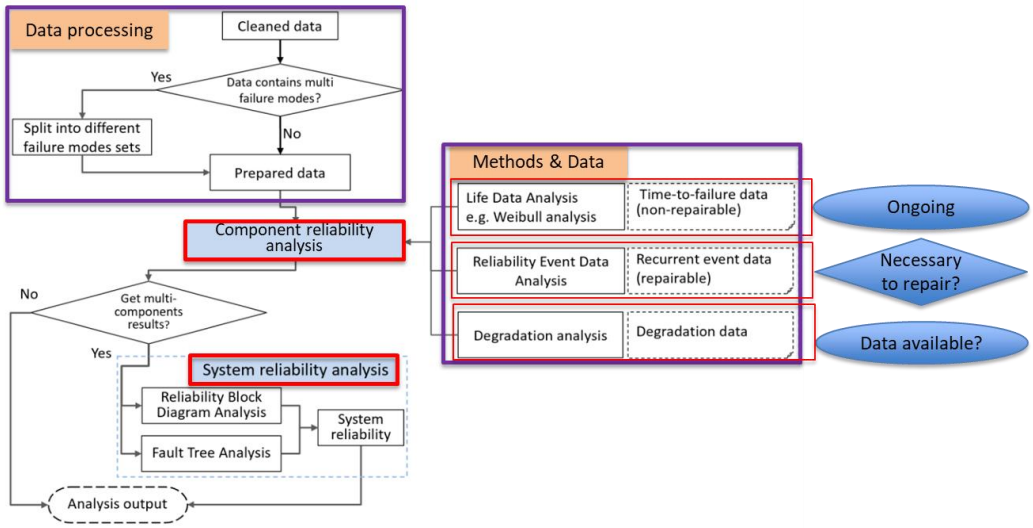

Figure 1.2: Established reliability framework.

Motivated by the demands for safe UAV operations this research aims to explore the topic of UAV reliability evaluation. In detail, the following objectives are expected to be achieved in this research project:

(a) **Evaluate UAV Propulsion Reliability**: Develop a framework to assess the reliability of electric UAV propulsion systems using Failure Mode and Effects Analysis Based on the preliminary research above, the quantitative method is developed to predict UAV propulsion system reliability.

(b) **Develop Quantitative Reliability Models**: Establish and validate quantitative methods, including statistical modelling, to predict the reliability of UAV propulsion systems based on empirical data and system performance metrics.

(c) **Simulate Health Conditions for Octorotor UAVs**: Develop a simulation method to model the health conditions of Octorotor UAVs under various operational assumptions, enabling the conceptualization and testing of reliability modelling approaches.

(d) **Conduct Experimental Data Collection**: Perform controlled experiments on UAV

propulsion systems to generate necessary failure data for model development and validation, ensuring reliability insights grounded in real-world performance.

(e) **Extend Methodologies Across UAV Components**: Expand the developed reliability evaluation methodologies to encompass other critical UAV components, contributing to a holistic evaluation of airworthiness.

(f) **Design a Comprehensive Testbed**: Create an advanced testbed capable of evaluating the time-to-failure of multiple UAV components simultaneously. Integrate hardware and software configurations to enable continuous, parallel experiments, supported by robust statistical methods such as Weibull and Bayesian analysis.

(g) **Enable Predictive Modelling for UAV Degradation**: Develop an experimental platform for manual UAV flight tests in controlled environments to collect real-time sensor data. Leverage advanced data mining and deep learning techniques to model and predict performance degradation, enhancing predictive maintenance strategies.

Based on the research output above, the quantitative method framework is needed to be conceptually developed and organized to be able to predict the UAV system or component's reliability with corresponding input information. The developed methodologies could support the airworthiness evaluation of the missioned UAV.

1.4 Scope

Darrah et al.[19] considers how - from a reliability research perspective - UAV performance and failure record data serve as the primary resources for basic analysis. This research leverages three types of data to explore effective methodologies, as illustrated in Figure 1.3:

1. Simulation-Generated Samples: In the early stages of the project, when information and material are limited, simulation-generated data under certain assumptions for defined failed components are utilized. This approach is particularly useful for exploring models with limited input data. The multiple rotors' various combinations and the resultant

controllability and reliability of the drone were analysed based on simulation data using Markov state generation and modelling methods.

2. Testbed Data: This data is generated from a constructed testbed for the UAV's critical components, such as motors, ESCs (Electronic Speed Controllers), and batteries. These components were tested under controlled environmental and operational conditions. The ability to perform continuous operations makes statistical methods, such as Weibull modelling, applicable. Time-to-failure data samples were collected to build the reliability models.
3. Experimental Flight Log Data: Collected from actual UAV flights, this data reflects real operational conditions and performance. The data, recorded by multiple sensors, is substantial in both size and dimension. Advanced deep learning algorithms were developed to characterize the UAV's health state and detect hidden degradation indicators from this extensive dataset.

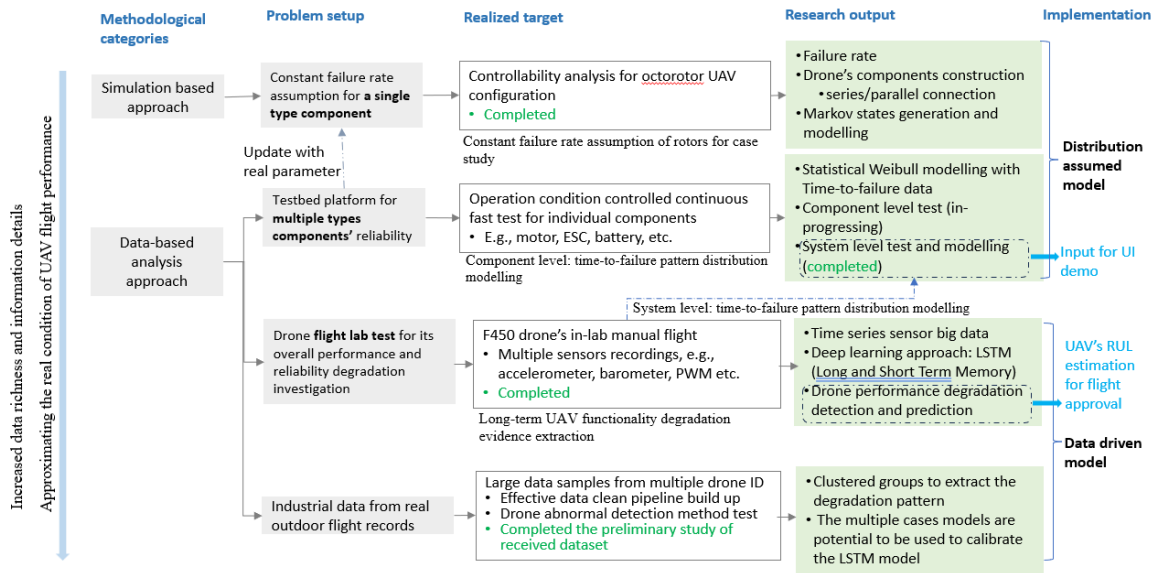

Figure 1.3:Research matrix of UAV reliability and performance degradation.

The research map in Figure 1.3 illustrates the progression from simulation data to real-time failure data generation, and from component-level to system-level characterization. The applied methods evolved from assumption-based approaches to more realistic, data-driven

methodologies. This project utilizes these three types of data and modelling methods for several reasons:

(a) Data Availability: The availability of data samples varies at different project stages, with manual flight data requiring significant effort during the experimental period.

(b) Comprehensive Reliability Modelling: Both component-level and system-level reliability parameters are essential for accurate UAV reliability modelling. For instance, component failure rates calculated from testbed data can update simulation model inputs. Additionally, combining multiple component reliability parameters helps build a system reliability model, which can be compared with deep learning methods for UAV system failure prediction.

(c) Diverse Data Formats: In real-world airworthiness management, data formats and types are diverse. This study aims to ensure the developed methods and models are applicable and useful during implementation. For example, a trained high-performance deep learning model can predict the Remaining Useful Life (RUL) of a drone based on its sensor readings during actual flights.

In summary, this research navigates through the complexities of enhancing UAV reliability by leveraging simulation-generated samples, testbed data, and experimental flight log data. By evolving the applied methods from strong assumption-based approaches to realistic data-driven models, the study addresses key challenges and provides robust solutions for UAV reliability and airworthiness evaluations.

1.5 Challenges Addressed

This research navigates the intricate challenges of enhancing the reliability and safety of Unmanned Aerial Vehicles (UAVs). The thesis aims to tackle the complexities associated with predicting component failures and establishing a robust testing framework that can operate

under diverse conditions. This endeavour is further complicated by the evolving regulatory landscape for UAV operations, highlighting the need for innovative solutions that align with safety standards and operational efficiency. The major technical challenges addressed in this research include:

(a) Sparse and Heterogeneous Data: Due to the limited occurrence of real-world failures and variability in operational settings, acquiring a comprehensive and diverse dataset for UAV propulsion system failures is challenging. Additionally, there is a lack of ready-made failure databases for multirotor-type UAVs, which is a bottleneck for data-driven reliability evaluations.

(b) Limited Testing Scenarios: Extensive real-world testing for UAV propulsion system dependability is often constrained by cost, time, and safety concerns. Strategies are needed to extend reliability assessments from small-scale testing settings to larger operational contexts. This includes developing precise accelerated testing methodologies, verified simulation models, and strategies for transferring knowledge from related disciplines.

(c) Short Product Lifecycles and Rapid Technological Advances: With constant breakthroughs in materials, design, and technology, the field of UAV propulsion systems is continuously evolving. Traditional reliability evaluation methodologies may struggle to keep pace with reduced product lifecycles and changing designs. Adaptive reliability evaluation approaches must be developed to assess the dependability of new and innovative propulsion system designs while accounting for the uncertainties introduced by evolving technology.

(d) Dependency on Setup and Environment: UAV failure mechanisms are heavily dependent on the specific drone setup and operating environment. Therefore, the assumed failure rates in simulation studies need to be representative of actual

conditions.

(e) Critical Component Identification: There are multiple components in a UAV system, but the most critical ones that determine the major failure causes are not transparently reported in the literature and require further study.

(f) Testbed Construction: Constructing the UAV component testbed requires harmonization of both hardware and software. Challenges include synchronization of data collection during parallel testing of multiple components and the development of proper data cleaning and model fitting methods to reflect component reliability accurately.

(g) Absence of Comprehensive Failure Database: The lack of a comprehensive UAV failure database presents a significant challenge for implementing data-driven approaches in drone health monitoring and degradation assessment. Designing and building a UAV experiment platform to continuously gather sufficient sensor data is the first crucial step. The subsequent challenge is developing data cleaning and deep learning-based algorithms to quantitatively predict the UAV's remaining useful life (RUL).

A significant challenge lies in the practical application and validation of the methods and models developed in this research. The objective is to quantitatively assess airworthiness by leveraging the available data and insights. This necessitates not only the theoretical formulation of models but also their empirical testing and refinement in real-world scenarios to ensure their effectiveness in supporting UAV airworthiness evaluations.

Overall, this research aims to address these challenges by developing and validating advanced methodologies for UAV reliability assessment, ultimately contributing to safer and more efficient UAV operations in urban airspace.

1.6 Outline

In this thesis, the research is arranged as follows:

Chapter 1: Introduction

Introduces the significance of UAVs, outlines the need for advanced reliability and degradation modelling, and sets the stage for the research scope and challenges.

Chapter 2: Literature Review

Reviews existing UAV reliability evaluation methods, focusing on Markov-chain models, statistical approaches, and the emerging role of deep learning in degradation prediction.

Chapter 3: UAV Propulsion System FMEA

Present the Failure Mode and Effect Analysis (FMEA) for the propulsion system of an Electric UAV assisting in the design of experimental models in Chapters 5 and 6

Chapter 4: Markov-chain Based Controllability Evaluation

Presents a Markov-chain analysis for assessing the controllability and reliability of multirotor UAVs, offering a novel framework for evaluation.

Chapter 5: Testbed for UAV Component's Reliability Analysis

Describes the setup and implementation of a testbed designed for empirical reliability analysis of UAV components along with the analysis of the data to create models.

Chapter 6: Degradation Flight Testing and Results

Details the methodology and findings from flight tests conducted to model UAV performance degradation, showcasing the application of Weibull models and LSTM autoencoders.

Chapter 7: Summary

Summarizes the key findings, contributions to UAV reliability modelling and suggests directions for future research to enhance UAV airworthiness through predictive maintenance strategies.

Chapter 2 Literature review

To lay the groundwork for the methods and strategies created in this thesis, this chapter examines the state of research on UAV airworthiness and reliability. There is a thorough examination of reliability analysis methods, such as statistical models, Fault Tree Analysis (FTA), and Failure Mode and Effects Analysis (FMEA). The conversation goes on to discuss contemporary strategies that make use of data-driven techniques like Markov models and deep learning, highlighting both their advantages and disadvantages. The need for this research is highlighted by the identification of important gaps in the body of existing literature, especially the dearth of reliability data specific to UAVs.

2.1 Related concepts

To evaluate the reliability of UAVs, a set of closely related terms and definitions are first emphasized herein.

Airworthiness: Refers to the ability of a system to meet its intended objectives and specifications.

Reliability: A term to measure the performance of a component operating the specified functions in a specified time. This defines the probability of a component to normally finishing its required mission without failure under stated conditions.

Component: Refers to a part or module of the off-the-shelf UAVs, not the raw material for product design in this thesis.

Criticality: A measure of the failure of UAV components in terms of the frequency and consequences.

Failure: An undesirable event in which the UAV component fails to operate normally as specified.

Failure mode: Consequences of failure.

Failure effect: Consequences of a failure mode.

Failure mode and effects analysis (FMEA): A process to analyse the failure mode of components and determine the effects.

Fault tree analysis (FTA): A technique of system analysis, which identifies all possible causes from a single potential failure mode and analyses system errors. FTA considers both interrelated and independent causes. In addition to the fault tree structure and all logical associations, FTA usually includes the identification of failure probability, so that the system reliability can be found from the reliability of components.

Failure rate (FR): The total number of failures of a UAV component in the given period.

Mean time between failure (MTBF): In the given duration under stated conditions, the mean number of life units of the tested components within specified limits. It is a reliability measure indicator for repairable components.

Mean time to failure (MTTF): In the given duration under stated conditions, the total number of life units of a component group is divided by the total failures within that group. This term is for non-repairable components reliability measurement.

Mean time to repair (MTTR): In the given duration under stated conditions, the total maintenance times are divided by the total number of failures within the repairable level of a component.

Redundancy: More than one component is used to obtain a specified level of reliability for a given function of objects.

Active redundancy: All redundant components perform the given function simultaneously.

Standby redundancy: Part of redundant components are activated only when the primary component failure happens.

2.2 UAV reliability evaluation

This section explores the various studies that have been conducted in the literature and their

associated data analysis method. Subsequently, the methods employed in these studies to estimate the propulsion system's reliability are also highlighted.

To perform UAV reliability analysis, qualitative methods, such as FMEA and FTA are widely used [20], [21], [22], [23]. In [20], the FTA was used to analyse the top event of the UAV critical component. The communication reliability of the UAV fleet was analysed by the method of FTA as described by Kladis et al. [21]. The failure causes between the UAV fleet and ground station were discussed to ensure safe missions. Also, Shlapatskyi [22], stressed the necessity of the FTA, in terms of UAV design and testing stages. And in Franco and Góes [23], both methods were employed to design failure analysis procedures and improve UAV reliability.

Various failure modes can worsen the reliability of the UAV propulsion system. Altinors, Yol and Yaman [24] talked about how the fault modes can be generally categorized into bearing, stator, rotor-shaft, and propeller faults. Bearing faults can be caused when there is an improper cooling effect, which leads to dust building up in the bearings. Secondly, stator faults refer to the breakdown of the stator winding insulation in the motors which are generally caused when there is an increase in temperature. This happens during an overload when the high temperature deteriorates the windings.

Rotor-shaft failures can be in the form of an imbalanced rotor or bent shaft whereas propeller faults can be due to deformation or chips in the propellers. Rotor-shaft and propeller faults usually occur when the UAV has endured physical damage due to an impact. Since there is no possibility of the propulsion system in the testbed enduring physical damage due to impact, stator and bearing faults will be considered.

There are various estimation methods studied in the literature and among them, some have demonstrated practical applications to the data that can be collected from UAV flight operations. This section also discusses how the methods employed in these studies can

potentially be applied in determining the reliability of the propulsion system following data collection from the experimental testbed. A summary of the methods discussed in this section is presented in Table 2.1.

Table 2.1: Summary of reliability prediction methods considered.

Reference	Type	Data and method considered
[25]	Theoretical	• Failure rate data from IEC 62380 • Markov chain model for fault-tolerant and redundant system scenarios • MTBF and MTBR for reliability estimation
[26]	Signal Processing	• Data from the current signal • Filters used on signal to determine bearing vibration signal. • Order analysis-based fault diagnosis
[24]	Empirical	• Data collected from bench tests of various BLDC motors. • Characterize BLDC motors' mathematical model parameters, torque-speed efficiency, and thermal properties. • Characterize the time and frequency domain of closed-loop performance
[26]	Data-driven	• Sound data collected from propulsion system operations. • Feature extractions using statistical equations. • Machine learning algorithms, SVM, and KNN to determine fault occurrence
[27]	Data-driven	• Temperature measurement and associated data collected. • Various machine learning techniques used to estimate stator temperature
[28]	Data-driven	• Input current and coupled generator’s output data. • LSTM is used to estimate remaining useful life (RUL)

In Thurlbeck and Cao [25], an electric propulsion system was studied using mission-based flight profiles under various fault-tolerant control and redundant system scenarios. Failure rates of the components are determined using IEC 62380 where the rates during healthy operations and postfault operations are considered for semiconductor devices in the propulsion subsystem. Secondly, Markov chain models were presented for the various operating states for the various system scenarios. Subsequently, reliability metrics using MTBF and MTBR were considered

to determine the reliability.

A signal processing methodology was proposed by Lu and Wang [26] to estimate the rotating phase under variable-speed conditions for bearing fault monitoring. A series of filters were applied to the current signal to achieve the bearing vibration signal. Subsequently, an order analysis is used to monitor the occurrence of a bearing fault.

As propulsion systems with brushless DC (BLDC) motors are becoming increasingly common in UAV applications, it is essential to obtain accurate and detailed specifications for them. These specifications can often be unreported and be important to determine the reliability of the propulsion system. As such, the study by Lee, Pan and Rouse [29] presented an empirical characterization of these propulsion systems by considering the motor's mathematical model, efficiency, as well as thermal properties during operation. By deriving the key parameters, the researchers were able to determine the trend when the propulsion system degraded.

In one data-driven study, features were extracted from flight sound data using several statistical metrics. These metrics are mean, standard deviation, variance, covariance, kurtosis, and skewness and they analyse the characteristics of the data. Subsequently, unsupervised machine learning algorithms, such as support vector machines (SVM) and K-nearest neighbour (KNN), were employed on these extracted features [24]. In another data-driven method, temperature measurements were collected for various load conditions, cooling conditions, and speed profiles. Machine learning techniques were used to train and test the developed models and the performance of the techniques was analysed [27]. Next, data from input current signals and coupled generator output were analysed to conduct a data-driven remaining useful life (RUL) for the propulsion systems [28].

To facilitate the data collection about reliability, a run to failure or degradation-based test seems to be optimal. This has previously been performed for BLDC motors in a few different forms using voltages and neural networks or developing diagnostic methods [30], [31].

However, there is a lack of testing data that uses real-world testing data to try to form a long-term reliability estimate.

With regards to the propulsion system, a lot of different accelerated testing procedures are possible [32], [33], [34], [35], [36]. These involve wearing out their primary known failure mode. With regards specifically to Brushless DC motors (BLDC), there has been some testing whereby the stator has been tested for reliability, or just a single wire has been tested to show that degradation occurs or demagnetization of the stator causes the motor to stop working[37], [38], [39]. Another testing method proposed by Abed et al [40], that has been conducted has been with regards to the rotor of the motor using Finite element analysis or a bearing fault. However, a lot of these tests have been for generic BLDC motors and not for UAV-specific motors. Hence there is a gap in the literature that can be explored.

In the same vein, a lot of the ESC (electric speed controller) related research in the UAV field tries to replace common ESCs with intelligent ESCs to develop neural models to still help the system run with faults. However, not much research has been conducted about the reliability of different types of speed controllers [41], [42].

Although a number of techniques, such as fault tree analysis and FMEA, are used to assess UAV reliability, there is a clear lack of application of these techniques to actual UAV operational data. The complexity of UAV operations in a variety of environmental conditions is not adequately captured by the evaluations that currently exist because they are frequently based on theoretical models or sparse experimental data. The breadth and difficulties of UAV reliability studies were covered in Sections 1.4 and 1.5, which emphasized the necessity of empirical research that makes use of copious operational data in order to validate and improve reliability assessment techniques. This is necessary to create reliable models that can be applied to the urban airspace operations certification procedure. In order to close this gap, Chapter 5 describes the planning and execution of run-to-failure experiments and provides the required

empirical data to enhance reliability models.

2.3 Statistical modelling approach of UAV reliability

To addresses the analytical strategies employed to evaluate the reliability of Unmanned Aerial Vehicles (UAVs) through the lens of time-to-failure data obtained from testbed experiments. This evaluation primarily focuses on extracting reliability parameters for various UAV components, utilizing sophisticated methods such as Weibull and Bayesian modelling. Weibull modelling stands out for its flexibility in characterizing the life distribution of components, making it particularly suited for analysing the wide range of failure patterns observed in UAV systems [43]. Its parameters offer insights into the failure rate and life expectancy of components, facilitating the identification of potential weaknesses and the prediction of their future performance. This method's strength lies in its ability to accommodate the varied nature of UAV component failures, from early failures to wear-out mechanisms, providing a comprehensive view of component reliability [44]. On the other hand, Gao et al [45] uses Bayesian modelling to introduce a probabilistic framework that incorporates prior knowledge and observed data to update the reliability estimates of UAV components. This approach is invaluable in scenarios where data are limited or incomplete, as it allows for the integration of expert judgment and historical data. Bayesian methods are particularly adept at handling uncertainty, offering a robust mechanism for predicting the reliability of UAV components under different operational conditions [46].

These methodologies not only enable the precise estimation of reliability parameters but also enhance the understanding of component behaviours under stress, contributing significantly to the development of more reliable and safer UAV systems.

2.3.1 Reliability event data analysis

Reliability event data analysis is a methodology used in reliability engineering to analyse

data on the occurrence of events or failures in a system. This methodology involves collecting data on the occurrence of events over time, identifying patterns in the data, and using statistical techniques to analyse the data and draw conclusions about the reliability of the system as shown by Powers and Xie [47].

The main goal of reliability event data analysis is to identify the causes of failures in a system and to develop strategies to prevent or mitigate those failures. This is typically done by analysing data on the frequency and severity of failures, as well as data on the conditions under which failures occur, such as temperature, humidity, and usage patterns [48].

Reliability event data analysis can be applied to a wide range of systems, including mechanical systems [49], [50], electrical systems [51], [52], software systems [53], and complex systems such as aircraft [54]. It can also be used to analyse data from different sources, such as field data, laboratory testing, or simulation models.

Some of the statistical techniques used in reliability event data analysis include:

- Failure mode and effects analysis (FMEA), which is used to identify and prioritize potential failure modes and their causes.
- Fault tree analysis (FTA), which is used to analyse the causes of a specific failure event and to identify the combination of events that led to the failure.
- Reliability block diagrams (RBDs) are used to model the reliability of a system by analysing the reliability of its components and their interactions.

Overall, reliability event data analysis is an essential tool for improving the reliability and safety of complex systems by identifying and mitigating potential failure modes. Within all of the reliability modelling domain, any one of these methods may be split into either parametric or non-parametric approach.

2.3.2 Weibull modelling theory for parametric systems

A parametric system is a system that can be described by a set of parameters that explain

its failure behaviour in the context of reliability engineering. The failure times or failure rates of system components are often used to obtain these characteristics through statistical or graphical analysis [55]. While many different types of models exist, such as the Normal distribution, the Log-normal distribution, the exponential distribution, and the Gamma distribution. This thesis will focus more on the Weibull distribution.

The Weibull distribution, which is frequently used to represent the failure behaviour of systems that encounter wear-out failures over time, is one typical example of a parametric system in dependability. The shape parameter (γ), which represents the slope of the failure rate curve, and the scale parameter (θ), which specifies the time at which the failure rate starts to climb, are the two parameters that define the Weibull distribution. With regards to the Weibull distribution the following equations help define the model as a whole [55].

$$F(t) = Prob(T \leq t), \quad F(0) = 0 \; and \; F(\infty) = 1 \tag{2.1}$$

$F(t)$ is the CDF (cumulative distribution function) of t, also called unreliability, indicating the probability that the system will fail before the specified time t.

$$f(t) = \frac{dF(t)}{dt}, \qquad F(t) = \int_0^1 f(t)dt \tag{2.2}$$

For Weibull distribution

$$f(t) = \frac{\gamma}{\theta} t^{\gamma-1} e^{\frac{-t^{\gamma}}{\theta}} \tag{2.3}$$

where $f(t)$ is the PDF (probability density function) of t.

$$f(t) = -\frac{dR(t)}{dt} \tag{2.4}$$

$$R(t) = e^{\frac{-t^{\gamma}}{\theta}} \tag{2.5}$$

where $R(t)$ is the reliability function (Survival Function): The probability that the item does not fail in the time interval (the probability that the item survives the time interval and is still functioning at time t).

$$h(t) = \frac{f(t)}{R(t)} \tag{2.6}$$

$$h(t) = \frac{\gamma}{\theta} t^{\gamma-1} \tag{2.7}$$

where $h(t)$ is the failure rate function. The probability that an item will fail in a time interval when how to know that the item is still functioning at any given time t.

2.3.3 Reliability analysis based on Weibull distribution.

In a previous report by Zhang et al. [56], the method of Weibull distribution is introduced to evaluate the UAV component reliability. The Weibull distribution is a continuous probability distribution that is widely used in reliability analysis to model the time-to-failure of systems or components. The probability density function (PDF) of the Weibull distribution is determined by two parameters, namely shape, and scale. In this section, a detailed analysis is done to reveal how the reliability changes with the parameters' shape and scale.

2.3.4 Weibull model shape parameter properties investigation

The parameter shape β, also called failure rate, determines the shape of the PDF. When β < 1, the PDF is decreasing and convex, which is characteristic of systems with increasing failure rates over time (reliability deteriorating over time). When β = 1, the PDF reduces to the exponential distribution, which is commonly used to model the failure rates of systems with constant hazard rates. When β > 1, the PDF is increasing and concave, which is characteristic of systems with decreasing failure rates over time (reliability improving over time). The changes in the shape parameter are shown in Figure 2.1.

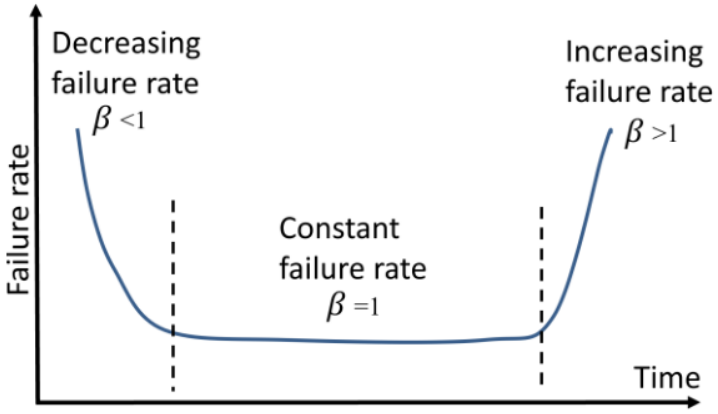

Figure 2.1: Bathtub curve of shape parameter β [57].

To analyses how the shape parameter affects the PDF and reliability of the Weibull distribution, three cases in terms of $\beta < 1$ with a constant scale are tested, as shown in Figure 2.2.

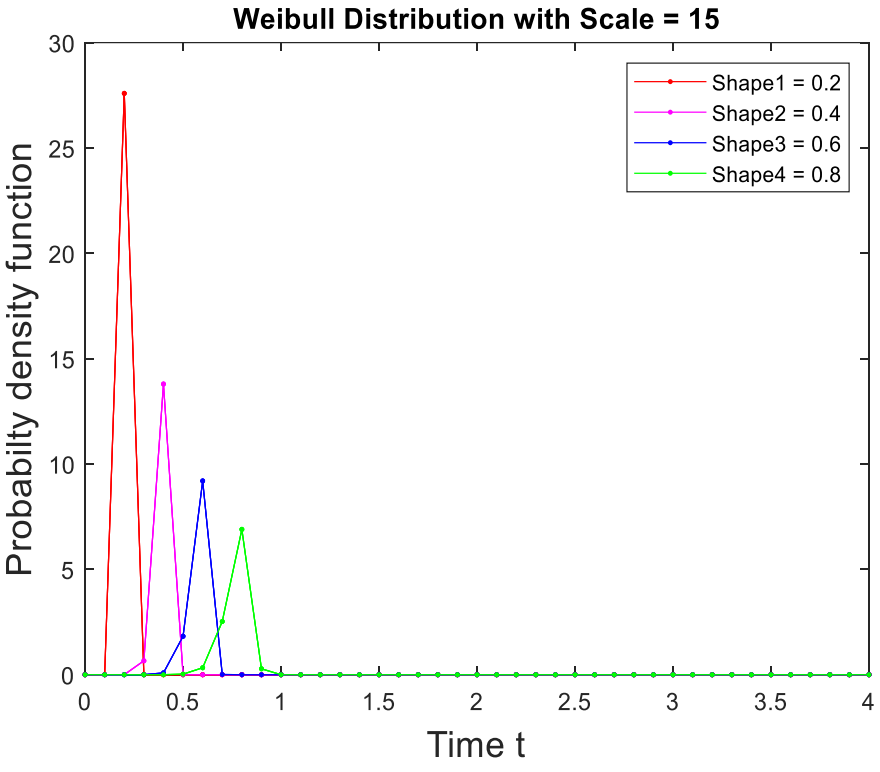

(a) PDF

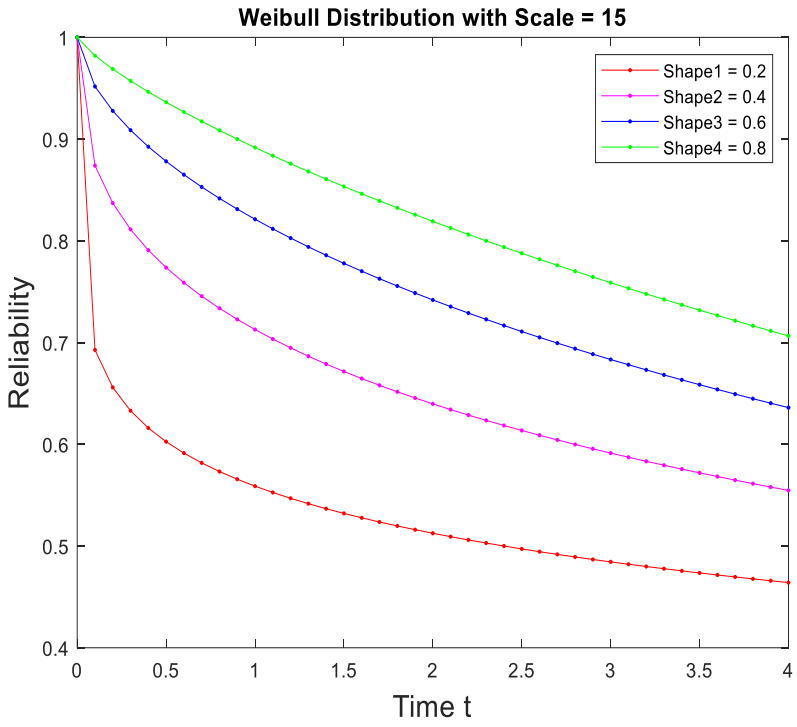

(b) Reliability

Figure 2.2: Weibull test with scale = 15 and shape < 1.

In the case that shape < 1 with scale = 15, four different shape values, including 0.2, 0.4, 0.6, and 0.8, are set to analyse the PDF and reliability of the Weibull model. As shown in Figure 2.2, when the shape values change from 0.2 to 0.8, the PDF of the failure reaches the maximum peak at shape = 0.2. With the step increase of the shape, the reliability shows a growth trend. This means the reliability is greater at shape = 0.8 than other shape values at the same test time. And the minimum reliability is at shape = 0.2. Such kind properties could be used for the analysis guide in the statistical result explain in the UAV component reliability modelling.

2.3.5 Degradation analysis

Degradation analysis is a measurement and extrapolation of degradation or performance data directly related to the presumed failure. It can either use model-based approaches (such as physics-based models or statistical models), knowledge-based approaches (such as expert systems and fuzzy logic systems), and data-driven approaches (such as neural networks (NNs)

and hidden Markov model (HMM) [58], [59]. The general degradation analysis process can be seen in Figure 2.3.

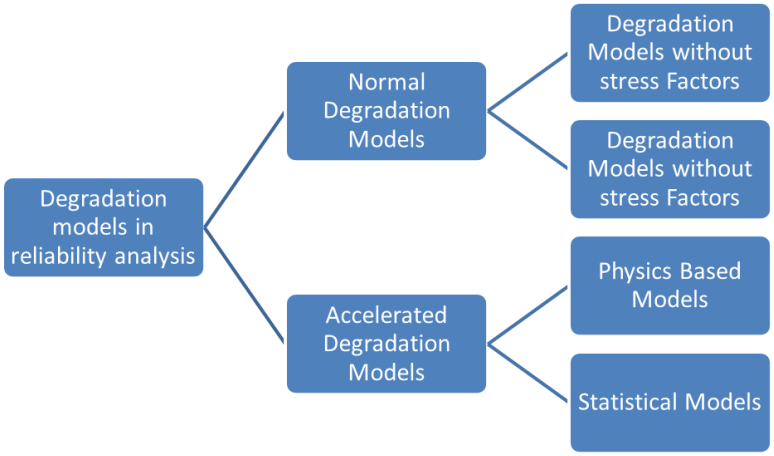

Figure 2.3: Degradation analysis flowchart.

2.3.6 Accelerated testing.

Accelerated testing is a method used to assess the performance and stability of materials or products over time. It involves subjecting the materials or products to harsher or more severe conditions than they would normally experience to accelerate their degradation and failure. This allows manufacturers to identify potential failure modes and design improvements and can also be used to estimate the expected lifetime of a product. Accelerated degradation testing is commonly used in various industries, including electronics, aerospace, and automotive [48], [60].

2.3.7 Use of Degradation Analysis for Censored Data

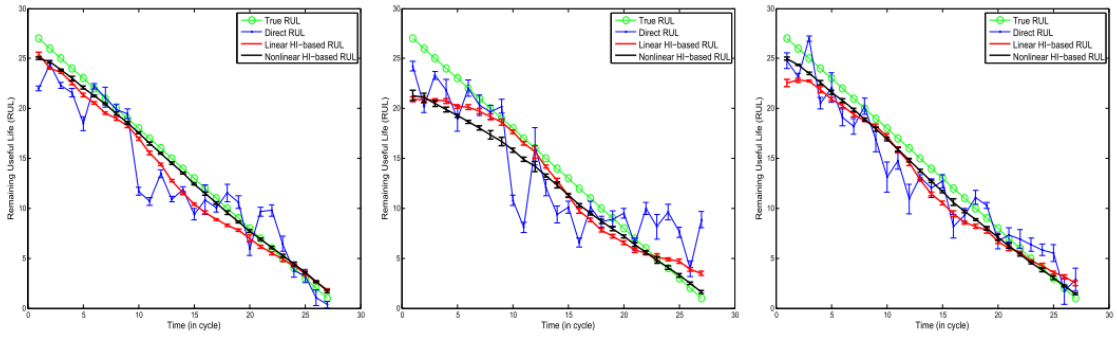

Figure 2.4: Example of Remaining Useful Life (RUL) prediction of Motors by Yang et al. [61]

Figure 2.4 displays graphs from a study that predicts the remaining usable life (RUL) of motors by monitoring a health index. The health index is a measurable indicator that represents the state of the motor over a period of time, calculated based on data collected from several sensors. Degradation study is conducted by monitoring the health index over multiple cycles. The actual remaining useful life (RUL), represented by the dotted line, is compared to forecasts produced by various models, including direct RUL prediction, linear, and nonlinear health-index-based RUL predictions. These models graphically represent the predicted RULs in relation to the actual operational cycles of the motors. The closeness of a model's prediction line to the actual RUL line reflects its precision in estimating the motor's deterioration and remaining operational lifespan. [61]

Degradation analysis is a technique employed in the fields of reliability engineering and quality control to evaluate the decline in performance of a system or component over time when subjected to regular operating circumstances [62]. Differing from conventional failure-time analysis, degradation analysis specifically investigates the gradual deterioration of a quantifiable performance attribute, commonly known as a degradation signal or health index [63]. This method is especially beneficial in situations when failures are few or where data is completely censored, indicating that failure occurrences are not observed throughout the

research period.

2.3.7.1 Types of Degradation Analysis

There are primarily three categories of degradation analysis. The first type of analysis is deterministic degradation analysis, in which the model assumes a consistent rate of deterioration across time for all units being studied. The models employed are simplistic and do not account for randomness in the degrading process.

Furthermore, stochastic degradation analysis has the potential to identify the inherent variability in the degradation paths across distinct units. This technique utilises probabilistic models, such as the Wiener process, gamma process, and inverse Gaussian process models, to accurately represent the uncertainty in deterioration.

Accelerated degradation analysis is performed when degradation data is obtained under situations of increased stress in order to forecast the lifespan of components during regular operating environments. This analysis facilitates the expedited estimation of the time to failure, as opposed to waiting for failures to occur under normal circumstances.

2.3.7.2 Why Degradation Analysis is useful for Fully Censored Data

Traditional reliability analysis approaches relying on failure times struggle with fully censored data when no units failed during the observation period. In many cases, degradation analysis can detect diminishing performance patterns before failure thresholds, enabling proactive maintenance and interventions. Degradation analysis analyses degradation signals up to the censoring point to make use of censored data since it focuses on performance deterioration rather than failure. Instead of waiting for failures, degradation analysis models the degradation process to monitor component health immediately and continuously. This helps in safety-critical situations where failure avoidance is crucial.

Thus, degradation analysis provides a comprehensive structure for analysing and

forecasting component and system reliability, even when failure-time data is unavailable. Measured performance degradation informs maintenance methods and design optimisations, improving system reliability and performance.

Reliability engineering and quality control employ degradation analysis to evaluate a system or component's performance over time under typical operating circumstances [62]. Degradation analysis tracks the deterioration of a quantifiable performance characteristic, such as a degradation signal or health index, rather than failure-time analysis [63]. This method is beneficial when failures are uncommon or data is entirely censored, producing no failure observations during the investigation.

2.3.7.3 Degradation Analysis as a Preliminary Exploration Tool

Degradation analysis is a useful method in reliability engineering, particularly when there is a lack of direct failure data. Once failure data becomes accessible, the knowledge acquired from degradation analysis may be utilised to enhance the accuracy of reliability predictions. This section will demonstrate how to improve the predicted accuracy of models by employing degradation analysis results after failure data is obtained.

The initial study identifies the baseline performance and important signs of decline, which are crucial inputs for predictive models. These inputs aid in the calibration of the models to detect early indications of probable breakdowns. Similarly, the quantified deterioration paths derived from historical data offer a comprehensive dataset for training prediction models. These paths enable the models to acquire knowledge about the usual pattern of wear and tear that components undergo in different circumstances, thereby enabling them to forecast future rates of degradation. The degradation analysis establishes thresholds that are utilised in prediction models to indicate imminent breakdowns. When the model anticipates that a component's performance will beyond a certain level, it may set off a warning for proactive maintenance.

Thus, degradation analysis serves as a way for understanding the degradation of components even when failure data is not available, and it also establishes the foundation to build complex prediction models. These approaches revolutionise the method companies take towards maintenance, lifecycle management, and design, transitioning from reactive to proactive techniques.

While statistical models like the Weibull distribution and Bayesian analysis are commonly employed in reliability engineering, there is still a lack of development in their application to unmanned aerial vehicle (UAV) propulsion systems. A significant research gap is highlighted by the lack of reliable statistical models and comprehensive failure data that can reliably forecast UAV component failures. The research roadmap highlights the requirement for quantitative analysis to support UAV certification, as stated in Section 1.3. Achieving this goal will require building thorough statistical models that consider the specific failure modes of UAV propulsion systems and incorporate real-time operational data.

2.4 System level reliability analysis

The discourse on "System-Level Reliability Analysis" extends beyond the examination of individual components to conceptualize the reliability of UAVs as integrated systems. This holistic approach, underpinned by statistical methodologies like Weibull and Bayesian analysis, provides a framework for assessing how different components interact to influence the overall reliability of the UAV system. Unlike component-level analysis, which isolates parts to determine their failure rates and lifespans, system-level reliability analysis synthesizes these individual metrics to model the UAV's collective performance and durability.

Key techniques in system-level analysis include Fault Tree Analysis (FTA) and Reliability Block Diagrams (RBDs), which map out the potential failure paths within a system and the interdependencies of components [64], respectively. These methods are instrumental in identifying critical failure modes that could compromise the UAV's operational integrity.

Weibull analysis, with its flexibility in modelling various life distributions, is adept at accommodating the diverse failure behaviours of components within the system context. Concurrently, Bayesian approaches offer the advantage of integrating prior knowledge and real-time data to refine system reliability estimates, especially under conditions of uncertainty or limited data [65].

By adopting these statistical approaches, researchers can construct a comprehensive model of UAV system reliability, accounting for the complex interactions between components and their collective impact on system performance. This integrated perspective is crucial for designing more resilient UAV systems, ensuring that they meet the rigorous demands of their intended applications.

Although statistical models such as Weibull distribution and Bayesian analysis are widely used in reliability engineering, their application to UAV propulsion systems remains underdeveloped. The lack of detailed failure data and the absence of robust statistical models that can accurately predict UAV component failures highlight a critical research gap. As outlined in Section 1.3, the research roadmap emphasizes the need for quantitative analysis to support UAV certification. Developing comprehensive statistical models that incorporate real-time operational data and account for the unique failure modes of UAV propulsion systems is crucial for achieving this goal. Chapter 6 addresses this gap by employing advanced statistical and machine learning techniques to model and predict UAV performance degradation.

2.5 Markov-chain based evaluation of multirotor drone reliability.

Zhao et al. [66] introduced s Markov-chain based controllability evaluation which represents a significant advancement in the assessment of multirotor drone safety and reliability. This methodology, grounded in the principles of stochastic processes, offers a novel approach to understanding how multirotor drones respond to component failures, specifically focusing on the rotors, which are critical to flight stability and control. By simulating failure

data based on assumed failure rates of the rotors, this technique provides a comprehensive framework for predicting the drone's behaviour under various failure scenarios [67].

The application of Markov chains in this context allows for the modelling of state transitions, from fully operational to partial or complete failure states, thereby offering insights into the controllability and safety of the drone under different operational conditions. This simulation-based approach not only enhances our understanding of the inherent risks associated with rotor failures but also contributes to the development of more resilient drone designs. Furthermore, it aids in the formulation of effective contingency strategies, ensuring that drones maintain a degree of controllability even in the event of component malfunctions. Overall, the Markov-chain based controllability evaluation marks a pivotal step towards improving the reliability and safety protocols of multirotor drones [46], paving the way for their safer deployment in increasingly complex and demanding environments. The derivation of specific theoretical methods will be introduced in the Chapter 4.

Although Markov-chain models present a promising method for assessing UAV reliability, the lack of empirical failure data for multi-rotor configurations limits their practical use. Predictions of reliability may be inaccurate because the majority of current models are predicated on theoretical premises that might not hold true in practical situations. The significance of creating quantitative approaches for UAV certification was emphasized in Section 1.3, and Figure 1.1 showed the stages of operation that depend on precise reliability evaluations. To close this gap, a great deal of experimental research is needed to collect failure data and improve Markov-chain models so that they can be used in real-world UAV operations. This data is provided by the experimental designs in Chapter 5, and the Markov-chain reliability models are integrated with the results in Chapter 4.

2.6 Deep learning-based degradation modelling and prediction

In the evolving landscape of Unmanned Aerial Vehicle reliability analysis, the

incorporation of machine learning and deep learning methodologies marks a significant paradigm shift. This subsection delves into the use of these advanced computational approaches for modelling and predicting the degradation of UAV functionality and performance. Leveraging large datasets derived from flight test logs and multiple sensor readings, these methods unlock new potentials in understanding the complex dynamics of UAV operations and their long-term sustainability.

Machine learning and deep learning algorithms excel in extracting patterns and insights from vast, multidimensional data, making them particularly suited for the nuanced task of degradation modelling. Among the spectrum of algorithms, Convolutional Neural Networks (CNNs) stand out for their ability to process spatial data, which can be instrumental in analysing images or spatial patterns from sensor data [68]. Similarly, Random Forest and Gradient Boosting Machines offer robust predictive capabilities and are adept at handling tabular data from sensors, providing a comprehensive view of UAV health [69].

The Long Short-Term Memory (LSTM) network, a specific type of Recurrent Neural Network (RNN), emerges as particularly promising for UAV degradation modelling [70]. Its architecture is uniquely designed to process sequential data, capturing temporal dependencies that are crucial for understanding how UAV performance evolves over time [71]. LSTMs are capable of learning from the historical performance data of UAVs, enabling the prediction of future degradation based on patterns of change in sensor readings.

The potential of LSTM and other deep learning algorithms to revolutionize UAV health monitoring and predictive maintenance is immense. By accurately forecasting degradation trajectories, these technologies can facilitate proactive maintenance strategies, enhance UAV reliability, and ensure operational safety, making them invaluable tools in the continuous effort to advance UAV technology [72].

2.6.1 The application LSTM for UAV health monitoring

The application of LSTM networks in UAV health monitoring represents a cutting-edge approach to predicting and mitigating potential failures before they compromise UAV operations. This detailed review explores the current landscape of LSTM applications within UAV health monitoring, addressing key challenges, methodologies, and the potential for future research directions.

A significant challenge in applying LSTM models for UAV health prediction is the reliance on labelled data, specifically health indicators that classify the operational state of the UAV [73]. Most existing studies necessitate a substantial dataset of labelled failures to effectively train the model [74]. Acquiring such data implies either the high-cost procurement of numerous failed drones for analysis or the simulation of failures under controlled conditions, both of which are resource-intensive. This requirement for extensive labelled data poses a significant barrier to the scalability and practicality of LSTM applications in UAV health monitoring [73].

Moreover, there is a noticeable gap in the literature concerning the use of long-term real flight test sensor data for model training. Most studies rely on short-term data or simulated datasets, which may not fully capture the complexity and variability of real-world UAV operations [75], [76]. Long-term data are crucial for understanding the gradual degradation patterns and the influence of environmental factors on UAV performance, offering a more robust foundation for LSTM model training and validation [77].

2.6.2 LSTM's core components and functions

An LSTM unit comprises several key components: the cell state (C_t), the hidden state (h_t), and three gates—forget gate (f_t), input gate (i_t), and output gate (o_t). These elements work in harmony to regulate the information flow through the network, allowing it to learn from and remember important information while forgetting the irrelevant.

Forget Gate (f_t): Determines parts of the cell state to discard from previous steps.

$$f_t = \sigma\big(W_f \cdot [h_{t-1}, x_t] + b_f\big) \tag{2.8}$$

Input Gate (i_t): Decides which new information is stored in the cell state.

$$\begin{aligned} i_t &= \sigma(W_i \cdot [h_{t-1}, x_t] + b_i) \\ \tilde{C}_t &= \tanh\,(W_C \cdot [h_{t-1}, x_t] + b_C) \end{aligned} \tag{2.9}$$

Update to Cell State (C_t): Combines the old state and new input to update the current state.

$$C_t = f_t * C_{t-1} + i_t * \tilde{C}_t \tag{2.10}$$

Output Gate (o_t): Determines the next hidden state reflecting the cell's output for this step.

$$\begin{aligned} o_t &= \sigma(W_o \cdot [h_{t-1}, x_t] + b_o) \\ h_t &= o_t * \tanh\,(C_t) \end{aligned} \tag{2.11}$$

Consider the application of LSTM networks in analysing UAV sensor data, such as temperature, vibration, and acceleration, to predict potential system failures. The LSTM model can process this sequential data, learning to recognize patterns indicative of normal operation and those suggesting an impending failure. For example, a sudden increase in vibration or temperature could be learned as a precursor to mechanical issues.

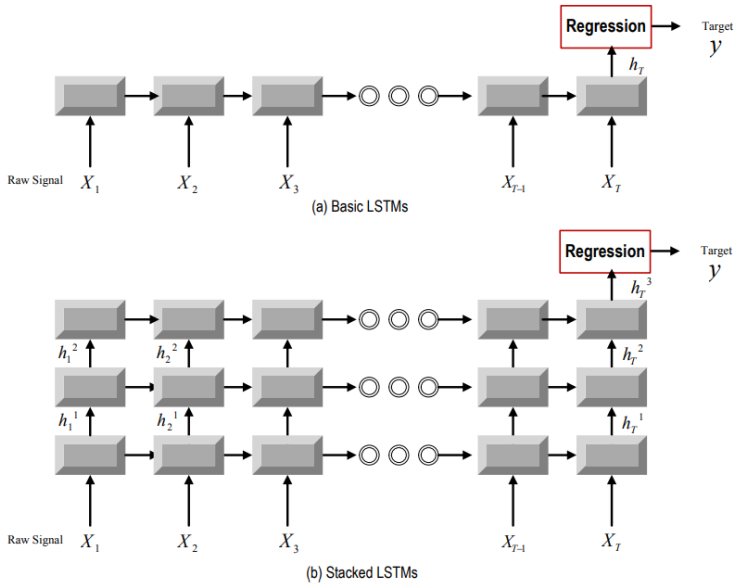

Figure 2.5: Illustrations for basic LSTMs and three-layers deep LSTMs model [78].

As shown in Figure 2.5, the paper investigates the application of a three-layered LSTM networks for machine health monitoring, presenting a pioneering empirical study. It leverages LSTM networks to predict tool wear from raw sensory data without requiring extensive feature

engineering or domain-specific knowledge. The study demonstrates LSTMs' superior ability to capture long-term dependencies and learn meaningful representations from sequential data, outperforming traditional models in tool wear prediction. This work underscores the potential of LSTMs in enhancing predictive maintenance strategies and advancing the field of machine health monitoring.

While LSTMs offer a powerful tool for degradation prediction, their effectiveness is contingent on the availability and quality of training data. The high cost of obtaining labelled datasets for UAV failures and the scarcity of long-term operational data pose significant challenges. Moreover, the complexity of UAV systems and the variability of operational environments can introduce additional complexities in model training and generalization.

2.6.3 Addressing Challenges with LSTM for UAV Health Monitoring

To overcome these hurdles, researchers are exploring innovative approaches, such as:

Data Augmentation: Generating synthetic data based on real-world patterns to enhance the diversity and volume of training datasets.

Transfer Learning: Applying knowledge gained from one domain to a related one, potentially leveraging models trained on similar sensor data from different contexts.

Semi-supervised Learning: Utilizing a mix of labelled and unlabelled data to improve model performance, especially when labelled data are scarce.

In the quest for reliable UAV health monitoring, LSTM networks represent a promising avenue for advancing degradation estimation. By harnessing their ability to analyse sequential sensor data, LSTMs can provide actionable insights into UAV health, supporting preventative maintenance and enhancing operational safety. However, addressing the challenges related to data availability and model adaptability remains crucial for realizing the full potential of LSTM networks in this domain.

Section 1.6 outlined the necessity of advanced modelling techniques. This research gap

highlights the need for extensive field studies that apply deep learning models to real-world UAV data, ensuring their robustness and reliability in predicting component degradation, which is essential for UAV certification in urban airspace. Chapter 6 addresses this by developing and validating LSTM-based models for predicting UAV performance degradation.

2.7 Artificial Neural Networks (ANN)

An Artificial Neural Network (ANN) is a computer model that draws inspiration from the neural networks found in the human brain. Comprising interconnected units or nodes, much like neurons, this system can analyse input and acquire knowledge of intricate patterns through training. In the field of reliability engineering, ANNs are employed to predict failures, evaluate system reliability, and enhance maintenance techniques by modelling the nonlinear relationships observed in operational data.

2.7.1 Components of ANN

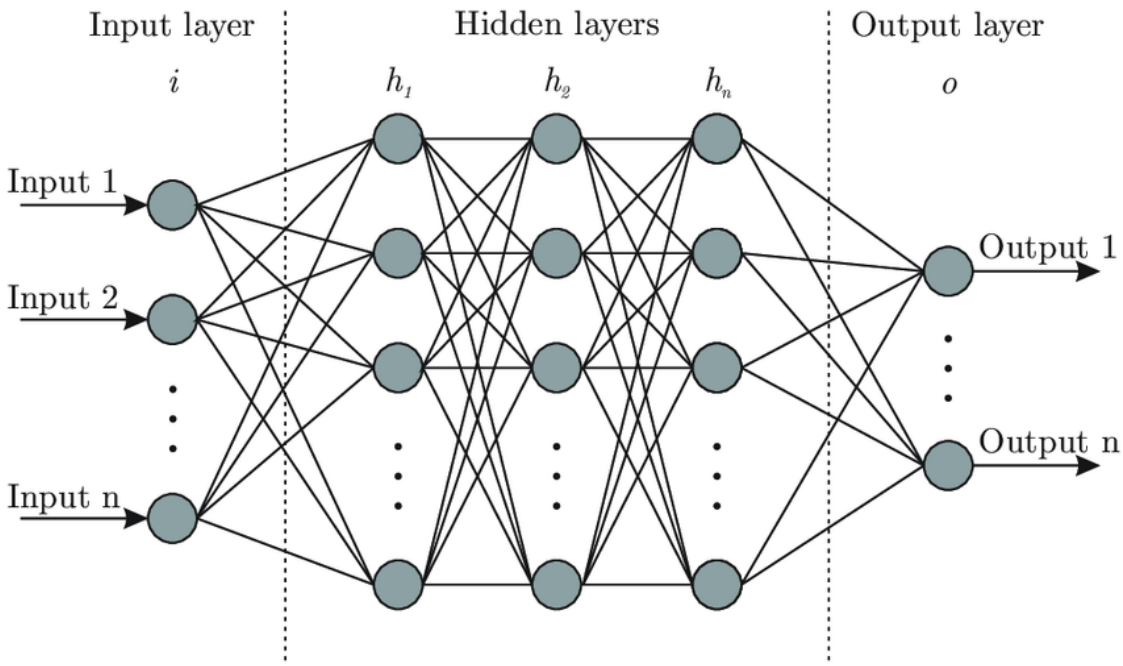

Figure 2.6: ANN Architecture [79]

This section explores the complexities of a typical Artificial Neural Network (ANN) and how its components work together to create an effective model. Figure 2.6 illustrates the

structure of a neural network, displaying a network of interconnected nodes divided into input, hidden, and output layers. The input layer acts as a gateway for data into the ANN. Each unit or neuron in this layer represents a distinct feature found in the dataset.. [80] In the field of reliability engineering, these characteristics could correspond to different sensor measurements that indicate the health of a system. The main purpose of this layer is to distribute the raw input to the neurons in the next layer without performing any computations.

The hidden layers are where the fundamental learning capabilities of ANNs lie. Situated between the input and output layers, these intermediate layers perform complex calculations on the received inputs. [80] Each neuron in these layers calculates a weighted sum of its inputs, incorporates a bias (an adjustable intercept), and then applies an activation function to the obtained outputs. The architecture can consist of multiple hidden layers, each potentially capturing different levels of abstraction from the input data.

Each neuron in these layers calculates a weighted sum of its inputs, incorporates a bias (an adjustable intercept), and then applies an activation function to the obtained outputs. The architecture can consist of multiple hidden layers, each potentially capturing different levels of abstraction from the input data.

The output layers represent the culmination of the network's computations and provide the final outcome.. [80] In regression applications, such as forecasting the time until failure in reliability engineering, the output layer may consist of a single neuron that produces a continuous value.

Activation functions play a crucial role in enabling the network to perform non-linear operations. Without these functions, the ANN would function as a linear regression model, lacking the ability to comprehend complex patterns. Typical activation functions include:

ReLU (Rectified Linear Unit): This popular activation function is commonly used in deep

neural networks. It is preferred for its simplicity and effectiveness in addressing the vanishing gradient problem. This problem occurs during training when the gradients used to update the network become extremely small as they are backpropagated from the output layers to the earlier layers.

Sigmoid function: This function produces an output ranging from 0 to 1, making it suitable for binary categorization applications.

Tanh function (Hyperbolic Tangent): Similar to the Sigmoid function, it produces output values between -1 and 1, providing a centred range that can be advantageous in certain situations.

The loss function, also known as the cost function, measures the difference between the model's predictions and the actual targets. It serves as a feedback mechanism, guiding the network to modify its weights and biases to reduce prediction errors.

Optimizers guide the network towards achieving the lowest possible loss by adjusting the weights and biases. This is done by considering the gradients of the loss function with respect to these parameters. The process used is called backpropagation. Optimizers such as Stochastic Gradient Descent, Adam (Adaptive Moment Estimation), and Root Mean Square Propagation differ in their approach to adjusting the learning rate during training, which affects the rate of convergence and the likelihood of reaching a global minimum.

Therefore, understanding the components of ANNs provides insight into their complex nature and adaptability, which explains their success in various fields, including reliability engineering. By adjusting these components, researchers and engineers can customize ANNs for specific purposes, such as classifying the condition of a system or forecasting the time until a part fails. This capability enables the development of predictive maintenance strategies and the improvement of system reliability.

2.7.2 Application of ANN in Reliability Engineering

In the field of reliability engineering, there are several factors such as stress, temperature, and material wear that interact with each other in complex and nonlinear ways. These interactions have a direct impact on the lifespan of components and their failure rates. Artificial neural networks (ANNs), with their layered structure and nonlinear activation functions, are highly effective in analysing historical data to uncover these patterns. By training on datasets that cover a wide range of operational conditions and outcomes, ANNs can accurately predict future failures or estimate the remaining useful life of components. A study conducted by Cheraghi et al utilized a combination of Monte Carlo simulation, ANNs, and the control variate technique to improve the efficiency and accuracy of reliability analyses in various engineering systems. [81]

For example, ANNs can be trained on sensor data obtained from machinery, enabling the network to identify subtle indicators that precede failure. The nonlinear activation functions of ANNs allow them to model the complex relationships between different sensor readings and the likelihood of failure, surpassing the capabilities of traditional linear models. [12, 16] This predictive capability of ANNs is valuable in maintenance planning, as it enables more precise scheduling and reduces downtime, ultimately extending the operational life of equipment. In this report, a similar approach is being used, where sensor data from a UAV is utilized as features to predict the likelihood of failure or the health index of the motor at a specific time period.

2.7.3 Markov Chain Monte Carlo (MCMC) Sampling

The No-U-Turn Sampler (NUTS) is a highly efficient technique called Markov Chain Monte Carlo (MCMC) that is used in Bayesian analysis to assess the reliability of UAVs. It improves upon the Hamiltonian Monte Carlo (HMC) method by automatically adapting simulation paths. This automation enhances the efficiency of sampling by minimizing the need

for manual adjustments and facilitates faster convergence to the regions of high probability in the posterior distribution. PyMC[84], a Python library, utilizes NUTS which uses the Metropolis-Hastings algorithm to accept new parameters. This approach optimizes the exploration of parameter space and reduces the tendency for random walks. NUTS is particularly well-suited for analysing complex models commonly encountered in UAV reliability studies.

The MCMC procedure is crucial for exploring the parameter space in UAV reliability analysis. It involves selecting initial values for the model parameters (θ). [85] The core of this procedure involves proposing new parameter values (θ') from a distribution that depends on its current parameters, ensuring a coherent exploration of the parameter space. The MCMC approach, particularly HMC, provides a sophisticated mechanism to achieve this goal. HMC, unlike typical MCMC approaches, uses Hamiltonian dynamics to propose new states, resulting in a more effective and systematic exploration of the parameter space instead of a random walk behaviour. [86]

Hamiltonian dynamics, which is crucial for HMC, uses a deterministic procedure to navigate the parameter space, resulting in a significant increase in sampling efficiency. The deterministic nature of this approach, influenced by physics, promotes substantial and consistent progression through the parameter landscape. This reduces the limitations of random walks and improves convergence towards the target posterior distribution. The fundamental principle of HMC relies on its acceptance criterion, which uses a method like the Metropolis-Hastings criterion to determine whether to accept new parameter sets (θ'). This criterion compares posterior probabilities to guide the sample towards regions with higher probability. The systematic method employed by HMC highlights its advantage in handling complex model predictions that are essential to UAV reliability analysis. It offers an effective structure that combines the exploratory capabilities of MCMC with the efficiency of Hamiltonian dynamics.

[86] Within the MCMC framework, the Metropolis-Hastings algorithm determines the acceptance probability of transition to a new state using the equation 2.12 below:

$$\alpha(\theta', \theta) = \min(1, \frac{P(data|\theta')P(\theta')q(\theta|\theta')}{P(data|\theta)P(\theta)q(\theta'|\theta)}) \quad (2.12)$$

In which, $\alpha(\theta', \theta)$ represents the likelihood of moving from the current state θ to a new proposed state θ', while $q(\theta'|\theta)$ is the proposal distribution that dictates the proposal of new sample values.

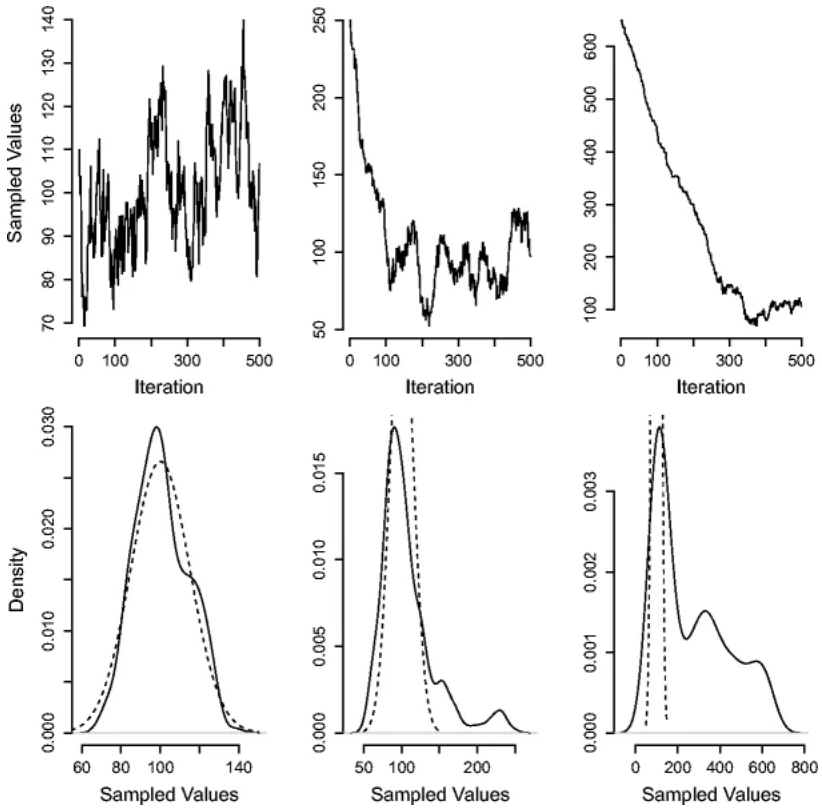

Figure 2.7: Example of MCMC sampling process [87]

Figure 2.7 depicts the MCMC sampling technique, which utilizes the Metropolis algorithm to generate samples from the posterior distribution of a population mean. This method involves using observed data and an initial estimate. In each iteration, a new sample is created by introducing random noise to the previous sample. The acceptance or rejection of this new sample is determined by the probability density of the posterior. The chain of samples explores the range of the distribution around the true mean of the data (100), with a provided standard

deviation of 15. The top row of trace plots shows the progression of sample values across iterations, starting from various initial estimates. The bottom row of density plots estimates the distribution of the sampled values, which corresponds to the actual underlying normal distribution (indicated by a dashed line). This process allows for the estimation of population parameters, such as the mean, by averaging the MCMC samples. [87]

The flexibility of MCMC is beneficial when integrated within a Bayesian framework, since it enables the sampling from posterior distributions that are difficult to compute. The flexibility of MCMC is advantageous when utilized within a Bayesian framework because it enables sampling from posterior distributions that are challenging to compute. The integration of MCMC and Bayesian inference is crucial for analysing reliability in UAVs.[88]

Although Artificial Neural Networks (ANNs) have shown significant promise in various fields, their application in UAV reliability engineering is still emerging. The current research lacks comprehensive studies that utilize ANNs to predict UAV component failures and enhance maintenance strategies based on real-time sensor data. Sections 1.3 and 1.6 emphasized the importance of advanced modelling techniques and the need for empirical data to support UAV certification. This gap necessitates the development of ANN-based models that can analyse complex, nonlinear relationships in operational data to predict failures and improve system reliability. Chapter 5 addresses this gap by applying ANN techniques to analyse the data from run-to-failure experiments and predict UAV maintenance needs.

2.8 Summary of the literature review

This chapter provides a comprehensive review of the existing literature, focusing on several critical aspects of the reliability and health monitoring of Unmanned Aerial Vehicles (UAVs). It begins by defining key terms and then delves into various studies conducted on UAV reliability, it then moves onto the exploration of statistical modelling approaches, covering

reliability event data analysis, Weibull modelling theory, and the application of Weibull distribution for reliability analysis, including an investigation into shape parameter properties. The chapter progresses to system-level reliability analysis. It then delves into Markov-chain based evaluation for multirotor drone reliability. It concludes with a focus on deep learning-based degradation modelling and prediction, emphasizing the application of LSTM networks for UAV health monitoring, detailing LSTM's core components, functions, and strategies for addressing challenges within UAV health monitoring frameworks.

The literature review highlights several important research gaps pertaining to UAV reliability and airworthiness assessment. These gaps encompass the need for empirical data to validate theoretical models, the development of integrated system-level analyses, and the utilization of advanced statistical and deep learning techniques specifically tailored to UAV operations. Sections 1.3 to 1.6, along with Figure 1.1, underscore the crucial role of these analyses in the certification process for UAVs in urban airspace. Addressing these gaps is critical for advancing the field of UAV reliability and facilitating the safe integration of UAVs into urban environments. The subsequent chapters of this thesis aim to address these gaps by employing detailed experimental designs (Chapter 5), advanced modelling techniques (Chapters 4 and 6), and comprehensive reliability assessments (Chapter 3). Thus, this review effectively covers the key elements as depicted in the research matrix of Figure 1.3.

Chapter 3 UAV propulsion system FMEA

As previously mentioned, the propulsion system is a critical component for the safe operation of a UAV. It is, however, susceptible to various types of failures that can compromise overall reliability and mission success. This chapter introduces the components of the UAV propulsion system in detail, followed by a thorough discussion of the failure evaluation metrics that serve as the foundation for reliability analysis.

Building on this foundation, a systematic Failure Mode and Effects Analysis (FMEA) is performed to identify and assess potential failure modes of UAV propulsion components. The analysis highlights critical failure mechanisms, their likelihood, and their impact on system performance. Additionally, the FMEA methodology is extended to other UAV components beyond the propulsion system, offering a comprehensive view of system-level reliability.

The structured steps of FMEA are presented in Figure 3.1., providing a clear roadmap for the analysis conducted in this chapter. This detailed examination not only underscores the vulnerabilities within the UAV system but also sets the stage for developing targeted mitigation strategies in subsequent chapters.

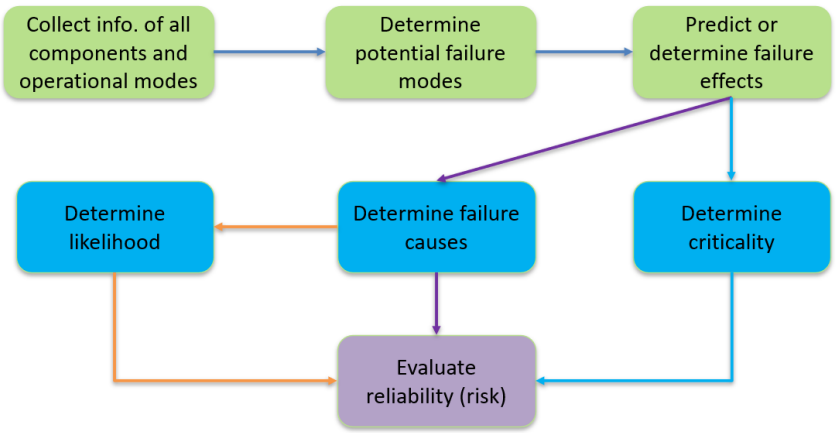

Figure 3.1: Flow chart to conduct FMEA for UAV components.

3.1 UAV propulsion system

The propulsion system is the core of the UAV power. There are three categories of the propulsion system:

Fuel propulsion: mainly consist of an engine, mechanical transmission, and propeller. This type of UAV is a high payload and can operate long-endurance extensive ranges.

Fuel-electric hybrid propulsion consists of an engine and electric motor. Compared with pure fuel propulsion, it can save fuel consumption.

Electric propulsion: consists of electric motors and control systems, mainly used in small and medium-sized UAVs. It is low pollution, cheap, and has high energy utilization.

In this project, the research is for electric UAVs. In detail, the electric propulsion system of UAVs consists of six components, as shown in Figure 3.2.

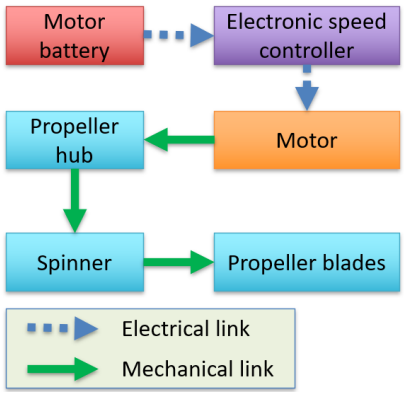

Figure 3.2: Components of electric UAV propulsion.

Component 1: motor battery, which provides power for UAV operations.

Component 2: electronic speed controller (ESC), send signals for motor rotation.

Component 3: motor, turn hub, spinner, and propeller to generate thrust.

Component 4: propeller hub: connect the motor driveshaft to the propeller blades.

Component 5: spinner, aerodynamic fairing for propeller hub.

Component 6: propeller blades, provide thrust.

3.2 UAV failure evaluation metrics

3.2.1 Rating scale of failure likelihood

In general, failure likelihood has three ratings based on the failure frequency, which is low, medium, and high. A detailed description of these three ratings is shown in Table 3.1.

Table 3.1: Rating scale of failure likelihood.

Rating	Description
High	Repeated failure
Medium	Occasional failure
Low	Unlikely failure

3.2.2 Criticality of failure modes

According to NASA, six categories of the criticality of failure modes are used in evaluating aircraft failure modes, and the specific descriptions are listed in Table 3.2.

Table 3.2: Criticality and description of UAV failure modes.

Category	Description
1 Catastrophic	Lead to vehicle and property damages, serious injury, or loss of life.
1R Catastrophic	Failed redundant components result in Category 1 effects.
2 Critical	Lead to the loss of one or more missions.
2R Critical	Failed redundant components result in Category 2 effects.
3 Significant	Lead to degradation of missions.
4 Minor	Lead to insignificant or no loss to missions.

3.2.3 Failure risk matrix

Combing three ratings of failure likelihood and six categories of the criticality of failure modes, the risk matrix of failure is shown in Table 3.3.

Table 3.3: Failure risk matrix.

Likelihood	Criticality					
	4	3	2R	2	1R	1
High	M	M	H	H	H	H
Medium	L	M	M	M	H	H
Low	L	L	M	M	M	M

3.3 FMEA of propulsion system

Based on the three failure evaluation metrics, failure likelihood, criticality, and failure risk describe in Section 3.2, the FMEA is performed in terms of the six UAV propulsion components mentioned in Section 3.1.

3.3.1 Motor battery

For the propulsion system, the motor battery provides UAV energy for operation. Therefore, it plays an important role in UAV safe flight. If the failure happens in the motor battery, the caused risk is evaluated as high. Details are shown in Table 3.4.

Table 3.4: FMEA of motor battery.

PC	FM	Cause	Likelihood	Effects	Criticality	Risk
1a	Internal	▪ Short circuit ▪ Overheating	M	▪ Thrust loss. ▪ Out of control	1R	H
1b	External	▪ Overcharging ▪ Over discharging ▪ Extreme temperature	M	▪ Thrust loss. ▪ Out of control	1R	H

Note: PC represents the UAV propulsion component; FM is the failure mode. The same for all the tables in this section.

3.3.2 Electronic speed controller

The electronic speed controller (ESC) is the electric UAV component to send signals for motor rotation. Its failure can cause circuit short or damage, damaged battery connection, which lead to at least medium risk for UAV operation. The detailed analysis is shown in Table 3.5.

Table 3.5: FMEA of ESC.

PC	FM	Cause	Likelihood	Effects	Criticality	Risk
2a	Wrong voltage output	Damaged/short circuit	M	▪ Wrong motor speed ▪ Out of control	3	M
2b	Power interruption	Damaged connection with batteries	H	▪ Thrust loss. ▪ Wrong motor speed ▪ Out of control	2	H
2c	Voltage output exceeds motor threshold	Damaged/short circuit	M	▪ Intermittent thrust loss ▪ Out of control	1	H
2d	Disconnection from motor battery	Damaged connection with batteries	H	▪ Total thrust loss ▪ Out of control	1	H

3.3.3 Motor

UAV motor failures include bearing failure, short circuit, and winding degradation. Bearing failure with a medium likelihood leads to high risk while winding degradation with a low likelihood result in a low risk. The medium risk may be due to the UAV motor short circuit. The details are shown in Table 3.6.

Table 3.6: FMEA of the motor component.

PC	FM	Cause	Likelihood	Effects	Criticality	Risk
3a	Bearing failure	Insufficient lubrication	M	▪ Motor spins difficult ▪ Thrust loss. ▪ Out of control	1	H
3b	Short circuit	▪ Propeller vibration ▪ Over-heating	L	▪ Motor stuck. ▪ Thrust loss. ▪ Out of control	1	M
3c	Winding degradation	▪ Propeller vibration ▪ Over-heating	L	▪ Wrong spin speed ▪ Out of control	3	L

3.3.4 Propeller hub

Disconnection from the motor driveshaft is the main failure mode of the propeller hub, which may cause mid-air collision and the bearing loose with a low likelihood and 1 criticality. So, the failure risk is medium (see Table 3.7).

Table 3.7: FMEA of propeller hub.

PC	FM	Cause	Likelihood	Effects	Criticality	Risk
4	Disconnection from motor driveshaft	▪ Midair collision ▪ Loose bearings	L	▪ Propeller loss ▪ Thrust loss. ▪ Out of control	1	M

3.3.5 Spinner

The spinner may damage or crack due to mid-air collision at a low likelihood, and it leads to low risk (see Table 3.8).

Table 3.8: FMEA of spinner.

PC	FM	Cause	Likelihood	Effects	Criticality	Risk
5	Damaged or cracking	Midair collision	L	▪ Maximum power reduction slightly	4	L

3.3.6 Propeller blades

Propeller blades may have a structural failure, crack, or blade loss from the propeller hub due to mid-air collision or vibration at a low likelihood leading to UAV thrust loss and out of control with a medium risk, as shown in Table 3.9.

Table 3.9: FMEA of propeller blades.

PC	FM	Cause	Likelihood	Effects	Criticality	Risk
6a	Structural failure/ cracking	Midair collision	L	▪ Maximum power reduction ▪ Total thrust loss ▪ Out of control	1	M
6b	Blade loss from propeller hub	Vibration	L	▪ Thrust loss. ▪ Out of control	1	M

3.4 FMEA of other UAV components

In addition to propulsion components, FMEA is also performed for other components, including airframe, power, and control and navigation.

3.4.1 Airframe

Airframe components mainly include a. cover; b. arm; c. landing gear. Structural failure mode due to midair collision or take-off/landing crash at a low likelihood. The failure risk is medium. The details are shown in Table 3.10.

Table 3.10: FMEA of airframe components.

OC	FM	Cause	Likelihood	Effects	Criticality	Risk
1a	Structural	Midair collision	L	▪ Altered aerodynamics. ▪ Vibration	1	M
1b	Structural	Midair collision	L	▪ Altered aerodynamics. ▪ Vibration	1	M
1c	Structural	Take-off/landing crash	L	▪ Crash during take-off. ▪ Fail to safely land	1	M

Note: OC represents other UAV components except for propulsion system components; FM is the failure mode. The same for all the tables in this section.

3.4.2 Power

UAV power components mainly include: (a) motor battery, (b) servo battery, and may have (c) camera battery for missions, like aerial photography or visual-based navigation. The failure modes for these three types of purpose-based batteries, the failure modes can be internal or external with a medium or low failure likelihood. As the battery provides power for UAV operations, any motor battery and servo battery failure can lead to high risks, while the camera battery with a low failure likelihood may bring about low risk.

Table 3.11: FMEA of airframe components.

OC	FM	Cause	Likelihood	Effects	Criticality	Risk
2a	Internal	▪ Short circuit ▪ Overheating	M	▪ Thrust loss	1R	H
	External	▪ Overcharging ▪ Over discharging ▪ Mechanical damage ▪ Extreme temperatures	M	▪ Thrust loss.	1R	H
2b	Internal	▪ Short circuit ▪ Overheating	M	▪ Power loss to servos ▪ Out of control	1	H
	External	▪ Overcharging ▪ Over discharging ▪ Mechanical damage ▪ Extreme temperatures	M	▪ Power loss to servos ▪ Out of control	1	H
2c	Internal	▪ Short circuit ▪ Overheating	L	▪ Mission loss if cameras are for aerial photography. ▪ Mission loss and out of control if the UAV is visual based	3	L

3.4.3 Control and navigation.

Generally, UAV control and navigation components include a. IMU (Inertial Measurement Unit); b. GPS; c. flight computer. The FMEA of control and navigation components is shown in Table 3.12.

For the IMU component, the main failure modes are circuit overload and de-calibration, which may lead to attitude or data loss at low and medium failure likelihood. The risk of IMU failure is rated as medium.

Table 3.12: FMEA of control and navigation components.

OC	FM	Cause	Likelihood	Effects	Criticality	Risk
3a	Circuit overload	▪ Power surge ▪ Electrostatic discharge	L	▪ Attitude/data loss	1	M
	De-calibration	▪ Load factory default parameters. ▪ Physical damage	M	▪ Wrong attitude, rate data, and flight data	2	M
3b	Circuit overload and failure	▪ Power surge ▪ Electrostatic discharge	M	▪ Navigation lost	1	H
	Disconnection from antenna	▪ Vibrations ▪ Damaged wiring	M	▪ Navigation lost	1	H
	Antenna fade	▪ Signal noise	M	▪ Navigation lost	1	H
3c	Disconnection from battery	▪ Vibrations ▪ Damaged wiring ▪ Software issue	M	▪ Loss of data and automatic control	1	H
	Disconnection from IMU	▪ Vibrations ▪ Damaged wiring ▪ Software issue	M	▪ IMU data loss ▪ Incorrect commands	1	H

The component of GPS is extremely important for UAV navigation. GPS failure will cause

navigation loss and lead to high risk because of circuit overload and failure, disconnection from the antenna, and antenna fade at a medium failure likelihood.

The flight computer like UAV's brain control and navigate all the UAV operations, so its failure will result in high risk. The common failure modes of flight computers include disconnection from battery or IMU at a medium failure likelihood.

3.5 Conclusion

This chapter has methodically applied Failure Modes and Effects Analysis (FMEA) to the motors, ESCs, and batteries—three essential parts of UAV propulsion systems. Through the identification of possible failure modes and the evaluation of their impact and likelihood, the analysis offers a strong foundation for comprehending the system's vulnerabilities. One of the most important failure mechanisms in UAV propulsion systems is motor failure, which is brought on by mechanical wear and overheating, and ESC failure, which is brought on by electrical anomalies like voltage surges.

Both the design of experimental tests and the development of comprehensive reliability models are informed by the FMEA described here. Through the run-to-failure experiments carried out in Chapter 5, these theoretical predictions will be reviewed and verified. Testing failures will be systematically examined to determine their underlying causes and contrasted with the failure modes anticipated in this chapter, guaranteeing consistency and scientific rigor in the application of theory to practice.

For the data-driven methods and reliability evaluations covered in later chapters, the FMEA provided in this chapter provides an essential basis by bridging the gap between theoretical analysis and empirical validation. The overall reliability framework is strengthened by this iterative feedback loop, which aids in the creation of reliable procedures for operational safety and UAV health monitoring.

Chapter 4 Markov-chain based controllability evaluation.

The Work presented in the Chapter was Published in ICUAS 2023 Conference under the title "A Reliability Framework for Safe Octorotor UAV Flight Operations" [89].

The ability of a UAV to maintain stability and control under varying operational conditions is paramount to its safe operation. This chapter introduces a novel framework for assessing UAV reliability through Markov-chain-based controllability evaluations. By modelling the transition probabilities between fully operational, degraded, and failure states, this methodology provides a quantitative means of evaluating the UAV's behaviour under different failure scenarios.

As illustrated in this chapter, the Markov-chain approach enables the assessment of multi-rotor configurations, focusing on their reliability and robustness to rotor and component failures. The results presented here emphasize how different configurations influence controllability and safety, offering key insights into design trade-offs for redundancy and reliability.

This framework not only enhances our understanding of UAV behaviour under stress but also contributes to designing more resilient systems. The findings from this chapter serve as a critical link between theoretical modelling and the experimental results discussed in Chapter 5, further informing reliability evaluation and UAV certification strategies.

4.1 Introduction of controllability assessment

Assessing controllability is vital for evaluating UAV reliability, emphasizing the propulsion subsystem's ability to maintain controlled flight, especially during a propulsion unit failure, as outlined in ASTM F3298-19. This focus ensures UAVs can safely navigate and recover from malfunctions, highlighting the importance of robust controllability measures in UAV design and operation standards [90]. This requires that a UAV retain its ability to manoeuvre based on

commands from the pilot or autonomous control systems in the event of single or multiple propulsion unit failures.

To achieve this, multi-rotor UAVs can be equipped with hardware redundancies, such as additional propulsion units, or analytical redundancies, such as fault diagnosis [91], [92], [93], [94] or active fault-tolerant control [95], [96], [97], [98]. If a UAV experiences a propulsion unit failure during a flight mission and must continue its flight, it should have its pitch, roll, altitude, and yaw channels remain controllable. Alternatively, if it chooses to land, the UAV should still have at least its pitch, roll, and altitude channels remaining controllable to manoeuvre away from high-risk airspace to recover.

Several controllability assessment approaches have been proposed for multi-rotor UAVs with different propulsion unit configurations [99], [100], [101], [102], including a reliability block diagram by Salazar et al. [103] and Markov chain-based approach by Aslansefat et al. [104]. To assess the reliability of the UAV's propulsion system, it is useful to integrate such controllability assessment approaches into a comprehensive framework.

4.2 Framework

Propulsion systems generate the thrust necessary for the UAV to change altitude and achieve rotation by varying the rotational speed of the units. However, when a propulsion unit fails, the remaining units may not provide enough thrust and torque for translational and rotational motions, potentially rendering the UAV uncontrollable. Also, even with redundancy, these remaining propulsion units do not guarantee controllability in all four crucial channels, which are altitude, pitch, roll and yaw. For instance, Quan et al [99] found a hexarotor to be uncontrollable in the yaw channel after a single propulsion unit failure. This can pose significant challenges for the UAV operator, especially when flying overpopulated areas or properties. Hence, evaluating the remaining thrust and torque available through controllability analysis is important to determine the reliability of the UAV's propulsion system.

Given that UAVs operate over an extended period and each propulsion unit has a distinct rate of failure, it is crucial also to understand the degradation of reliability over time. Hence, following a controllability analysis, a Markov-chain modelling will be useful to model the combinations of propulsion unit failures in which the multi-rotor UAV is controllable in the four critical channels. Then, the reliability can be evaluated over a timespan.

A framework to assess the reliability based on controllability analysis and Markov chain modelling is presented in Figure 4.1. First, the multi-rotor UAV configuration is selected, and its parameters are collected. These parameters are necessary for the controllability analysis in the following step, which is based on the controllability assessment introduced in [100], [101]. The UAV is initially subjected to various combinations of complete propulsion unit failure, ranging from one to six. For each of these combinations, the controllability assessment is performed, generating an available control authority index (ACAI), which helps determine whether a particular combination of fault-free propulsion units is controllable.

If the UAV becomes uncontrollable with just one propulsion unit failure, the analysis is rejected. This is because such a UAV is deemed unsafe to fly in a high-risk environment. On the other hand, if it remains controllable with one propulsion unit failure, a Markov chain is then generated with all the controllable combinations, as Markov states. Finally, the probability of the UAV being in state is evaluated, and subsequently, the UAV's reliability is determined over a time span of 50 hours.

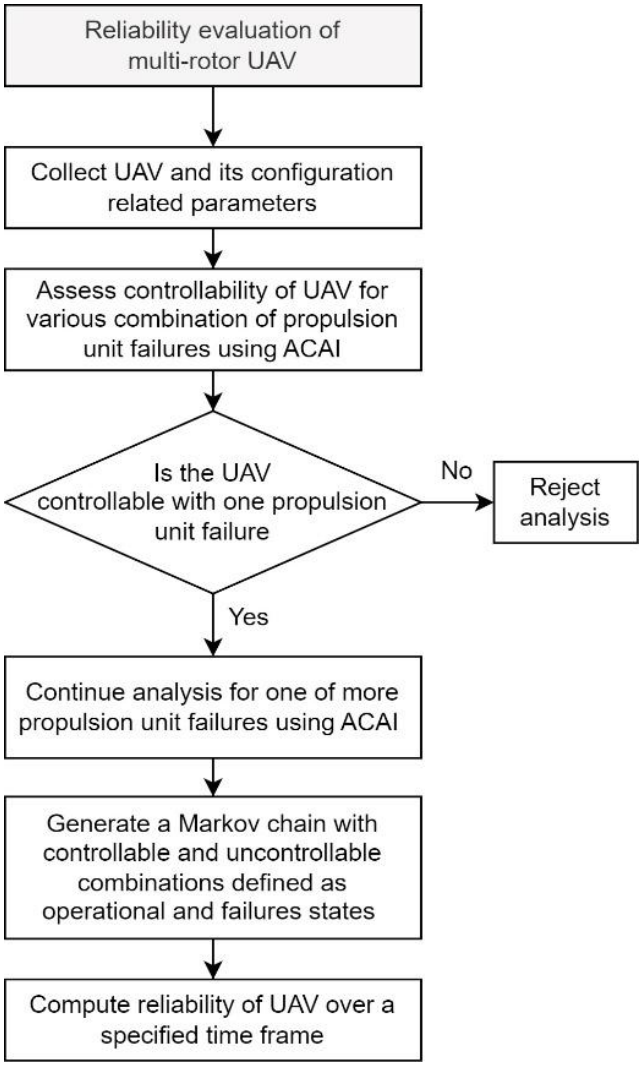

Figure 4.1: Framework of reliability evaluation for multi-rotor UAV.

4.3 Reliability estimation of octorotor UAV

In this section, an octorotor UAV is used an example, and its corresponding reliability is evaluated using controllability analysis and Markov chain modelling.

4.3.1 Controllability analysis

The objective of this analysis is to evaluate the controllability of a multi-rotor UAV in the event of a single propulsion unit failure. To determine the remaining thrust and torque, a controllability metric is used as a metric to generate an attainable control set, as introduced in Du et al.[101] and discussed in Liscouët et al. [105].

The available control authority index (ACAI) is a metric that evaluates the positive controllability of the UAV's propulsion system. Unlike classical Kalman-based controllability analysis, which involves a rank test, ACAI accounts for propulsion unit failure. The ACAI is computed based on a linearized dynamic model of a hovering UAV, where the four essential channels for control are altitude, roll, pitch, and yaw. The largest enclosed sphere in four dimensions is defined as $\partial\Omega$ is obtained by computing the control constraint set Ω. The ACAI, ρ, is computed as follows [101]:

$$\rho(g, \partial\Omega) \triangleq \begin{cases} \min\|g - x\|, & g \in \Omega, x \in \partial\Omega \\ -\min\|g - x\|, & g \in \Omega^C, x \in \partial\Omega \end{cases} \tag{4.1}$$

In this equation, Ω represents the control set in which UAV is controllable with boundaries defined by $\partial\Omega$, while Ω^C is the complementary set of Ω, in which the UAV is no longer controllable. ρ measures the distance from g to $\partial\Omega$. The higher the value of ρ, the greater the available control. A system is considered controllable if and only if $\rho > 0$. This analysis assumes that the UAV has a symmetrical structure, with its center of gravity fixed at the center of the structure. A step-by-step guide to the ACAI calculation process is presented in [101].

Next, the number of combinations for failed propulsion units is calculated for N_P propulsion units. A combination is deemed controllable only if $\rho > 0$. Otherwise, it is considered uncontrollable.

4.3.2 Markov chain modelling

Markov Modelling is a mathematical technique commonly used for evaluating the reliability of complex systems over time. This method is particularly useful for modelling systems with dependent failure and considers the operational and failure states of the systems, as well as the transitions between these states.

The following assumptions are considered before generating a Markov model:

(1) At the beginning, the system is always operational;

(2) There is no common cause of failure in the system;

(3) During the mission, the repair is not possible;

(4) The failure rates of a propulsion unit are constant and obey an exponential distribution;

(5) Any propulsion unit is either in an operational or failure state.

In this convention, each state has no self-transition [106], and the resulting continuous time Markov state transition equations can be expressed as follows:

$$\frac{d}{dt}\boldsymbol{P}(t) = \boldsymbol{M} \cdot \boldsymbol{P}(t), \qquad \text{where } \boldsymbol{M} = \begin{bmatrix} -\lambda & 0 \\ \lambda & 0 \end{bmatrix} \tag{4.2}$$

In this equation, $\boldsymbol{P}(t)$ represents the vector of probabilities that the system is in a particular state at a specific time. This concept can be extended octorotor UAVs using Markov chain modelling. The resulting state transition diagram involves a fully operational state, several post-fault states where the UAV is still controllable, and a failure state. Assuming that the failure rate of each propulsion unit is the same, a simplified state transition diagram is presented in Figure 4.3. As observed, the octorotor UAV remains controllable in all channels, even with a complete failure of two rotors. However, beyond the failure of two rotors, there is a probability that the UAV will become uncontrollable, reaching the failure state, F.

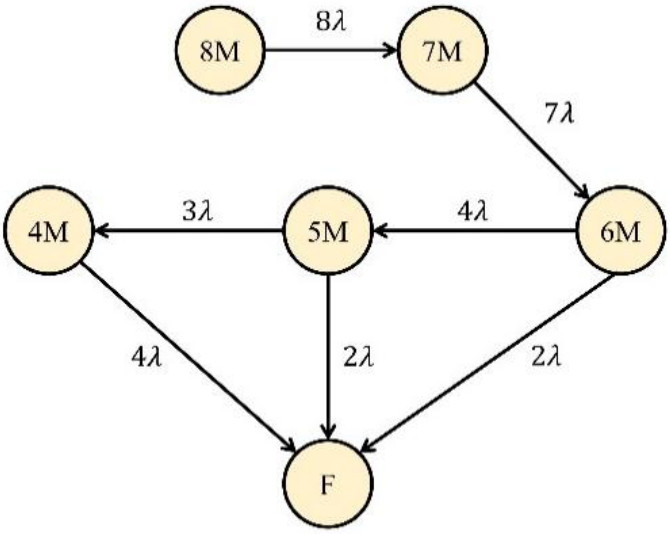

Figure 4.2: Simplified continuous-time Markov state transition diagram of a component.

A set of state transition equations can be generated to describe the transitions among the

Markov states. Then, by solving the system of state transition equations, the probabilities of each state can be determined over time. The sum of the probabilities across all states for a timestep would be 1. Summing up all the probabilities over all controllable states, without including the final failure state, would provide the reliability curve of the UAV over the timespan.

It is also assumed that the UAV's propulsion system has not undergone any repair or maintenance during the timespan during which the reliability is being evaluated.

4.3.3 Octorotor configurations

For this study, three octorotor configurations are analysed. Figure 4.4 (a) and (b) illustrate two octorotors in the 'X' configuration with rotor spin direction alternating every one rotor (PNPNPNPN) and every two rotors (PPNNPPNN), respectively. Here, 'P' means positive, and 'N' means negative, corresponding to clockwise and counterclockwise spin direction. Illustrations in Figure 4.4 (a) and (b) show 'X' configuration octorotors with rotor spin direction alternating every one rotor and two rotors, respectively. As such they are referred to as Octo-1 and Octo-2. The illustration in Figure 4.4 (c) shows an octorotor with 'H' configuration with rotor spin direction alternating every one rotor, and as such will be referred to as Octo-H. It should be noted that r refers to the distance of the rotor from the center of gravity and $r = \sqrt{2}r_d$ in Figure 4.4 (c).

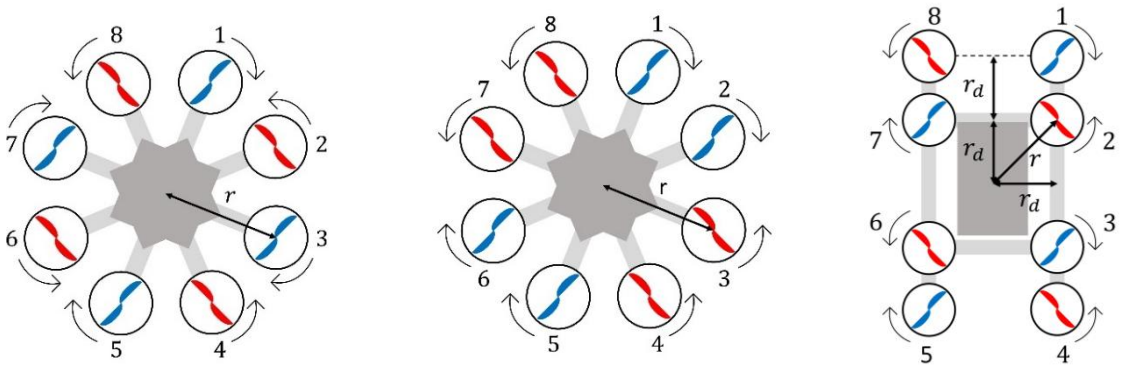

Octo-1 Octo-2 Octo-H

(a) (b) (c)

Figure 4.3: Illustration of different types of octorotor configurations.

For comparative analysis, a quadrotor and a hexarotor in 'X' configuration with rotor spin direction alternating every two rotors (PPNNPN) is also included. Table 4.1 presents the multi-rotor UAVs used in this reliability analysis. The hexarotor with the PNPNPN configuration is included because its yaw channel becomes uncontrolled after one propulsion unit failure, including the hexarotor with 'H' configuration [99], [101].

No. of propulsion units	Config.	Rotor spin arrangement	Name
Eight	X	PNPNPNPN	Octo-1
	X	PPNNPPNN	Octo-2
	H	PNPNPNPN	Octo-H
Six	X	PPNNPN	Hexa-2
Four	X	PNPN	Quad

Table 4.1: Configurations of multi-rotor UAVs considered for this study.

4.4 Results and Analysis

In this section, the reliability of three octorotor UAV configurations are compared with that of hexarotor and quadrotor UAVs. The UAV parameters used in [101] is also used for ACAI calculation in this thesis. The controllable states are determined following the computation of ACAI and a Markov chain with transition links between the controllable states is established.

Assuming a 0.05 failure rate of the propulsion unit, reliability curves are generated for the quadrotor, Hexa-2 configuration, and the three configurations of octorotor UAVs.

Figure 4.5 presents the reliability curves for all five multi-rotor UAVs considered, where the reliability value starts at 1 and degrades over time. The reliability curves of Quad and Hexa-2 show that they are less reliable than the octorotor UAVs, described by their steeper descent. Among the octorotors, the Octo-1 exhibits marginally greater reliability, and another observation is that Octo-2 initially has lower reliability than Octo-H but surpasses it after a certain time span.

Further investigation was conducted to determine the reliability of the hexarotor and three octorotor UAVs relative to the quadrotor across the timespan, as presented in Figure 4.6. Here, the difference in the reliability of the multi-rotor UAV and the quadrotor is plotted across the time span of 50 hours. It can be observed that between 5 to 6 hours, the difference in the reliability is at the greatest, after which, the differences start to subside.

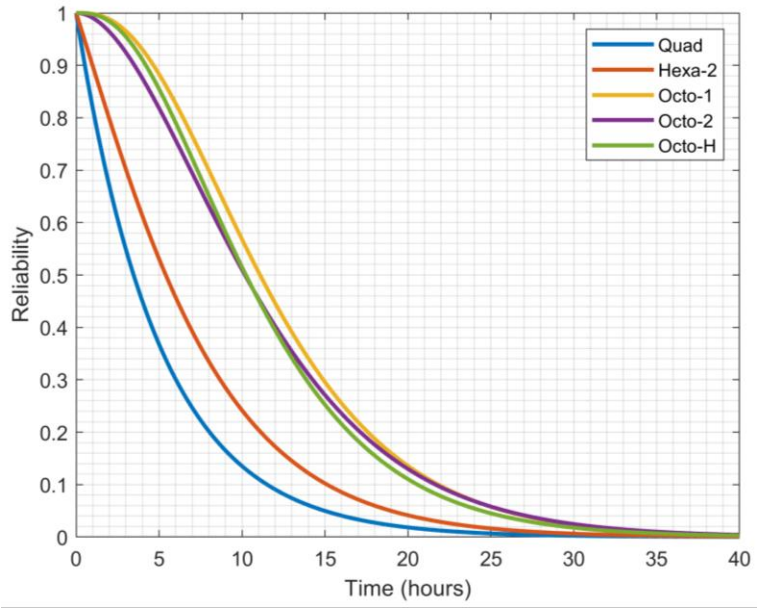

Figure 4.4: Reliability curves of the multi-rotor UAVs over a time span of 50 hours with propulsion unit failure rate 0.05 failures/hour.

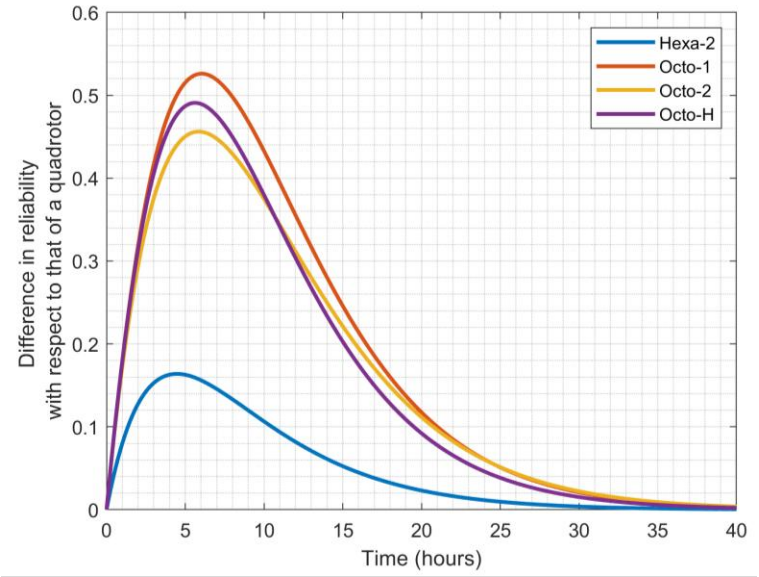

Figure 4.5: Difference in reliability levels multi-rotor UAVs relative to quadrotor, 50 hours.

Furthermore, two methods are used to evaluate the reliability of the multi-rotors. One is mean time to failure (MTTF) curves, which are generated by computing the area under the curve across the timespan for various failure rates. Another is studying the characteristics of the inflection point in Figure 4.6.

Figure 4.7: presents the plot of the MTTF curves for various failure rates of the propulsion unit that ranges from 0.01 to 0.1 failures per hour. As observed, the overall reliability of the multi-rotors decreases gradually. Octo-2's curve initially starts below the other octorotors but eventually goes above Octo-H, similar to the pattern observed in Figure 4.5.

Figure 4.6 shows the inflection point, which represents the point at which the advantages of using a multi-rotor other than a quadrotor become less significant. After this point, the rate of reliability degradation for the multi-rotor UAVs becomes higher than that of the quadrotor. The time at which this inflection point occurs for each multi-rotor is recorded for various failure rates and presented in Figure 4.8. Here, Hexa-2 reaches its inflection point earlier than the octorotors. The octorotors' times of inflection are close, which suggests that there is little benefit in scheduling maintenance or repair earlier for one octorotor over the others.

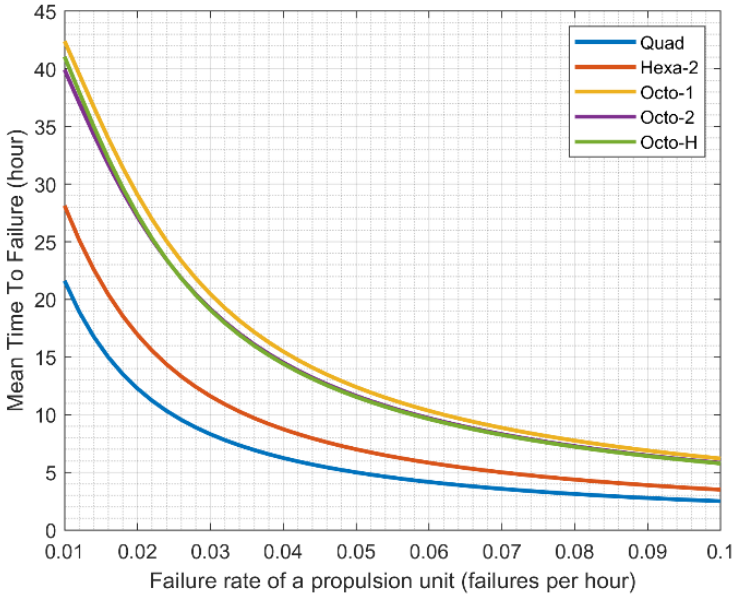

Figure 4.6: MTTF curves for multi-rotor UAV for various failure rates of a propulsion unit.

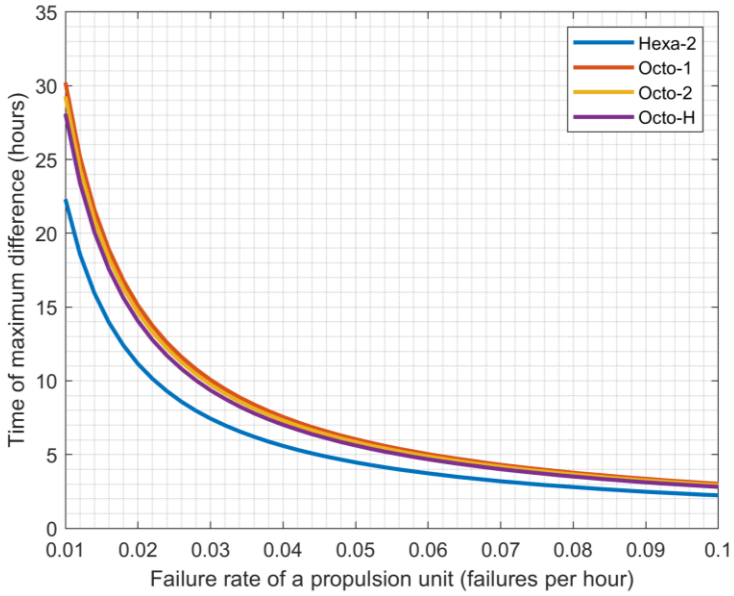

Figure 4.7: Time variations of inflection point for multi-rotor UAVs relative to quadrotor propulsion unit failure rates ranging from 0.01 to 0.1 failures/hour.

Table 4.2 displays the percentage difference in reliability at the inflection point, which is calculated as the average difference in reliability values over a range of failure rates from 0.01 to 0.1 failures per hour. Hexa-2 shows a 40% increase in reliability compared to the quadrotor at this point. However, the octorotors exhibit more than twice the reliability value of the quadrotor. Specifically, the percentage difference in reliability at this peak difference is 176%, 147%, and 151% for octorotors Octo-1, Octo-2, and Octo-H, respectively.

Multi-rotor	Difference (%)
Hexa-2	40.0
Octo-1	176.1
Octo-2	147.1
Octo-H	151.1

Table 4.2: Percentage difference in multi-rotor's reliability relative to quadrotor at inflection point

4.5 Payload analysis

Multirotor UAVs may be required to carry payloads in particular missions. Evaluating their dependability while carrying various payloads might give authorities with insights during flight authorization. The dependability curves for the three octorotor UAV types are estimated in this section, with payload amounts ranging from 0.5 to 1.5 kg. The maximum payload amount is roughly similar to the mass of the UAVs. Figure 4.9 illustrates the reliability curves for the three octorotor configurations for the three stated payloads, whereas the Quadrotor reliability curve depicts one that does not have a payload.

Figure 4.9 (a) shows how the reliability of Octo-2 and Octo-H is much higher than that of Octo-1 when considering a payload of 0.5 kg. It also shows the reliability of Octo-2 and Octo-H are almost similar. The lower reliability curve of Octo-1 is probably due to the 44.3% drop in controllable states when comparing the "no payload" and "0.5 kg payload" circumstances. This is in contrast to the 24.7% and 18.2% drop experienced by Octo-2 and OctoH, respectively. The similar reliability curves of Octo-2 and Octo-H can be attributed to their almost equivalent number of controllable states.

When increasing the payload to 1.0 kg, Octo-H is shown to have greater reliability, whereas Octo-1 and Octo-2 have similar reliability, as seen in Figure 4.9 (b), again attributed to having the same number of controllable states. Finally, when increasing the payload value to 1.5 kg, all the reliability curves are very similar. Zooming in, one can see that Octo-1 has a marginally greater reliability than the other two, as presented in Figure 4.9 (c).

Furthermore, after 6 hours, the octorotor UAVs' reliability curves fall below the quadrotor's

curve. This also implies that the propulsion system of octorotors that are always carrying a payload, such as an extra subsystem or cargo, may require more frequent maintenance than when no payload is present. The volume of cargo will also play an essential role in the authorization or certification procedure from a regulatory standpoint.

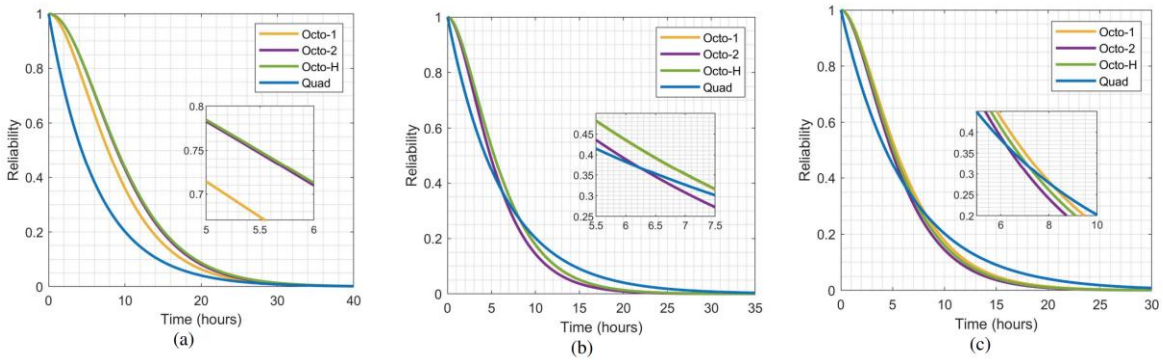

Figure 4.8 Reliability curves of the three octorotor configurations with payload values of (a) 0.5 kg, (b) 1.0 kg and (c) 1.5 kg, over a time span of 50 hours. The failure rate of a propulsion unit is taken to be 0.05 failures per hour.

4.6 Conclusion

This chapter concludes by noting the variability in reliability among different multi-rotor UAV configurations, highlighting that UAVs designed with higher redundancy levels exhibit enhanced reliability. The results from the controllability evaluation and Markov-chain modelling provide significant insights into the reliability and safety of multi-rotor UAVs under various failure conditions.

The controllability analysis showed that depending on the configuration, the UAV's capacity to sustain flight control in the event of a propulsion unit failure varies considerably. The controllability of the UAV was evaluated using the available control authority index (ACAI), which showed that configurations with symmetrical rotor arrangements were more resilient to single rotor failures. The significance of building UAVs with resilient configurations that can keep control even in the event of critical component failure is highlighted by this analysis.

For the UAV configurations, Markov-chain models were developed to give a

comprehensive view of the system's reliability over time. The state transition diagrams showed that the reliability of most configurations dropped sharply with multiple rotor failures, but most configurations could withstand single rotor failures. The UAV's transition from fully operational states to different degraded states was precisely predicted by the continuous-time Markov models, providing important insights into the probabilistic nature of UAV failures.

It was clear from comparing various UAV configurations that some offered better controllability and reliability than others, such as the Octo-H configuration. These configurations demonstrated their suitability for high-risk environments over extended periods of time by maintaining higher ACAI values and lower failure probabilities. Based on particular operational requirements, a clear framework for choosing and designing UAVs is provided by this comparative analysis.

The payload analysis assessed how various payload weights affected the controllability and dependability of UAVs. It was found that heavier payloads typically resulted in less control authority being available, increasing the likelihood of UAV malfunctions. Nonetheless, some configurations, like the Octo-H, performed better with larger payloads because of their sturdy build and efficient lift distribution. Planning a mission requires careful consideration of this analysis to make sure that UAVs are not overloaded beyond manageable limits.

From a regulatory perspective, the evaluation of reliability, interestingly, does not necessitate flight data but rather relies on UAV parameters for reliability estimation. The framework discussed offers a valuable tool for pre-flight airworthiness assessments, enabling the determination of UAV flight readiness. This method provides a foundational basis for flight approval, ensuring UAVs meet critical safety standards before operation, aligning with regulatory expectations and enhancing overall flight safety.

This chapter fills in a number of significant gaps in current approaches by introducing a novel application of Markov-chain modelling to UAV reliability and airworthiness assessment.

The dynamic and probabilistic character of UAV failures is frequently ignored by conventional fault-tree or theoretical reliability models, particularly when operating in a variety of conditions. This method offers a more detailed understanding of failure propagation and controllability across various UAV configurations by integrating state transition diagrams and continuous-time Markov models. Additionally, the analysis incorporates factors that have a significant impact on operational reliability but are rarely taken into account in traditional studies, such as payload weight and rotor symmetry. A useful innovation of the methodology is its capacity to assess UAV reliability without requiring a large amount of flight data, allowing for pre-flight evaluations that comply with legal requirements. These contributions provide practical insights for developing and certifying UAVs for safe operations in challenging environments, bridging the gap between theoretical frameworks and practical applications.

As mentioned in chapter 1 that, the individual motor's failure rate assumption could be updated based on the component's reliability testbed modelling results in Chapter 5.

Chapter 5 Experimental design

This Chapter is currently submitted for Review to be published in the Journal for Reliability Engineering and System Safety under the title "Comprehensive Reliability Analysis and Degradation Modelling of Electric UAV Propulsion Systems: An Integrated Qualitative and Quantitative Approach" [107]

The propulsion system's vulnerability to failures demands rigorous experimental evaluation to ensure UAV reliability. This chapter details the design and implementation of a testbed tailored to analyse UAV components' reliability under controlled conditions. The testbed focuses on capturing time-to-failure data for critical components such as motors, Electronic Speed Controllers (ESCs), and batteries, providing empirical insights into their failure mechanisms.

To address the complexities of UAV reliability analysis, this chapter outlines the testbed's experimental objectives, setup, and methodologies. The experimental framework encompasses continuous testing to simulate real-world operational conditions, enabling the collection of high-fidelity data for model development and validation.

By bridging the gap between theoretical reliability analysis and practical data collection, this testbed plays a pivotal role in refining the statistical and machine learning models discussed in later chapters. The results obtained not only validate the methodologies proposed earlier in the thesis but also provide actionable insights for designing more reliable UAV systems.

5.1 Experimental objective

Given the limited data on multi-rotor propulsion systems, the objective of this experiment is to test the reliability of the components within the propulsion system. Using NATO paper [108] and EASA paper [109] as references, this chapter aims to design and implement run-to-failure experiments for UAV propulsion systems. These experiments will include stress tests

using cyclical loading to identify potential motor degradation phenomena or functional failures. Various configurations will also be tested to estimate the performance of different motor types and identify trends in motor degradation. The goal is to generate empirical data essential for validating the reliability models developed in previous chapters. By linking the experimental design to the theoretical frameworks and analyses discussed earlier, this section ensures a cohesive and comprehensive approach to UAV reliability assessment.

Chapter 3 provided a detailed Failure Modes and Effects Analysis (FMEA) of the UAV propulsion system's components. The critical failure modes identified in Chapter 3 guide the selection of components and conditions for the run-to-failure experiments. This ensures that the experiments target the most vulnerable points in the propulsion system, as highlighted by the FMEA, to effectively simulate real-world failure scenarios.

To further replicate long-term wear and tear observed in real-world UAV operations, the experimental setup integrates controlled stress factors such as cyclical thermal and mechanical loading. These parameters simulate degradation patterns typically seen in motors, ESCs, and batteries under diverse operational conditions. Advanced statistical models, including Weibull and Bayesian frameworks, are employed alongside real-time monitoring to capture high-resolution data. This methodology ensures that the results accurately represent the degradation trends encountered during real-world missions, bridging the gap between theoretical reliability frameworks and practical applications. The ability of the testbed to predict degradation and failure scenarios with high fidelity highlights its utility for both research and operational planning.

The obtained degradation data can then be integrated into Weibull models and Markov Controllability models (Chapter 4) to derive a reliability estimate. This estimate can be used for drone licensing in the licensing phase and assist in maintenance cycle planning during pre-flight and post-flight periods. By observing how actual failures impact UAV control and

stability, the experiments provide critical feedback for refining the theoretical models discussed in Chapter 4. This feedback loop enhances the accuracy and reliability of UAV controllability assessments.

This process links back to Figure 1.1, which illustrates the phases of UAV operations, highlighting the importance of pre-licensing, planning, operational, and post-flight phases. The experimental objectives in Chapter 5 align with these phases by providing empirical data that inform each stage of UAV operation. For instance, the pre-licensing phase benefits from validated reliability models, while the planning and operational phases use this data to ensure safe and efficient UAV missions. The post-flight phase leverages the findings to improve maintenance protocols and predict future failures.

By linking the experimental objectives to the foundational analyses and models from Chapters 3 and 4, as well as the overarching research roadmap in Section 1.3, this chapter ensures a comprehensive and integrated approach to UAV reliability assessment. The empirical data generated through these experiments not only validate the theoretical models but also provide practical insights for improving UAV design, operation, and maintenance.

5.2 Experimental setup

Figure 5.1 illustrates the overall design of the experiment, which aims to identify faults in the three major components of the propulsion system: the motors, the Electronic Speed Controllers (ESCs), and the batteries.

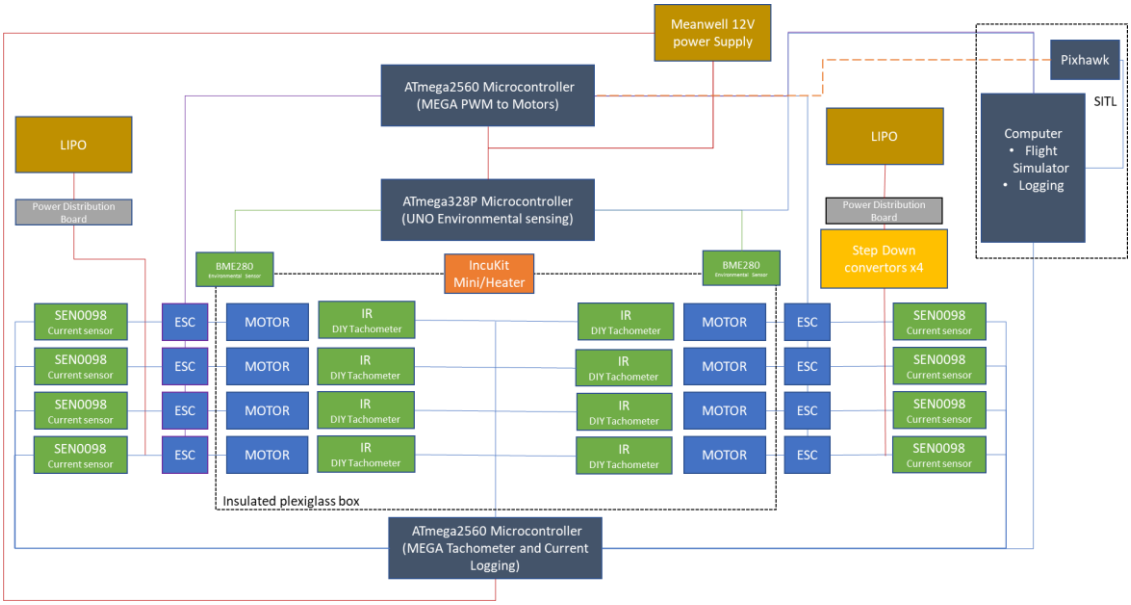

Figure 5.1: Overall Experimental Block Diagram

The experiment focuses on examining three major factors:

- Motor Degradation: Assessing wear and performance deterioration over time.
- ESC Power Draw: Monitoring the power consumption of the ESCs under various conditions.
- Battery Life Cycle: Evaluating the longevity and performance of the batteries through multiple charge and discharge cycles.

Figure 5.2 provides a summarized view of the inputs, outputs, and assumptions for the experiment.

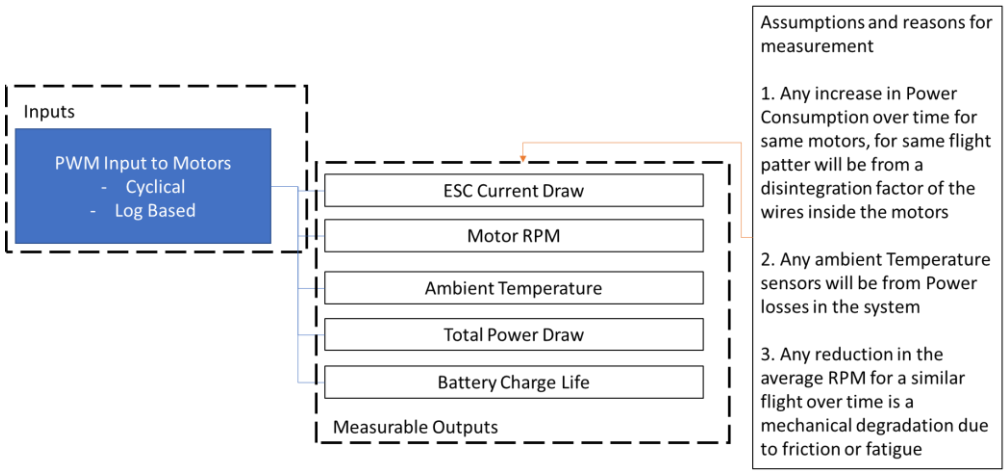

Figure 5.2: Summarized inputs, measurable outputs, and assumptions.

5.3 Motor degradation

To facilitate a broader range of motor reliability data, a combination of Brushless DC (BLDC) motors will be selected to represent different classes of drones. While this approach generalizes the results, it is more efficient given the extensive variety of motor manufacturers and models, which makes exhaustive testing impractical.

To ensure the testbed provides a comparatively comprehensive data set for failure rates, UAVs were first classified according to the criteria presented in Table 5.1. The classification is based on the three most common categories, which consider size, weight, and flight times.

FPV/Racing (≤1kg)	**Hobby/Industrial inspection (≤7kg)**	**Logistical/Farming**
		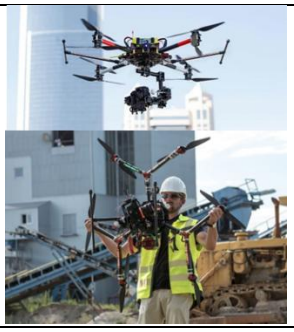
Small, compact, used for photo/video and racing	Medium sized. Used for hobby photography and industrial inspection	Large and Extra-large sized. Used for long flights, heavy loads, farming etc
10-20 min flight times	20-30 min flight times	>30 min (up to a few hours)
10xx-22xx motors	22xx-40xx motors	38xx-48xx motors

Table 5.1: Drone classification

5.3.1 Cyclical loading

The cyclical loading component of the experimental procedure was developed using guidelines from the NATO White Paper.

This document specifies that for any aircraft under 150 kg utilizing electrical motors, reliability testing should adhere to the protocol outlined in Annex D UL.EE.22.c of the white paper [60]. According to this protocol, the motors must undergo cyclic loading for 50 major cycles to assess motor endurance. Each major cycle is divided into four sub-cycles: three 90-

minute cycles at different temperatures (cold, ambient, and hot) and one longer 105-minute cycle at ambient temperature.

These cyclical loading protocols was tailored to mimic real-world conditions by incorporating variable temperature settings and representative power cycles. This approach ensures that the failure modes observed in the testbed align closely with those experienced during actual UAV operations.

However, for most multi-rotor copters, the specified test cycle durations of 90 minutes or 105 minutes per cycle are not practical. Most modern multi-rotor flights typically last between 20 to 40 minutes [61] , varying based on several factors. Additionally, considering the climate of Singapore, where the weather is consistently tropical with an average annual temperature of 26–27.5°C and a high likelihood of precipitation [62] , the cold temperature sub-cycle can be omitted. To better align with the actual usage conditions of multi-rotor copters in a tropical environment, a modified testing protocol is proposed, as shown in Table 5.2.

Sequence	Environmental Temperature	Duration [min]	Power setting
1.1	Ambient	2	Maximum continuous power
1.2	Ambient	8	Nominal power
1.3	Ambient	2	Maximum continuous power
1.4	Ambient	8	Nominal power
TOTAL CYCLE 1 DURATION: 20 [minutes]			
2.1	Hot	2	Maximum continuous power
2.2	Hot	8	Nominal power
2.3	Hot	2	Maximum continuous power
2.4	Hot	8	Nominal power
TOTAL CYCLE 2 DURATION: 20 [minutes]			
3.1	Ambient	2	Maximum continuous power
3.2	Ambient	18	Nominal power
TOTAL CYCLE 3 DURATION: 20 [minutes]			
TOTAL SEQUENCE DURATION (1 to 3): 60 [min] Iterate the previous 3-cycle sequence up to 50 times or a failure, whichever occurs first.			
Ambient temperature setting = 26°C Hot temperature setting = maximum temperature according to the design usage spectrum as per UL.0			

Table 5.2: Modified experimental design of cyclical loading.

5.4 Measuring motor degradation

To measure motor degradation, two primary methods will be employed: speed-based assessment and electrical power-based assessment.

5.4.1 Speed-based assessment.

Most of the degradation from running a motor continuously is expected to result from friction and heat generation. Consequently, it can be assumed that for any given RPM input, the speed output will decrease over time. This implies that tachometers can be used to measure the RPM for a given PWM signal when the motors are new, compared to their performance after extended use. Significant degradation in motor performance should become evident as a lower output RPM over time for similar inputs. The observed degradation can then be used to build a predictive model.

To measure this degradation, IR sensors will be employed as tachometers to track the RPM outputs of the motors. These RPM outputs can be compared over time; if degradation occurs, the output RPM should decrease for the same PWM inputs as time progresses. The rough circuit for measuring the speed of the motors is shown in Figure 5.3.

To measure motor degradation comprehensively, two major methods will be used: a detailed speed-based assessment and an electrical power-based evaluation.

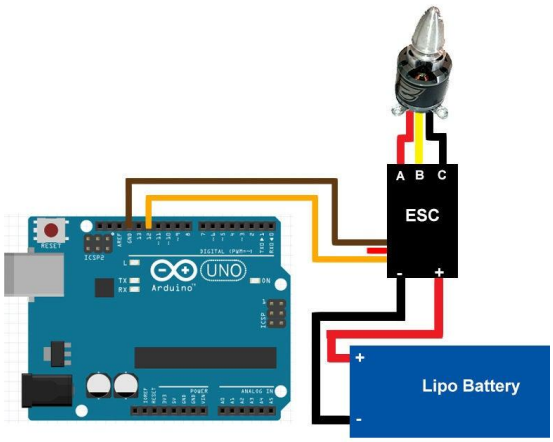

Figure 5.3: Motor connected to Arduino for PWM output.

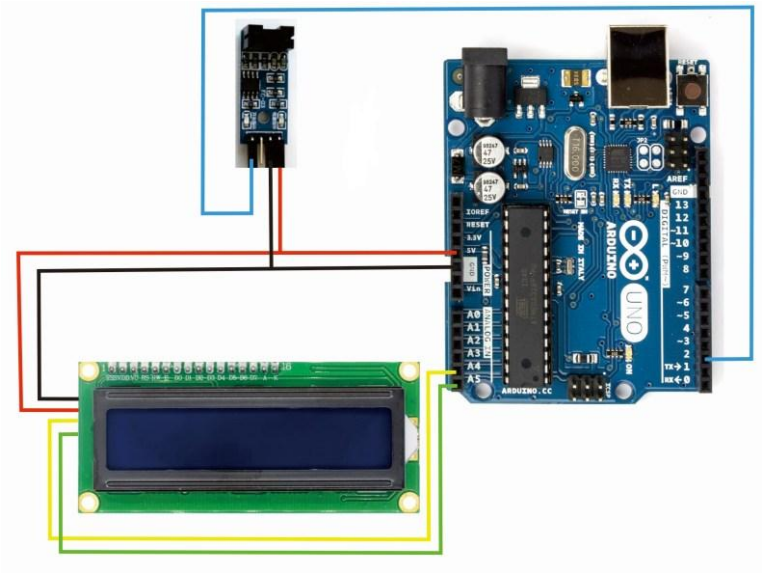

Figure 5.4: DIY Tachometer.

5.4.2 Electrical degradation testing

The motors are connected to power via the ESCs (Electronic Speed Controllers), which control the motors based on the PWM (Pulse Width Modulation) input. The load current drawn by the motor is proportional to its RPM. If a motor begins to draw more current to maintain the same RPM, it can be inferred that there has been some form of electrical or physical degradation. This increase in current indicates that the motor requires more power to overcome increased friction or other resistance, suggesting wear and tear.

To effectively measure this degradation, inline current sensors will be used to monitor the current draw of the motors during operation. By comparing the current drawn over time for the same RPM inputs, it will be possible to identify any significant increases that indicate degradation. This approach will provide a clear and quantifiable measure of motor health and performance over extended use.

5.4.3 Addressing propellors

To ensure that the tests reflect real-world conditions, the impact of motor degradation while equipped with a propeller also needs to be considered. An initial test was conducted to compare

the voltage drop measurements with and without propellers. This test utilized a 4S battery as a power source, and the drones typically had a flight time of 20 minutes.

The initial test involved running motors A2212, A2820, and BR4114 on existing drones in the lab. The voltage drop was measured over a 6-minute cycle for both scenarios:

- Without Propellers: The voltage drop was less than 0.1V.
- With Propellers: The voltage drop was 0.8V.

These results indicate that the voltage drop is significantly higher when the motors are running with propellers. This finding highlights the necessity of testing the motors with propellers to simulate the actual load conditions they will experience during flight. Testing without propellers does not provide an accurate representation of motor performance and degradation.

By testing the motors with propellers, the experiment will provide a more accurate representation of motor degradation under real-life conditions. The observed voltage drops and increased current draw will offer valuable insights into motor performance, helping to develop reliable predictive models and maintenance schedules. This approach ensures that the data collected can be extrapolated to real-world scenarios, improving the overall reliability and safety of UAV propulsion systems.

5.5 ESC testing

ESCs are selected to match the motor specifications, ensuring the testing system accurately reflects the configuration of a commercial UAV. This alignment is crucial for generalizing the test results to real-world applications. The objective is to detect deterioration or faults through electrical power draw assessment and temperature monitoring.

For this experimental setup, the existing motor electrical power testing circuit will be employed to measure the current drawn by the ESCs. By monitoring this current, we can identify potential issues: an increased current draw may indicate a fault in the ESC or an

increased power demand from the motor due to degradation.

In either scenario, the data collected will be used to develop a comprehensive reliability model for the entire propulsion system. This model will enable us to predict system performance and identify potential failure points, thereby enhancing the overall reliability and safety of the UAV.

5.6 Battery testing

To simulate real-world scenarios, a LiPo (Lithium Polymer) battery is utilized to power the propulsion system. Although using bench power supplies might provide a more controlled environment for run-to-failure tests, employing a LiPo battery introduces real-world limitations, thereby offering a more comprehensive understanding of system-level trends. This approach not only evaluates the performance of the propulsion system but also measures battery degradation within the context of its operational environment.

During each test run, the initial and final voltages of the battery will be recorded. By analysing the voltage drop across successive runs under consistent operating conditions, we can identify signs of battery degradation. Specifically, an increased discharge rate over time for identical test conditions will indicate a decline in battery performance. This method provides a dual assessment of both the propulsion system's reliability and the battery's longevity, yielding valuable insights into the overall endurance and efficiency of the UAV's power system.

5.7 Environmental control

To maintain temperature and environmental control, particularly for higher-than-ambient testing as detailed in Chapter 5.3.1, it is crucial to have precise environmental control and measurement. To facilitate this, the experimental setup will include the following considerations:

5.7.1 Plexiglass box

An enclosure made of Plexiglass or Acrylic will be utilized for two primary reasons. Firstly, it provides a safety barrier in case of motor failure or other hazardous incidents. Secondly, it creates a controlled environment essential for accurate testing.

BME280 environmental sensors will be deployed to continuously monitor temperature, barometric pressure, and humidity inside the enclosure. These sensors will also detect any heat generated by the system, allowing for real-time adjustments and precise environmental control.

By implementing this setup, the experimental environment will be both safe and controlled, providing reliable data for assessing the performance and reliability of the UAV propulsion system.

5.7.2 Box temperature control.

A heater/fan combination with a proportional thermostat will be used to heat and maintain constant temperatures within the enclosure. This setup ensures precise temperature control and uniform heat distribution. For this purpose, a 3D printer main voltage heated silicone bed equipped with a thermocouple is ideal, as it provides efficient and reliable heating capabilities. The thermocouple will continuously monitor the temperature, allowing the thermostat to make real-time adjustments and maintain the desired temperature accurately.

5.8 Testbed component selection

Based on Table 5.1, the selection process was further refined to identify the most common motor types for each UAV category. The final selection criteria included compatibility with a 12V power supply, which lies between the commonly used 3S and 4S battery configurations across various UAV types. Although FPV/racing drones typically use 1S or 2S LiPo batteries and industrial drones often use multiple 6S LiPo batteries, the selected motors are rated to operate at 12V, making them suitable for these scenarios as well. The selected motors are

detailed in Table 5.3.

To ensure accurate and effective testing, the motors were paired with appropriate ESCs and propeller sizes, as specified in their respective datasheets. This combination provides a realistic load on the motors, facilitating proper fatigue testing and ensuring that the results are relevant to real-world applications.

MT2204	**A2212**	**BE4108**
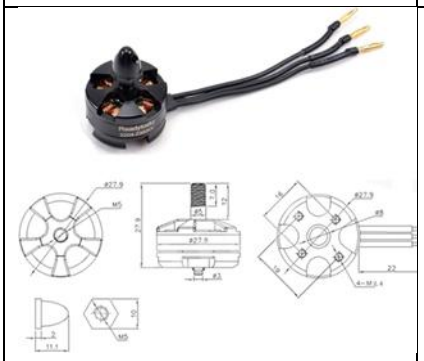		
12A ESC	20A ESC	40A ESC
5” prop	9” prop	13” prop
2.94N thrust (300 grams)	4.65N thrust (475 grams)	20.4N (thrust) (2080 grams)
2S-4S	3S-4S	3S-6S
2300KV	1400KV	480KV

Table 5.3: Motor choices and relevant ESC and propeller choices

5.9 Experimental runtime

The orange graph in Figure 5.5 represents a "High/Low" cycling pattern, while the blue graph depicts a "Min/Max" cycling pattern. These cycles were specifically chosen based on the criteria outlined in Table 5.2, which were influenced by Annex D UL.EE.22.c of the NATO white paper [108].

The runtime of tests was optimized to balance experimental feasibility with the need for long-term reliability insights. The simulated flight cycles were designed to replicate diverse

operational scenarios, ranging from short-term missions to extended endurance tests, thereby enhancing the applicability of results. This allows for degradation behaviours of critical propulsion components, including motors, ESCs, and batteries, were evaluated under controlled yet realistic operational stresses. This approach allowed for the identification of failure modes that are commonly observed in real-world UAV operations.

Each set of motors was divided into groups of four for each test to ensure consistent and reliable results across the different cycling patterns as described by Table 5.6.

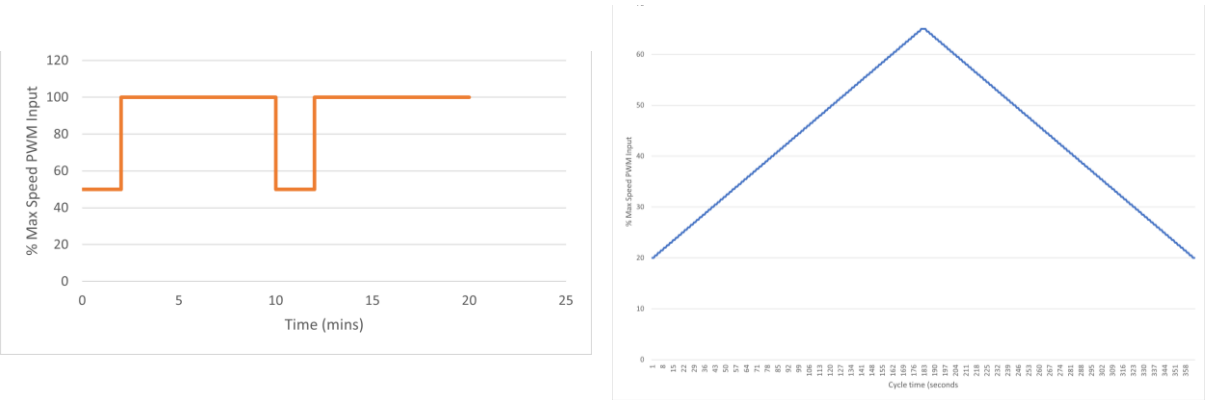

Figure 5.5: Cyclical loading of motors.

Motor Type	Test Pattern	Number of motors	Hours Run	No of Failures/ Errors
MT2204	High/Low	4	40.3	0
	Cycle	4	40.2	1*
A2212	High/Low	4	40.2	0
	Cycle	4	40.3	0
BE4108	High/Low	4	30.3	0
	Cycle	4	30.0	0

Figure 5.6: Motor runtime.

5.9.1 Error in MT2204 Min-Max

At the 21st hour of testing the MT2204 motors under the Min-to-Max cycle, a fault was detected. Upon initiating the testing cycle, both the current sensor and the tachometer for Motor 1 recorded errors. After completing the initial cycle, the test was temporarily suspended to diagnose the issue. Consequently, this particular cycle was excluded from the final results discussed in subsequent chapters.

The fault was identified as loose signal cables on the Arduino interface, likely caused by inadvertent physical disturbance of the test bench, which displaced the wires enough to disrupt pin contact. Following the identification and securing of the loose connections, the testing resumed without further incident.

TimeStamp (s)	Time Stamp (Mins)	Time (Hrs)	Input RPM	Temp	Motor 1	Motor 2	Motor 3	Motor 4	Current Sensor 1	Current Se	Current Sensor 3	Current Sesnor 4
75695	1261.583333	21.02639	8280	23.46131	7676.215	7940.495459	7919.267904	7275.236	2.207878347	2.120732	2.030947795	2.152663013
75696	1261.6	21.02667	8004	26.2483	6969.552	7543.733953	7468.257352	7564.904	1.933363889	1.93121	2.008803882	2.126232391
75697	1261.616667	21.02694	7728	26.44393	7218.984	6769.243279	6800.697038	6812.3	2.038062763	2.044861	1.864062896	1.997748831
75698	1261.633333	21.02722	7452	24.22903	6811.129	6806.979691	6610.755814	6993.748	1.889968894	1.971047	1.815922133	1.921575868
75699	1261.65	21.0275	7176	24.91075	6384.534	6788.676618	6705.412706	6534.931	1.867943251	1.785017	1.738482744	1.804679605
75700	1261.666667	21.02778	6900	26.53684	ERROR	6034.808357	6595.55213	6036.436	ERROR	1.680522	1.70767412	1.749607587
75701	1261.683333	21.02806	7176	23.42624	ERROR	6402.617022	6617.799857	6314.373	ERROR	1.855914	1.814414635	1.743275954
75702	1261.7	21.02833	7452	25.23917	ERROR	6489.209761	6517.066672	6513.746	ERROR	1.854215	1.976046014	1.817094388
75703	1261.716667	21.02861	7728	24.82496	ERROR	7355.244991	7198.073681	7211.38	ERROR	1.884095	2.03538443	1.952433831
75704	1261.733333	21.02889	8004	24.91126	ERROR	7295.437881	7593.762725	7195.186	ERROR	2.019388	1.981320165	2.034612282
75705	1261.75	21.02917	8280	26.98638	ERROR	7234.866275	7809.238224	7597.193	ERROR	2.001194	1.99233474	2.119791961
75706	1261.766667	21.02944	8556	23.98556	ERROR	7983.429394	7927.349771	8042.572	ERROR	2.080182	2.281613232	2.118450757
75707	1261.783333	21.02972	8832	25.10258	ERROR	7904.701488	8413.262518	7873.113	ERROR	2.347499	2.306068054	2.322131433

Figure 5.7: MT2204 Error in data set.

5.10 Initial Results discussion

While no failures were observed during the experimental tests, the degradation trends captured through real-time monitoring align with the failure modes predicted in Chapter 3's FMEA. For example, gradual RPM reductions in motors reflect wear-out mechanisms, and minor voltage irregularities in ESCs are indicative of electrical anomalies. These observations validate the FMEA framework and provide critical insights for refining reliability models.

5.10.1 Initial findings

To analyse the motors, the initial step involves examining the raw data outputs to identify any emerging patterns. Although the initial graphs may appear cluttered due to the large volume of data, they will be refined in subsequent stages. This preliminary graphing is intended to

provide an early indication of potential patterns, which will then inform the data cleaning process and guide the detailed investigation that follows.

5.10.1.1 RPM outputs over time.

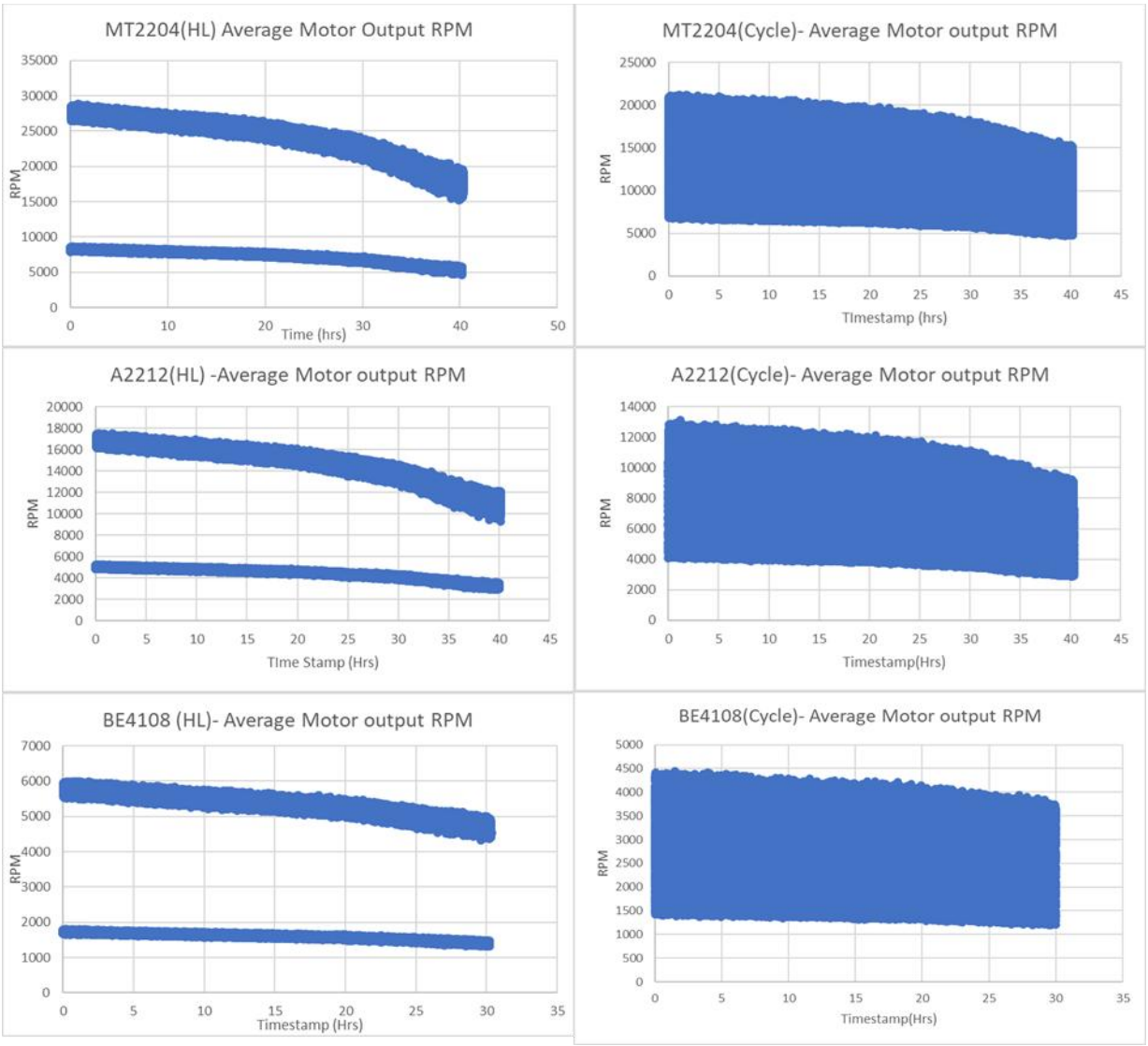

Figure 5.8: AVG RPM for each test case against time.

Figure 5.8 illustrates that, contrary to the common assumption of linear degradation of electronic components in an overall system as often suggested in literature [110] , the observed data indicates an exponential degradation pattern. Specifically, the RPM degradation demonstrates nearly a 30% reduction over time. Initially, the graphs display a linear trend;

however, as time progresses, the rate of degradation accelerates exponentially, which aligns more closely with the behaviour of more complex systems.

This finding suggests that modelling the degradation process may benefit from considering exponential trends rather than linear ones. Figure 5.9 presents a typical equipment performance cycle that could serve as a basis for this more nuanced modelling approach. This approach better captures the dynamics observed in the experimental data, providing a more accurate representation of the degradation process over time.

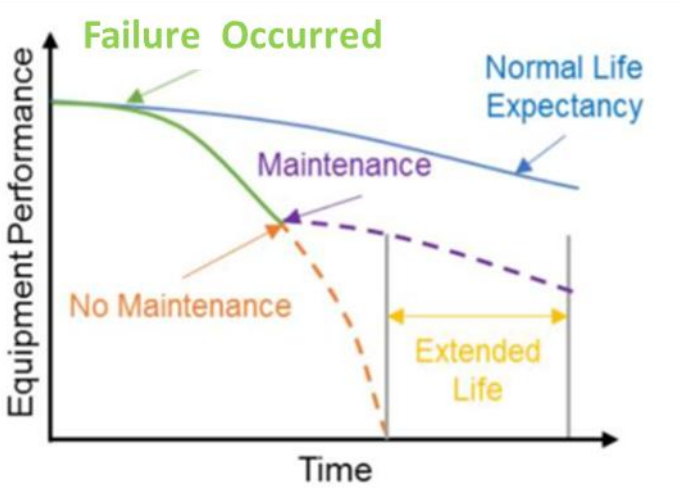

Figure 5.9: Reliability prediction results for maintenance strategies decisions.

5.10.1.2 Current draw over time

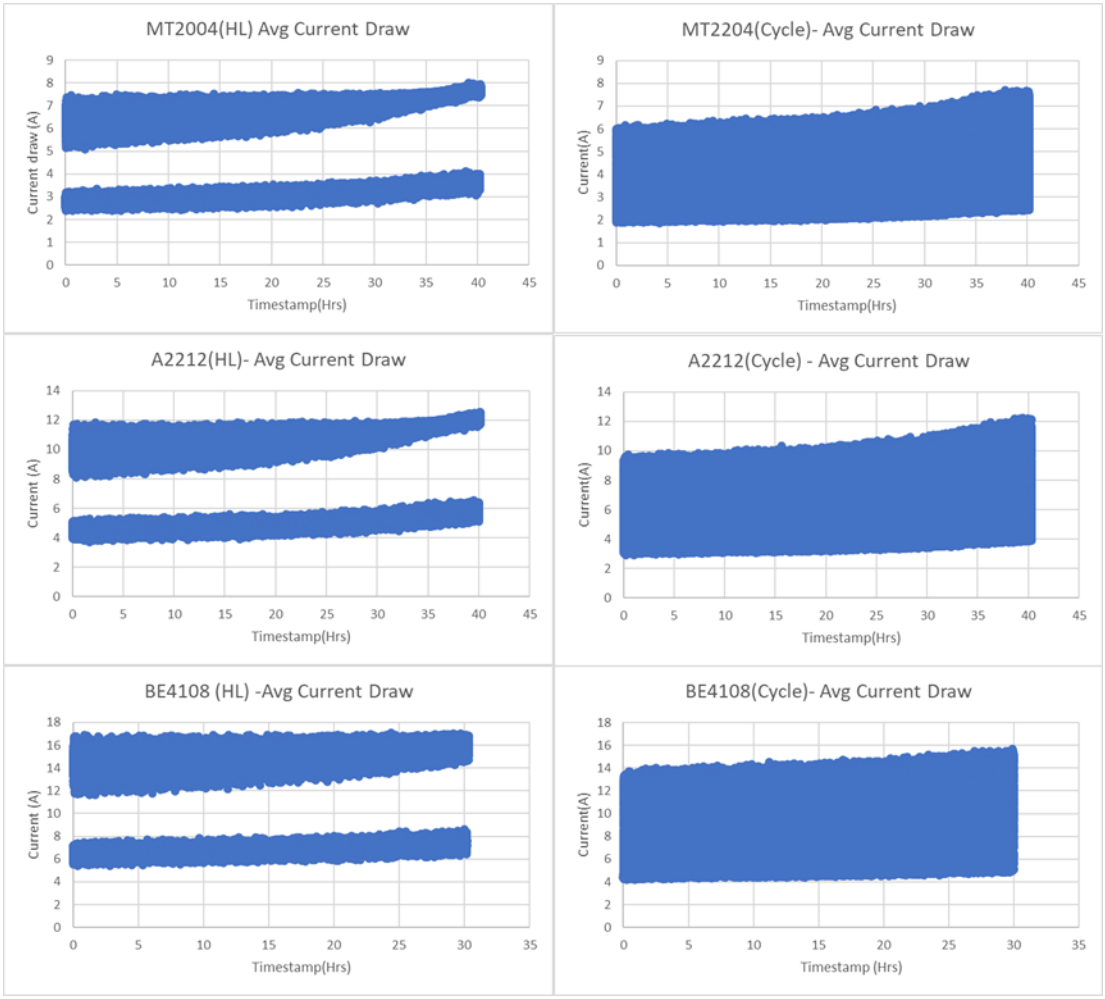

Figure 5.10: Average current drawn per test over time.

Figure 5.10 illustrates an interesting phenomenon observed during the test period. Although the RPM decreases over time, as discussed in Section 5.10.1.1, the current draw actually increases to maintain output stability.

This relationship is noteworthy because the percentage change in average current (%ΔAvgCurrent) almost inversely coincides with the percentage change in average RPM (%ΔAvgRPM) over time. Specifically, as the RPM decreases to approximately 70% of the initial input RPM, the required current increases by around 30% compared to the beginning of the test. This inverse linear relationship highlights the compensatory increase in power consumption required to maintain performance as motor efficiency declines.

5.10.2 Lines of best fit

By utilizing a random sample of 200 data points from each test case, the output RPM and input RPM of the motors can be compared. This comparison facilitates the creation of degradation curves for each of the three motors, enabling the prediction of their degradation patterns.

As illustrated in Figure 5.11, the degradation curves exhibit an exponential trend. Although the degradation pattern for the 2204 motors fits a second-order polynomial best, the RPM loss over time closely aligns with an exponential curve. For the 2212 and 4108 motors, the degradation curves share similar coefficients and exponents.

The best-fit function for the 2212 motors is $y = 1.9693e^{0.0752x}$, and for the 4108 motors, it is $y = 1.9054e^{0.0783x}$. Both functions exhibit coefficients of approximately 1.9 and exponents around 0.07, indicating a consistent exponential degradation pattern across these motor types. This similarity in the degradation models suggests a predictable pattern that can be applied to estimate the performance decline of these motors over time.

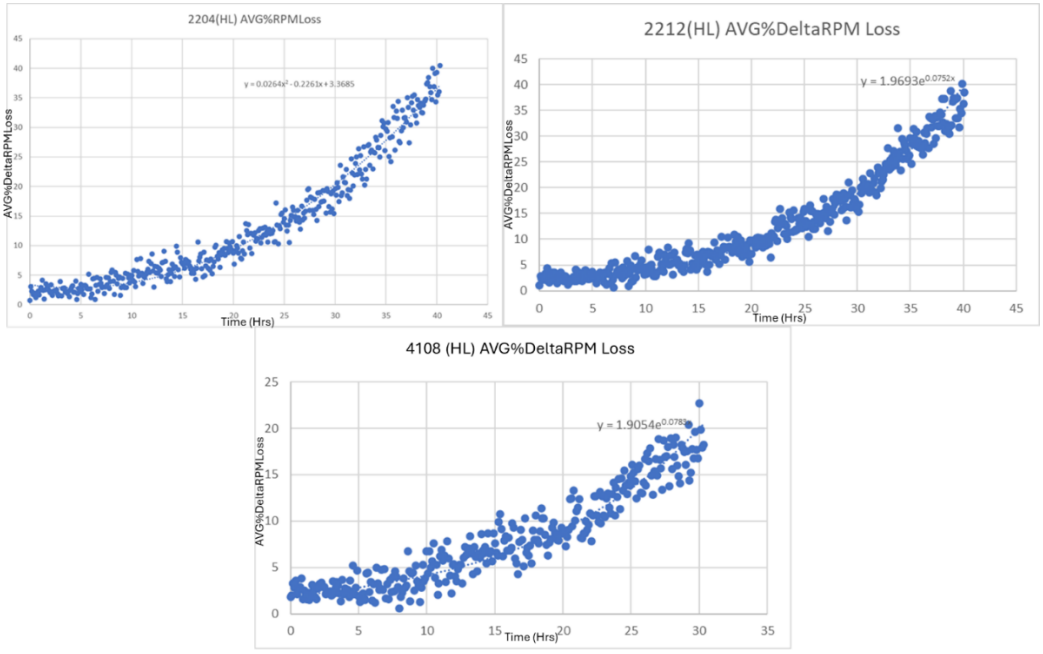

Figure 5.11: Fitting the High Low functions for the loss of average RPM difference vs RPM input.

Following this, an overall average fitting was conducted to determine if a generalized function could be generated to estimate the degradation and remaining useful life (RUL) of the motors, regardless of type.

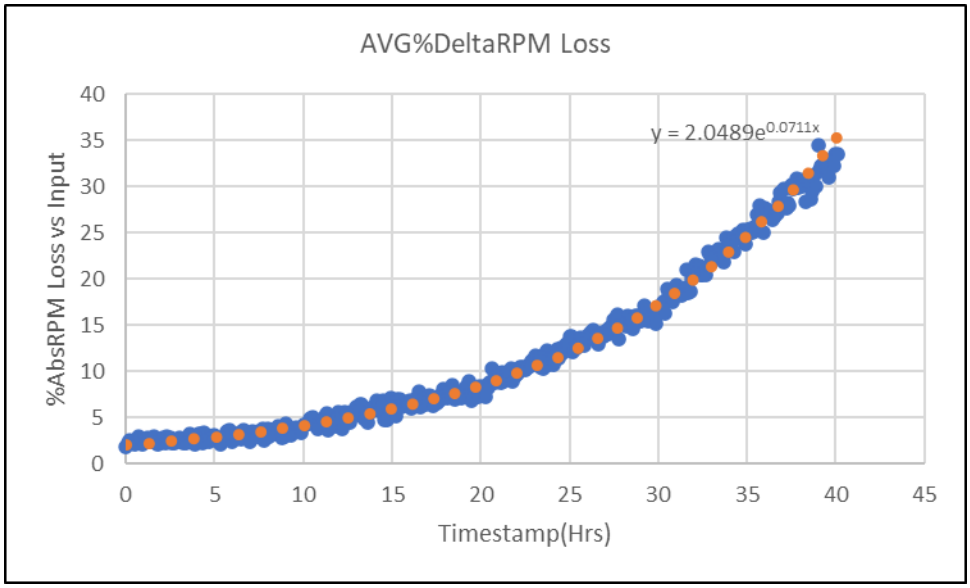

Figure 5.12: Average fitted function.

When the RPM loss over time is averaged, the best fit follows Equation 5.1, as illustrated in Figure 5.12.

$$y = 2.0489e^{00711x} \tag{5.1}$$

Where:

- x: x represents the number of hours flown.
- y: y represents the amount of RPM loss.

Using this exponential degradation model, we can make critical assumptions about motor performance and drone stability. Specifically, it is assumed that a 25% RPM loss results in the drone becoming unstable due to power thrust losses. This threshold allows for a quick estimation of the RUL (Remaining Useful Life) of the motor.

5.11 Modelling

This Section follows the base procedure laid out in Quantitative evaluation of multi-rotor

UAV propulsion system reliability[111] and is not elaborated here

5.11.1 Model Result Analysis

5.11.1.1 Weibull Model Result Analysis

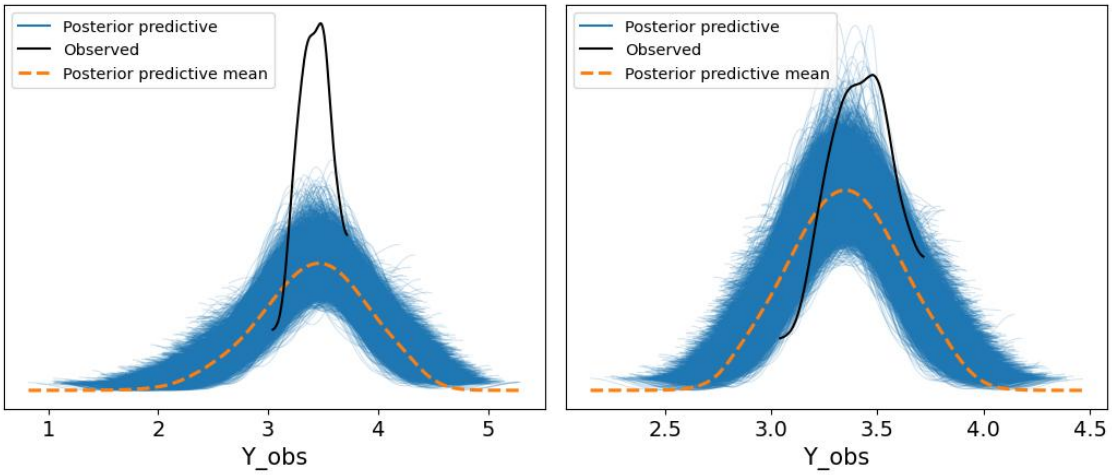

Figure 5.13: a) Posterior Predictive Plot (LWMM) b) Posterior Predictive Plot (NWMM)

Figure 5.13a shows the posterior predictive plot for the Linear Weighted Mean Model (LWMM), while Figure 5.13b shows the posterior predictive plot for the Non-Linear Weighted Mean Model (NWMM).

In the LWMM, the highest point of the observed data aligns with the mean of the predicted values on the x-axis. This alignment suggests that the model's average prediction closely matches the average value of the observed data, indicating an absence of bias on average. However, there is a noticeable difference in the distribution peaks on the y-axis, where the observed data has a higher concentration around its central value compared to the model's predictions. This discrepancy indicates that the LWMM underestimates the probability of the most common outcomes seen in the data.

Approximately 30% of the observed data falls within the blue shaded region, representing the spread of predictions. This suggests that the model's predictions carry significant uncertainty and fail to accurately capture the true variability of the data.

In contrast, the NWMM's posterior predictive plot shows that most of the observed data falls within the blue highlighted region, indicating that the model effectively captures both the average and the range of the data, thus outperforming the LWMM. However, a discrepancy remains in the alignment of the highest points, with the maximum observed data point slightly shifted to the right compared to the maximum point of the posterior predicted mean. This shift suggests that the NWMM tends to underestimate the average value of the observed variable. Additionally, the highest point of the observed data exceeds the highest point of the predicted average, indicating that the model underestimates the likelihood of the most frequent occurrence in the data.

When comparing both plots, it is evident that the NWMM provides a better fit. It more accurately represents the central tendency and variability of the observed data and offers more reliable predictions. This improved fit suggests that the NWMM is better calibrated and can generalize more effectively to previously unseen data. Conversely, the LWMM exhibits higher bias and less variation in predictions, which aligns less closely with the true variability of the data.

In summary, the NWMM demonstrates superior performance in modelling the data, capturing the essential characteristics of the observed distributions, and providing more accurate and reliable predictions. This makes it a preferable choice for applications requiring robust predictive accuracy.

5.11.1.2 NN Model Analysis

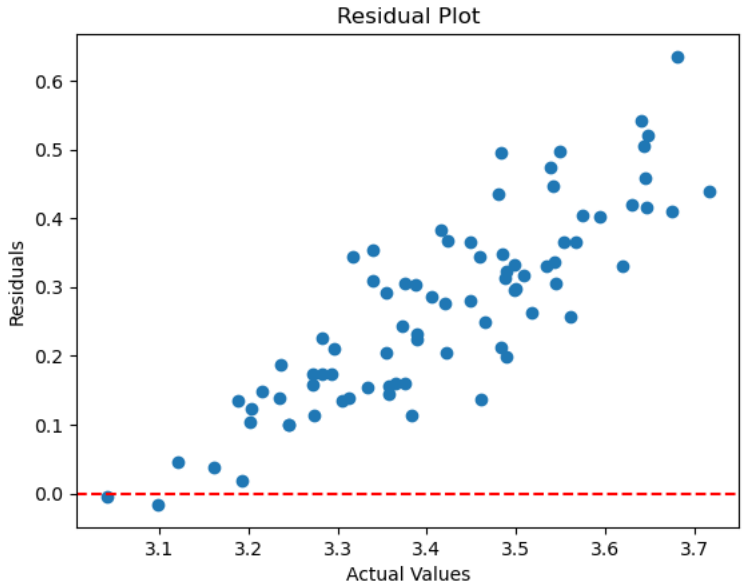

Figure 5.14: Residual Plot for NN

Figure 5.14 depicts the residual plot for the 2212 High-Low cycle, illustrating the differences between the actual values and the model-estimated values. The residuals are plotted on the vertical axis, while the actual values are shown on the horizontal axis.

The plot reveals a clear trend where residuals consistently increase with the actual values. This pattern indicates that the model systematically underestimates the target variable as the actual values rise.

The increasing residuals with higher actual values suggest a systematic bias in the model, indicating that the model's predictions become less accurate for larger actual values, resulting in consistent underestimation. Ideally, residuals should be randomly distributed around zero if the model accurately captures the underlying data patterns. The observed non-random distribution implies that the model fails to account for specific characteristics or relationships within the dataset.

The clear pattern in the residuals suggests that the current model inadequately captures the potential nonlinear relationship between the input features and the target variable. This

inadequacy is particularly evident for higher values of the target variable. The trend in the residuals indicates that a nonlinear relationship may exist between the input features and the target variable. The current model's inability to capture this nonlinearity results in systematic prediction errors. To improve predictive performance, it is recommended to explore more sophisticated modelling approaches, such as nonlinear regression techniques or advanced machine learning algorithms, which can better accommodate the complexities observed in the dataset.

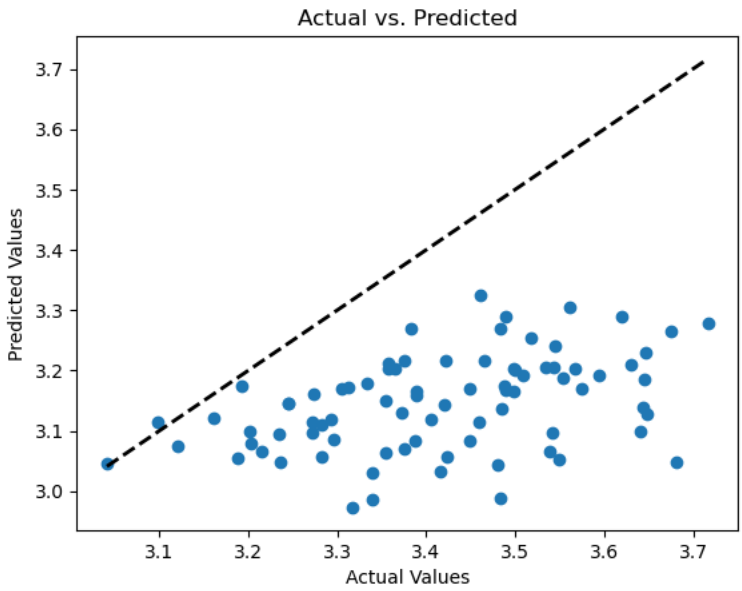

Figure 5.15: Actual vs Predicted Plot for NN

Figure 5.15 presents a scatter plot comparing real values with predicted values. The figure includes a dotted line representing the ideal prediction line, where the predicted values would perfectly align with the actual values.

A significant number of data points fall below the dotted line, indicating that the model tends to overestimate the actual values. The tendency of the model to predict higher values than the actual ones indicate a systematic overestimation error, which suggests that the model's assumptions or structure are insufficient to capture the underlying patterns of the data. The consistent overestimation implies that the current neural network model does not possess the necessary complexity to capture the nonlinearity, and intricacies present in the dataset.

To address this issue and improve the model's ability to capture the data's complexity, more Long Short-Term Memory (LSTM) units were added to the neural network. The number of LSTM units was increased from 64 to 128, resulting in the updated model referred to as NN128. By increasing the number of LSTM units, the enhanced model is expected to better capture the nonlinearity and intricacies in the data, leading to more accurate predictions and reducing the systematic overestimation observed in the original model.

Based on these findings, it can be concluded that the original neural network model was inadequate for accurately capturing the nonlinearity present in the data. By increasing the number of LSTM units from 64 to 128 (NN128), the model's complexity is enhanced, which should improve its ability to represent the data accurately and reduce prediction errors. This adjustment aims to create a more robust model capable of effectively handling the complexities inherent in the dataset.

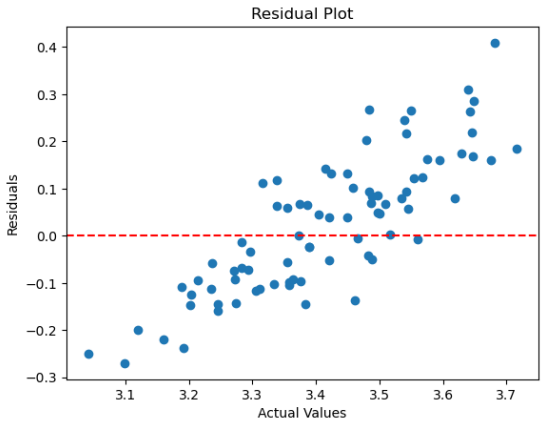

Figure 5.16: Residual Plot for NN128

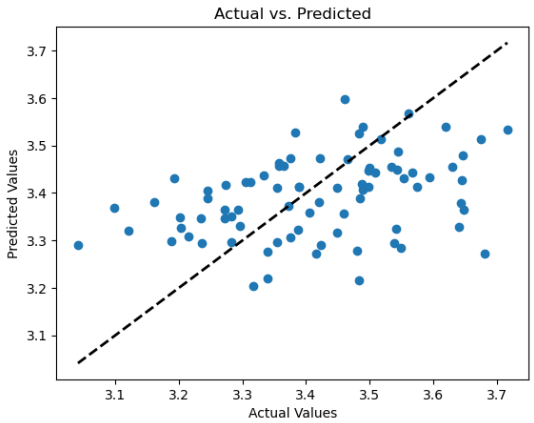

Figure 5.17: Actual vs Predicted for NN128

The revised neural network model demonstrates improved accuracy in predictions. The residual plot indicates that the residuals are uniformly distributed around the zero line, suggesting that the model's prediction errors follow a normal distribution without noticeable bias. The dispersion of the residuals indicates that the model does not consistently overestimate or underestimate the observations.

The revised neural network model, with increased LSTM units, successfully addresses the limitations of the previous model. The uniform distribution of residuals and the symmetrical scatter of data points around the perfect prediction line confirm that the model adequately captures the complexity and variability of the data. The lack of bias and the presence of symmetry are critical indicators of the model's reliability and flexibility in making accurate predictions. This improvement highlights the model's enhanced capability to handle the nonlinear relationships inherent in the dataset, making it a robust tool for predictive analysis.

5.12 Model Evaluation

5.12.1 Model Evaluation Metrics

To evaluate the accuracy of the models, three measures have been selected: Root Mean Squared Error (RMSE), Mean Absolute Percentage Error (MAPE), and R-squared (R^2). [81]

- Root Mean Squared Error (RMSE): RMSE is used to measure the average magnitude of the errors between predicted and actual values. It is particularly sensitive to larger errors, providing a clear indication of the model's prediction accuracy.
- Mean Absolute Percentage Error (MAPE): MAPE measures the accuracy of the model in terms of the percentage error, making it easy to interpret and compare across different datasets.
- R-squared (R^2): R^2 represents the proportion of variance in the dependent variable that is predictable from the independent variables. It provides a measure of how well the model captures the data's variability.

To evaluate model complexity, several criteria have been selected: training duration, number of parameters, and number of divergences (specifically for Weibull models).

1. Training Duration:

This refers to the time required to train a model, reflecting the computational efficiency and complexity of the model's learning process. Training duration is crucial when time resources are limited, especially in scenarios requiring iterative experimentation. Since these models aim to validate the reliability of drones, shorter training durations enable faster repetition cycles, providing more opportunities for experimentation within a given timeframe.

2. Number of Parameters:

   This measures the total count of trainable parameters in a model, indicating its complexity and ability to learn patterns from data. The number of parameters serves as a direct measure of the model's intricacy. While increasing the number of parameters can enhance the model's capacity to learn complex patterns, it also increases the risk of overfitting, particularly with limited data. Therefore, understanding the model's parameter count is crucial for managing the trade-off between model complexity, overfitting potential, and available data.

3. Number of Divergences (Specific to Weibull Models):

   This criterion applies to Weibull models and refers to the instances where the model fails to converge to a solution during training. High numbers of divergences indicate issues with model stability and training efficiency, highlighting areas where the model's complexity may need to be adjusted for better performance.

By assessing both the accuracy and complexity of the models, this study aims to balance the trade-offs between computational efficiency, predictive accuracy, and the potential for overfitting. The chosen criteria provide a comprehensive framework for evaluating and optimizing the performance of models used to validate the reliability of drones, ensuring robust and reliable predictions in practical applications.

5.12.2 Model Evaluation

	LWMM	NWMM	NN	NN128
RMSE	0.1117	0.1105	0.7478	0.8266
R2	0.2234	0.2150	-29.0724	-35.8410
MAPE (%)	3.2598	3.2119	0.1922	0.2166
Training Time (s)	815	245	52	98
Number of Parameters	594667	382636	21121	74881
Divergences	0	4		

Table 5-4: Evaluation Results for Cycle

The RMSE quantifies the dispersion of residuals, indicating how accurately a model predicts observed outcomes with fewer errors. Table 5-4 shows that the LWMM and NWMM have low RMSE values of 0.1117 and 0.1105, respectively, suggesting that these models provide more accurate predictions closer to the actual values. In contrast, the NN models, with larger RMSE values, appear to deviate more from the actual values, potentially due to overfitting or underfitting.

The R^2 value of 1 implies a perfect fit of the regression predictions to the data. While a value close to 1 is desirable, a low R^2 indicates that the model explains little of the variability in the response data around its mean. The low positive R^2 values for LWMM and NWMM, such as 0.2234 and 0.2150, respectively, indicate that they capture only a modest proportion of variance in the data. The significantly negative R^2 values in NN and NN128 may indicate overfitting to the training data, resulting in poor generalization to the test data.

A lower MAPE score suggests that a model's predictions closely match the actual data in terms of percentage error. The disparities between the MAPE and RMSE of the NN and NN128 models may be attributed to skewed errors. If the neural network models consistently overestimate or underestimate the real values, the MAPE may remain low, while the RMSE would be large due to the squaring of the errors. This indicates that the neural network models struggle with specific portions of the data.

When comparing the NWMM and LWMM models, both demonstrate similar levels of accuracy. However, the LWMM model requires substantially more time to train due to its higher number of parameters.

Overall, the Weibull models (NWMM and LWMM) appear to strike a harmonious balance between precision and complexity. Despite their longer training times and higher number of parameters, these models exhibit lower RMSE and positive R^2 values, indicating a better representation of the underlying process compared to the NN models. Although the NN models train quickly, they lack the necessary precision to be considered reliable. The presence of negative R^2 values is concerning and suggests that either the model structure is unsuitable for the data, or the model inadequately reflects the underlying process.

	LWMM	**NWMM**	**NN**	**NN128**
RMSE	0.1291	0.1103	0.2367	0.1773
R2	0.1542	0.2589	-1.7363	-0.7749
MAPE (%)	3.3367	2.9504	0.0622	0.0476
Training Time (s)	403	236	58	112
Number of Parameters	594667	594667	21121	74881
Divergences	0	40		

Table 5-5: Evaluation Results for High-Low

The Weibull models exhibit greater stability and moderate prediction accuracy in the High-Low cycle. However, they require longer training times and have higher complexity, as shown in Table 5-5. Among the Weibull models, the NWMM, despite experiencing some divergences, demonstrates slightly better compatibility than the LWMM.

In contrast, the neural network (NN) models offer faster training times and reduced complexity. However, their negative R^2 values suggest they may not accurately capture the underlying data distribution. The significant difference between their low MAPE and higher RMSE likely results from consistent overestimation or underestimation of data, as noted in the cycle findings.

The NN models appear more effective in handling the High-Low cycle compared to the

Cycle models. This observation suggests that NN models are better suited for dynamic environments characterized by frequent variations in operational stress due to alternating power levels during flight. However, this also implies that NN models might be responsive to specific conditions but may not generalize well under different stress scenarios.

	LWMM	NWMM	NN	NN128
RMSE	0.1204	0.1104	0.4923	0.5020
R2	0.1888	0.2369	-15.4043	-18.3080
MAPE (%)	3.2982	3.0812	0.1272	0.1321
Training Time (s)	609	241	55	105
Number of Parameters	594667	488651	21121	74881
Divergences	0	22		

Table 5-6: Total Average Evaluation Results

Overall, the nonlinear approach demonstrated by the NWMM is more effective at capturing the complexities of the data compared to the linear approach. However, the divergences observed in the NWMM may indicate issues with sample selection and model convergence, which could affect the reliability of its predictions. This may require adjustments to the model's priors or sampling technique.

This shows that while Weibull models consistently perform well across many cycles, demonstrating their robustness and reliability in various operational scenarios that drones encounter, neural network models offer quicker training but may require further refinement to improve accuracy and generalization.

5.13 Conclusion

This chapter presents a new testbed for UAV propulsion systems that can carry out extensive run-to-failure tests in a controlled environment. This testbed fills a crucial gap in UAV reliability research—which frequently lacks empirical data for model validation—by mimicking operational environments. Advanced sensors and data acquisition systems are integrated into its design to record high-resolution performance metrics, allowing for in-depth examination of failure mechanisms and degradation patterns. An important development is the

application of NWMM for predictive modelling, which provides a reliable and precise way to identify nonlinear degradation trends that are usually missed by traditional linear models. These developments establish a new benchmark for UAV propulsion reliability studies by offering a scalable framework for creating predictive maintenance plans.

The tests consistently showed a decline in motor performance due to mechanical wear and overheating. As the motors approached failure, there was a noticeable decrease in RPM and an increase in current draw. Weibull analysis identified wear-out failure as the primary mode, emphasizing the need to monitor motor temperature and load conditions to predict and prevent failures. ESC failures were primarily attributed to voltage variations and current surges. The data highlighted the vulnerability of ESCs to electrical anomalies, underscoring the importance of reliable electrical monitoring systems to promptly detect and address such issues.

The Nonlinear Weibull Mixed Model (NWMM) outperformed both the Linear Weibull Mixed Model (LWMM) and neural network models in terms of accuracy and reliability across various assessment criteria and operating cycles. Despite the NWMM's longer training time due to its complexity, it demonstrated lower RMSE and positive R^2 values, indicating a more accurate representation of the degradation process compared to the neural network models. Although faster, neural network models lacked accuracy in predicting outcomes, as evidenced by negative R^2 values and higher RMSEs. These models struggled with generalization across different scenarios, potentially oversimplifying the nonlinearity present in the data.

The experimental findings provide a comprehensive understanding of the degradation mechanisms affecting essential components of UAV propulsion systems. By utilizing this data, UAV operators can enhance safety, increase reliability, and improve maintenance protocols. Future studies should aim to broaden the scope of these experiments by incorporating a wider range of operating conditions and advanced monitoring technologies to further refine the predictive models. These insights underscore the importance of continuous monitoring and

advanced modelling to ensure the longevity and reliability of UAV propulsion systems, guiding future research and development in this critical area.

Chapter 6 Degradation flight testing and results

The Work presented in the Chapter was partially published in DASC 2023 Conference under the title "UAV flight test and its endurance degradation modelling by considering the energy efficiency and flight stability factors" [112]

This Chapter covers the other half of the concurrent tests conducted during the course of this Research. Namely in contrast to the is propulsion system degradation by analysis of the different component level degradation over time on testbench, as discussed in Chapter 5, this chapter covers a test of a full UAV system to simulate real-world degradation over time.

The rapid advancement and deployment of Unmanned Aerial Vehicles (UAVs) in recent years, fuelled by breakthroughs in AI and robotics, have revolutionized a myriad of sectors including agriculture, disaster management, surveillance, logistics, and more [113]. However, despite the proliferation of UAV applications, accurately estimating flight endurance remains a daunting task. This challenge originates from the intricate interplay of various factors influencing UAV performance such as payload, environmental conditions, aerodynamic properties, and the state of the UAV itself, particularly its energy source and mechanical health [114]. In the context of UAV failures, Zahra et al. [115] disclosed that nearly half of all accidents can be attributed to machine failure, with the propulsion systems of UAVs accounting for almost 40% of these failures. However, it's imperative to recognize that beyond the costly analysis based on total failure samples, the detection and prediction of UAV performance degradation trends are of substantial research significance. This consideration is especially relevant when considering the practical constraints related to experimental costs and feasibility.

The lack of comprehensive and contextually-rich data hampers the ability to develop precise predictive models [116]. Moreover, the complex nature of UAV systems necessitates sophisticated analysis techniques capable of decoding intricate correlations and causality in large, multi-faceted datasets.

6.1.1 DJI F450 Drone Platform Setup

The drone setup for the flight test is the DJI F450, a versatile drone renowned for its adaptability and performance. The DJI F450 as shown in Figure 6.1 has a diagonal wheelbase of 450mm and a frame weight of just 282g, promising a balanced combination of stability and lightness that should enable efficient flight dynamics.

Figure 6.1: F450 drone platform [112]

As shown in Figure 6.1 the propulsion system of this sophisticated drone is engineered with precision, incorporating 2212 920KV Brushless Motors as its core. Each of these high-efficiency motors, with a weight of 53 grams, is capable of delivering an impressive maximum power output of 370W. Furthermore, they are designed to produce a formidable maximum thrust of 1200 grams, ensuring the drone's capability to achieve and maintain superior flight performance. At the heart of the propulsion mechanism are the meticulously designed 1045 ABS propellers. Each propeller, part of a pair and weighing 22 grams, spans 10 inches in length and features a pitch of 4.5 inches. The strategic dimensions and materials of these propellers contribute significantly to the overall aerodynamic efficiency, offering the agility and lift essential for the drone's aerial manoeuvres.

Enhancing the drone's flight capabilities, the propulsion system's efficacy is seamlessly integrated with the advanced Holybro Pixhawk Mini flight controller. This compact yet powerful flight controller stands out for its ability to optimize flight performance, ensuring a smooth and responsive control experience. It plays a pivotal role in flight management, adhering to the highest standards of precision and reliability. Throughout all flight tests conducted in this experiment, altitude control mode was meticulously utilized, highlighting the controller's versatility and efficiency.

The drone's sensory apparatus is nothing short of state-of-the-art. It is equipped with an MPU9250 sensor, providing critical data from its accelerometer, gyroscope, and magnetometer. This is complemented by an MS5611 barometer, renowned for its precise altitude measurements. Together, these sensors supply real-time data to the flight controller, empowering the drone with the ability to navigate with unparalleled stability and accuracy across a multitude of flight trajectories.

Powering this technological marvel is the ACE 5300mAh 14.8V 30C Lithium Polymer Battery, chosen for its optimal capacity and voltage to guarantee prolonged flight times and a consistent power supply during all phases of operation. This ensures that the drone remains operational for extended periods, catering to the demands of various flight missions without compromise.

For operational management and monitoring, the drone utilizes the sophisticated QGround Control software. This powerful software suite is instrumental in configuring flight parameters, managing the drone's operations, and most importantly, collecting and analysing flight data. The capabilities of QGround Control software extend far beyond basic flight control, offering in-depth insights into flight dynamics, thereby enabling precise adjustments and improvements in drone performance based on empirical data.

In summary, the integration of high-performance 2212 920KV Brushless Motors,

aerodynamically efficient 1045 ABS propellers, the cutting-edge Holybro Pixhawk Mini flight controller, advanced sensory equipment, a high-capacity ACE Lithium Polymer Battery, and the comprehensive QGround Control software, collectively forge a drone propulsion system that is designed to excel. This system not only meets but exceeds the requirements for agile, stable, and extended flight capabilities, setting a new benchmark in drone technology and performance.

6.1.2 Flight Test Specifications

The flight tests, as depicted in Figure 6.2, were undertaken in a controlled indoor setting. The drone was controlled manually to follow a rectangular trajectory with dimensions of 3.5 by 4.5 meters in a counterclockwise direction (from point A to until point D in Figure 6.2). This routine commenced from a fully charged state and persisted until the battery voltage reached the predefined threshold. The flight altitude, denoted as h, is subject to operator control and maintained an approximate average of 1.5 meters throughout the test.

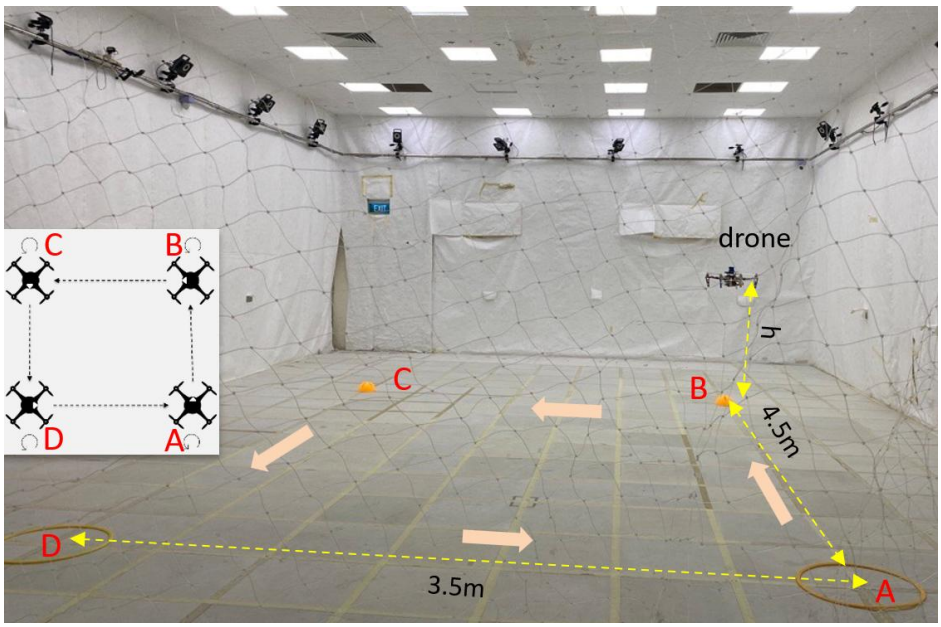

Figure 6.2: Indoor UAV flight environment [112]

6.1.3 Flight test data

In a flight test, constraints from battery endurance and pilot focus typically limit flights to

15 to 20 minutes. After each session, a comprehensive .ulg formatted log, approximately 50Mb for a 20-minute flight, is saved for subsequent data processing by a developed pipeline. Extracted CSV files from such a log expand to around 120Mb. Notably, different sensors possess varied sampling frequencies. This study specifically leverages readings associated with the motors' instantaneous rotational speeds as training data for the LSTNet model, marking a foundational explorative approach.

To ensure high-quality inputs for model training and analysis, preprocessing steps were employed to manage noise, handle outliers, and align data across sensors:

- Data Fusion and Resampling: Sensor data with varied sampling frequencies were aligned using linear interpolation, ensuring consistency and compatibility for analysis. This step allowed seamless integration of multi-source data for the model.
- Exploratory Data Analysis (EDA): Prior to analysis, EDA was conducted to inspect the structure and quality of the data, identifying anomalies, trends, and inconsistencies. These inspections informed preprocessing strategies tailored to the dataset.
- Noise and Outlier Management: Advanced filtering techniques were applied to smooth fluctuations caused by noise. Additionally, the LSTM autoencoder model itself was leveraged for anomaly detection, flagging deviations from expected reconstruction outputs as potential outliers.
- Sequence Reconstruction and Error Minimization: The LSTM autoencoder reconstructed sensor data sequences, with the reconstruction error serving as an indicator of legitimate degradation patterns versus noise. This ensured that the model retained essential degradation signals while mitigating the impact of noise.

Concurrently, meta-data from each flight test was meticulously documented. The dataset encapsulates variables such as the unique identifiers for the log, pilot, and battery, the initial

battery voltage, drone take-off and landing timestamps. Moreover, the dataset chronicles the number of laps completed counterclockwise along the predefined rectangular trajectory, as depicted in Figure 6.2. Furthermore, anomalies in flight patterns, like abrupt lateral deviations or vertical fluctuations, were also noted which could be further converted to the indicators for the flight stability characterization.

6.2 Flight test outcome

The manual flight test in the laboratory of this project has finally collected around 60 hours' effective log data of the F450 drone. The flight test operation was conducted from April-2023 until end of August-2023 by the multiple pilots within the ATMRI group and the supervisor who stand beside pilot for the security alert and data recording purpose also contributed throughout the test process.

The recent series of tests revealed critical reliability issues in the system, manifesting as a trifecta of failures. As shown in Figure 6.3, the gimbal responsible for transmitter control (as in dictated as (a)) ceased functioning around the 30-hour mark, with its legacy status and lack of usage history complicating diagnostics. Subsequently, at the 40-hour threshold, the battery connector (as in dictated as (b)) succumbed to abrasion and fatigue, indicating a potential oversight in material endurance. Finally, the flight controller's failure (as in dictated as (c)) after approximately 60 hours raises concerns about the overall system integrity, necessitating a comprehensive review of the design and maintenance protocols to enhance future test outcomes.

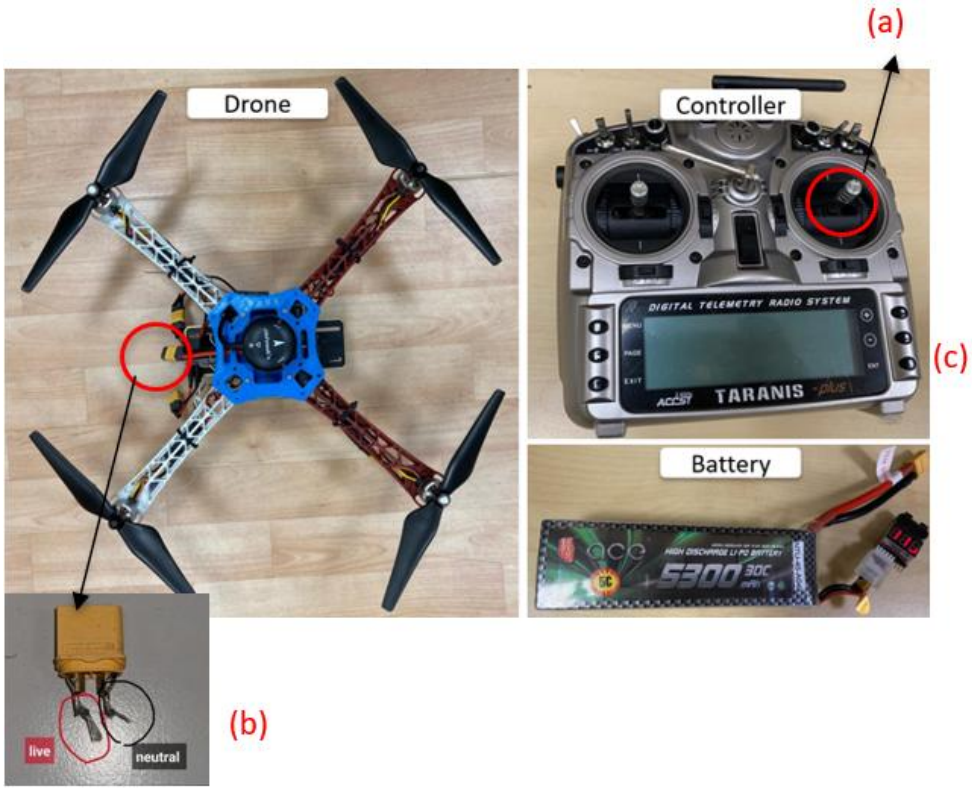

Figure 6.3: The F450 done failure event during the flight test.

Different from the testbed test in Chapter 5 which aims to generate multiple total failure data samples for the interested components, these full system event failure data samples provide meaningful reflection of the overall reliability properties of the drone used in the flight test.

6.2.1 Weibull model for the UAV failure event data analysis

Given the constraints of limited failure data samples from disparate components, it is imperative to adopt a methodological approach that accurately reflects the overall reliability of an Unmanned Aerial Vehicle (UAV) across its lifecycle. The Weibull Non-Homogeneous Poisson Process (NHPP) model [117] stands out as the preferred analytical tool for this purpose. It is particularly well-suited to our context, where the UAV's reliability assessment must incorporate data from three distinct failure incidents, each followed by repairs that only partially restore the system's functionality, thereby allowing the effects of wear and tear to accumulate progressively over time.

The inherent advantage of the Weibull NHPP model lies in its ability to handle non-constant

failure rates, which is a realistic reflection of the UAV's operational conditions [118]. Unlike traditional models that assume a constant failure rate, the Weibull NHPP acknowledges that the failure mechanisms evolve and the hidden failure rates vary as the UAV ages, and as it experiences different environmental conditions and operational stresses [119]. This model's flexibility to adapt to changing failure rates makes it an indispensable tool in forecasting the UAV's reliability, enabling a more robust and comprehensive understanding of its performance and maintenance needs.

6.2.2 Weibull NHPP model fitting and results.

Two types of NHPP structures were selected for comparison of their performance. On is Power Law Weibull NHPP model and another one is Polynomial Weibull NHPP model.

The Power Law Weibull Non-Homogeneous Poisson Process (NHPP) model refines the approach to reliability analysis by incorporating the principle that the failure rate does not remain constant but instead follows a power law relationship with respect to time [120]. This model posits that the rate of failure escalates or decelerates proportionally to time raised to a certain exponent. In essence, this exponent, often referred to as the shape parameter in the Weibull distribution, dictates the trend of the failure rate: if the shape parameter is greater than one, the failure rate increases over time, indicating a wear-out mechanism, while a value less than one suggests a decreasing failure rate, often associated with an initial 'burn-in' period.

In the context of UAV components, where the effects of aging, environmental wear, and operational stress dynamically alter reliability, the Power Law Weibull NHPP model enables a nuanced understanding of how these factors influence failure rates. By fitting the model to empirical data—such as the three documented failure incidents—it becomes possible to discern the underlying failure pattern, whether it be a gradual degradation or intermittent faults. This modelling is critical for predicting future reliability, scheduling preventive maintenance, and improving UAV designs to mitigate the identified risks.

The detailed equations of the Power Law Weibull Non-Homogeneous Poisson Process are presented in the following part.

Reliability function:

$$R(t) = \exp(\Lambda(t)) = \exp(-\alpha t^{\beta}) \tag{6.1}$$

Failure rate function:

$$\lambda(t) = \alpha\beta t^{\beta-1} \tag{6.2}$$

Expected cumulative number of failures upon time *t*:

$$\Lambda(t) = \alpha t^{\beta} \tag{6.3}$$

Based on the equations listed above, the actual parameters and fitted reliability functions are as shown in the following:

Reliability function:

$$R(t) = \exp(-4.879 \times 10^{-5} \times t^{1.349}) \tag{6.4}$$

Failure rate function:

$$\lambda(t) = 4.879 \times 10^{-5} \times 1.349 \times t^{0.349} \tag{6.5}$$

Expected cumulative number of failures upon time *t*:

$$\Lambda(t) = 4.879 \times 10^{-5} \times t^{1.349} \tag{6.6}$$

The Polynomial Weibull Non-Homogeneous Poisson Process (NHPP) model extends the capabilities of reliability analysis by describing the change in failure rate over time with a polynomial function [121]. This model is particularly adept at capturing complex behaviours of systems where the failure rate (λ) does not follow a simple linear or exponential trajectory but may exhibit a variety of patterns—increasing, decreasing, or stabilizing as time progresses.

In this model, the polynomial function, typically a sum of powers of time with corresponding coefficients, is used to fit the observed failure data. The degree of the polynomial—whether it is a quadratic, cubic, or higher degree—reflects the complexity of the system's failure dynamics. For example, a quadratic function can model a scenario where the

failure rate initially decreases, reflecting early detection and rectification of faults, before increasing due to aging and wear. A cubic or higher-degree polynomial can model more intricate behaviours, such as a failure rate that decreases, then stabilizes, and finally increases.

Applying the Polynomial Weibull NHPP model to the UAV's failure data allows for a comprehensive depiction of how its components' reliability evolves throughout its operational life. This is crucial for pinpointing periods of increased risk of failure, thereby informing targeted interventions, optimizing resource allocation for repairs, and ultimately enhancing the UAV's design for resilience against complex failure patterns.

The detailed equations of the Polynomial Weibull Non-Homogeneous Poisson Process are presented in the following part.

Reliability function:

$$R(t) = \exp\left(-\alpha t - \beta t^2\right) \tag{6.7}$$

Failure rate function:

$$\lambda(t) = \alpha + 2\beta t \tag{6.8}$$

Expected cumulative number of failures upon time *t*:

$$\Lambda(t) = \alpha t + \beta t^2 \tag{6.9}$$

Based on the equations listed above, the actual parameters and fitted reliability functions are as shown in the following:

Reliability function:

$$R(t) = \exp\left(-5.015 \times 10^{-4} \times t - 9.632 \times 10^{-8} \times t^2\right) \tag{6.10}$$

Failure rate function:

$$\lambda(t) = 5.015 \times 10^{-4} + 2 \times 9.632 \times 10^{-8} \times t \quad (6.11)$$

Expected cumulative number of failures upon time *t*:

$$\Lambda(t) = 5.015 \times 10^{-4} \times t + 9.632 \times 10^{-8} \times t^2 \quad (6.12)$$

The F450 drone's corresponding reliability and failure rate development feature over the 60 hours' test time period is displayed in Figure 6.4. Upon examining the reliability and failure rate over time, it has been observed that both metrics exhibit non-linear progression, eschewing a straightforward path in favour of more complex patterns. When plotted, the reliability curves derived from both models bear a striking resemblance in shape, suggesting a degree of synchronicity in the overall reliability trends they predict. However, a discernible divergence appears in the failure rate curves, particularly noticeable at the extremities of the timeline. In the nascent stages, the initial failure rates differ significantly, potentially due to initial quality variances or 'burn-in' effects. Conversely, in the later periods, the models predict contrasting failure rate trajectories, which could be indicative of varying degrees of wear-out mechanisms or maintenance effectiveness as the system matures. This bifurcation in trend underscores the complexity of the system's failure dynamics and highlights the criticality of time-specific analysis in understanding and forecasting reliability.

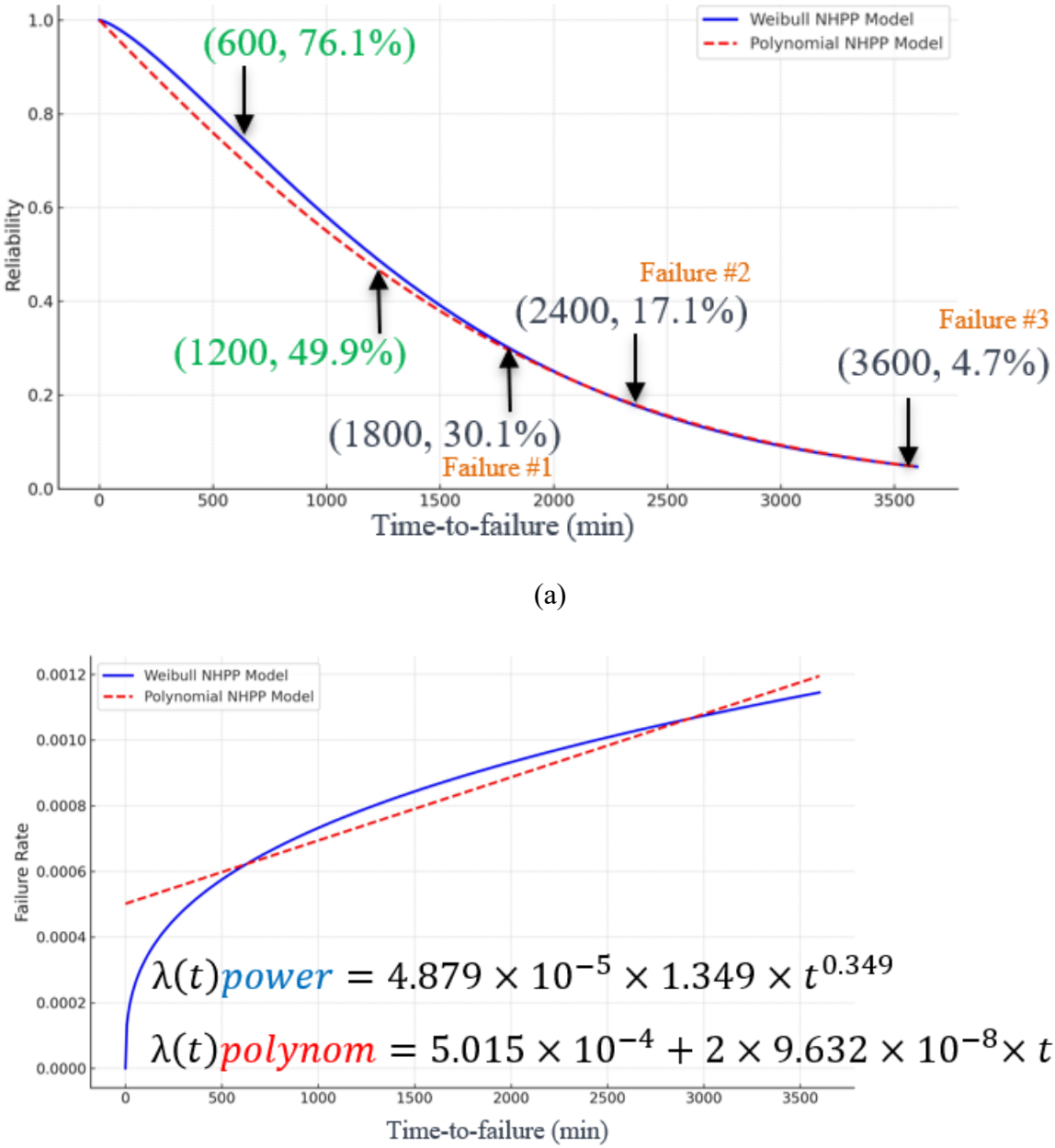

Figure 6.4: F450 drone reliability development over cumulative flight time: (a) Reliability curve; (b) Failure rate curve.

6.3 Exploratory data analysis of the flight test log data samples

The primary objective of this flight test is to evaluate the real-time degradation patterns within the propulsion system. Following the completion of the test flight, meticulous efforts in data collection, cleansing, and processing will have been executed. It is then imperative to engage in exploratory data analysis (EDA) on the refined dataset. Conducting EDA is a critical

step that serves as a prelude to the actual modelling work, as it provides an initial inspection and understanding of the data's characteristics [122]. This preliminary examination is instrumental in identifying trends, detecting anomalies, and understanding the data's underlying structure, thereby informing the subsequent modelling approach, and ensuring that the analysis is grounded in a robust understanding of the dataset's nuances.

This subsection has selected several representative parameters groups to show the physics feature behind the flight log data. The selected data sample is a flight test for about 10 mins.

6.3.1 Selected sensor data analysis individually and comparatively

Figure 6.5: The accelerometer temperature variation during the test.

As shown in Figure 6.5, the accelerometer's temperature increased quickly after the drone was armed, and it reached a relatively stable constant level after around 3 mins (200M timestamp value), as the green line indicated, which means the heat generation and dissipation come to a balance statement. A higher *Z* value represents the drone flying at a higher vertical space location than the start positions on the ground floor.

The dashed line circle indicated that two low-position record data points demonstrated a rapid temperature drop, indicating that when the drone came near the floor, the enhanced airflow from the floor reflection increased the heat exchange rate.

The solid line circled data points from a higher position (a more negative Z value) induced a sudden increased temperature. This phenomenon inspired that the flight height or the space gap between the drone and the nearby obstacle or floor affects the airflow and the heat dissipation. Thus, the heat load cycle and degrading damage, which can be accumulatively applied to the drone through multiple individual flight tests, would be different even though the flight time length is approximative.

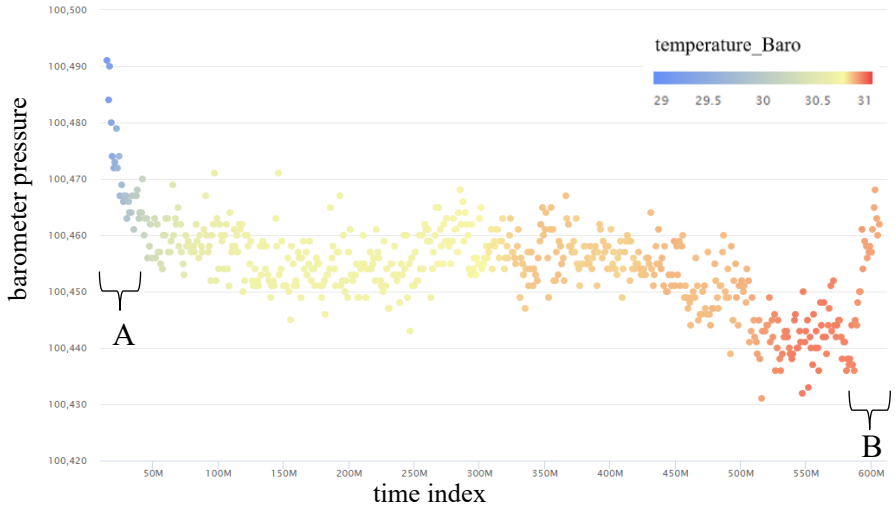

Figure 6.6: Barometer pressure and temperature.

Apart from the accelerometer signal readings, another sensor called a barometer which is used for UAV's height location detection. The pressure value would decrease when the height is increased. Figure 6.6 indicates that the temperature of the barometer is continuously increasing along the flight time. The pressure value is used as an indicator for height estimation. A hysteresis manner appeared when comparing the take-off period, A, and landing period B. Therefore, in future analysis, the barometer-based height estimation will be more accurate for the normal flight period.

The sampling frequency of the barometer and the accelerometer are the same. Therefore, the

comparative study of the parameters between such files is convenient. As Figure 6.7 shown that the temperature of both the barometer and accelerometer increased after the UAV took off. However, the heat build-up and temperature rise characteristics are diverse. This comparison plot also illustrated that the temperature variation of the accelerometer is much higher than the barometer. And the barometer's temperature continuously increases without a precise, stable period.

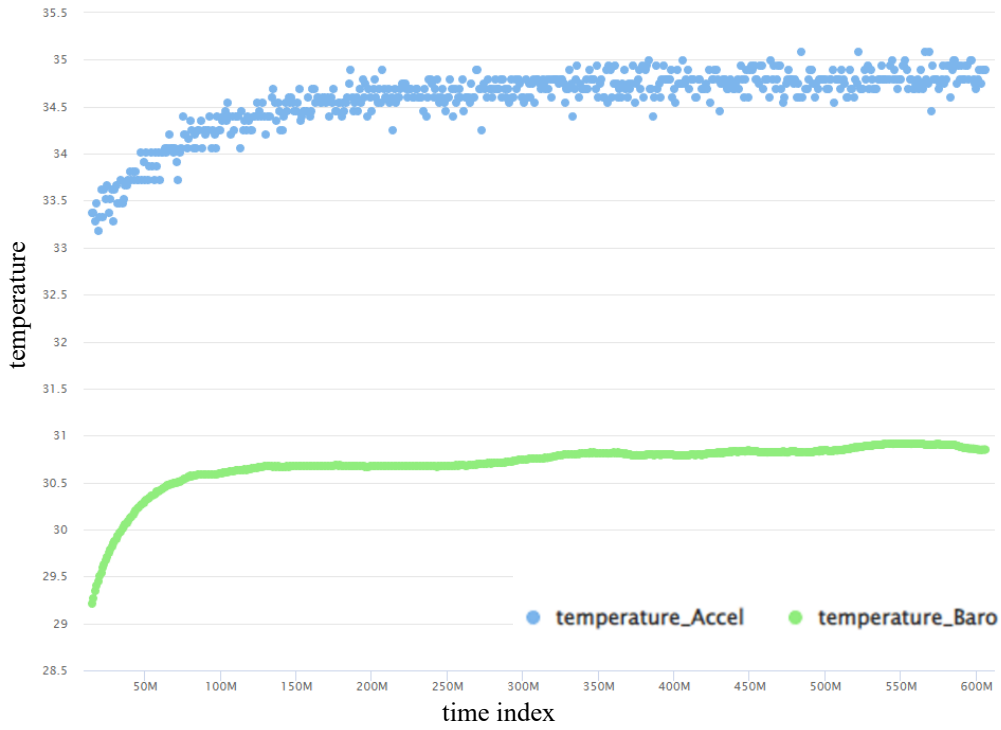

Figure 6.7: Temperature comparison between accelerometer and barometer.

A 3D plot can take four different parameters into consideration at the same time. Figure 6.8 aims to reflect the relationship of the parameters between the accelerometer and barometer. And such an intuitive 3D plot helps to understand the complex physics performance during the same test history.

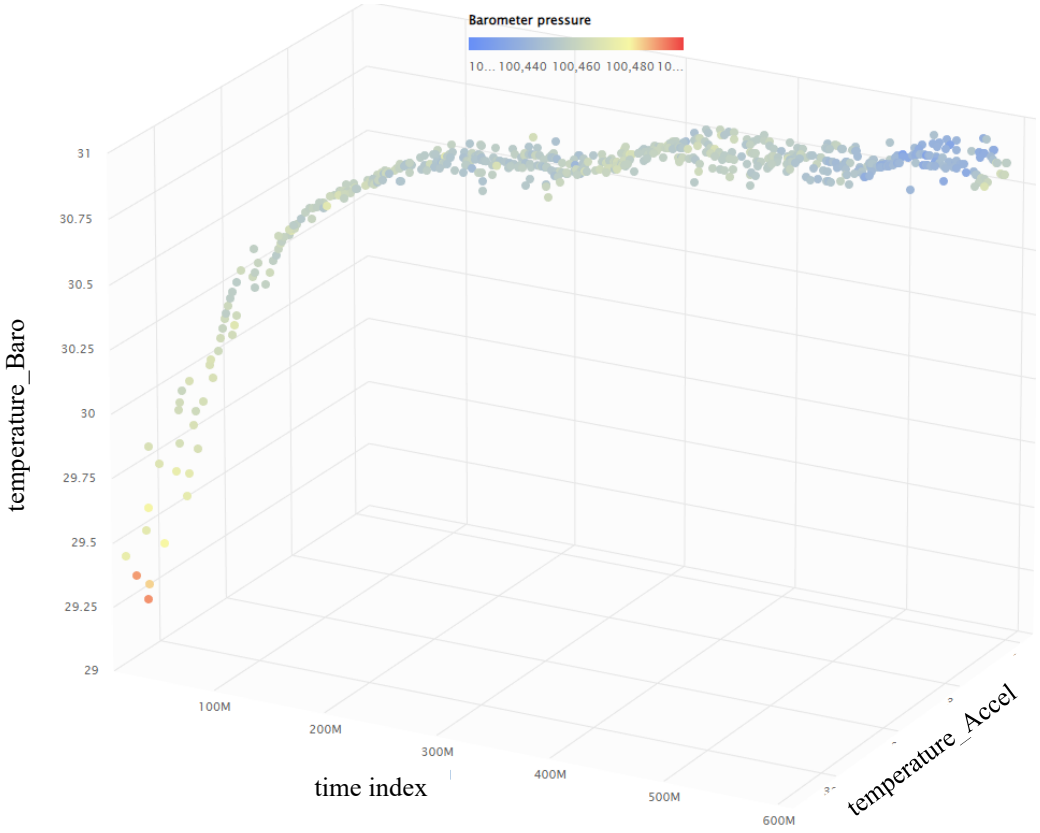

Figure 6.8: Relative features plot between barometer and accelerometer.

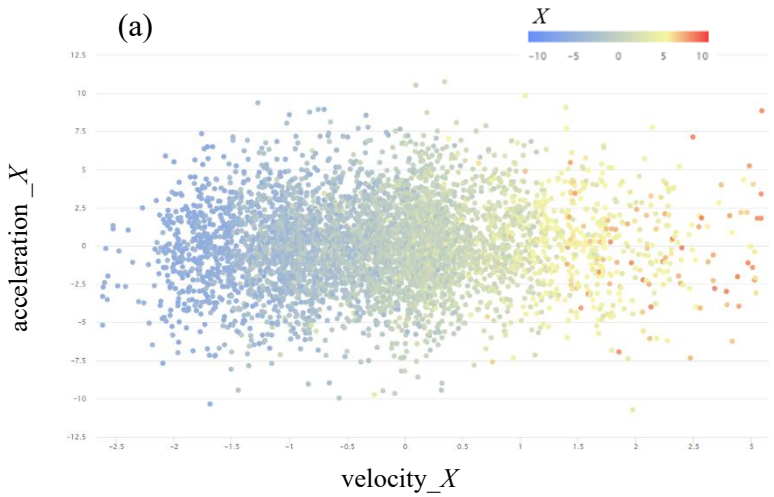

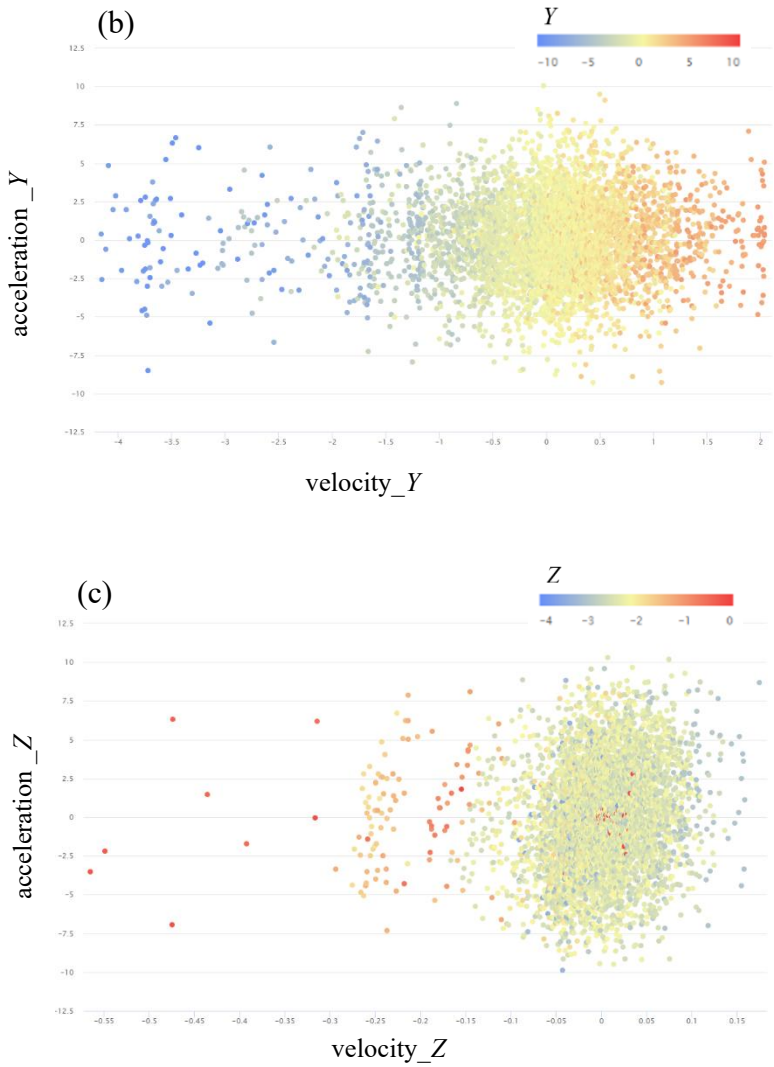

Figure 6.9: Position, velocity, and acceleration plot for (a) X; (b) Y; (c) Z.

The Figure 6.9 presents this typical rectangular route flight generated space location-related parameters comparison between the *X*, *Y*, and *Z* directions. It can be found that the velocity and acceleration instant values in the *X* direction are distributed more uniformly than the other two. The velocity and acceleration values in *Y* and *Z* directions gathered close around the 0 mean value correspondingly. Therefore, such parameters' distribution in *Y* and *Z* directions are suitable for evaluating the overall stability of a particular flight. And this kind of information could be potentially effective input for future UAV performance degradation analysis.

The next critical component of a drone is the battery which provides all the power supply.

The battery's output voltage and average current value are plotted in Figure 6.10, along with the timestamp. The highest power output happens in the take-off period. The average current was reduced to very low during the stable flight. Therefore, the electricity supply-induced degradation calculation to the propulsion system (here means, the motors) is more affected by the take-off period with a high current value. The voltage and current decreasing characteristics are relative to the battery health. When enough life-to-failure test data samples are available, such parameters can be used to build up the battery degradation and failure prediction model.

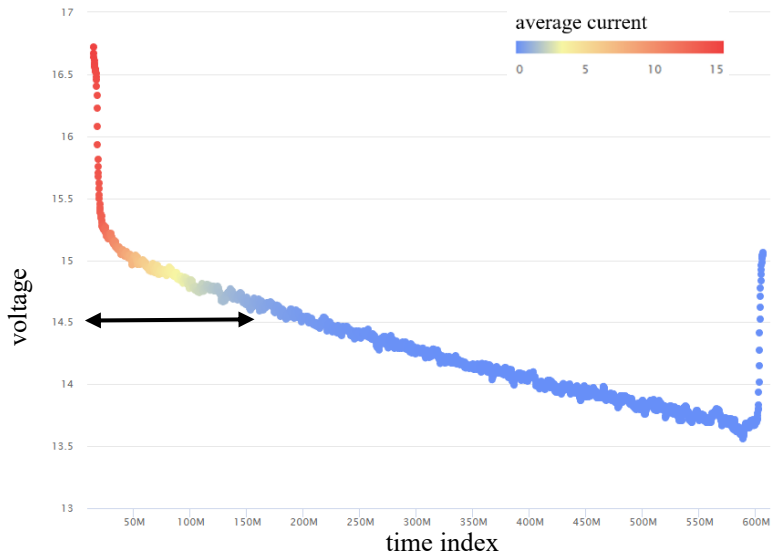

Figure 6.10: Battery performance during the flight test.

6.3.2 Data fusion for cross-sensor data integration and analysis explore.

The aforementioned investigation plots are all based on the groups' parameters with the same sampling frequency respectively. In order to analyse the different sensors' effects on each other, this study applied an interpolation method to realize the data resampling between multiple sensors.

Taking this 10 mins log data set as an example, the data recording samples' number of acceleration sensor parameters and X, Y, and Z position information is 592, while the battery-related information samples' number is 2963. The proposed interpolation method can be used to increase the low data file (containing 592 samples) to match the high one (containing 2963

samples) to realize the data fusion and analysis efficiently.

The interpolation method by Oh et al. [123] used in this analysis is linear interpolation as an initial exploratory attempt. There are different methods that can be used for data integration. The choice of such a method depends on the nature of the target data and the specific requirements of the analysis [124]. Generally, the linear approach is a good choice for data that has a relatively smooth variation between consecutive data points. It assumes that the rate of change in the data is constant between two data points. Other methods, such as the nearest interpolation, can be used to fill the missing values with the nearest non-missing value in the data, and this is useful when the data has sudden changes or discontinuity properties.

In contrast, the quadratic method can perform quadratic interpolation, which considers the curvature of the data. It can be helpful when the data has a quadratic trend. And when the data trend becomes more complex, methods such as cubic or nearest-neighbour interpolation are also potential good choices. In practice, trying different interpolation methods and comparing the results is often a good idea to determine which method works best for a particular dataset and analysis.

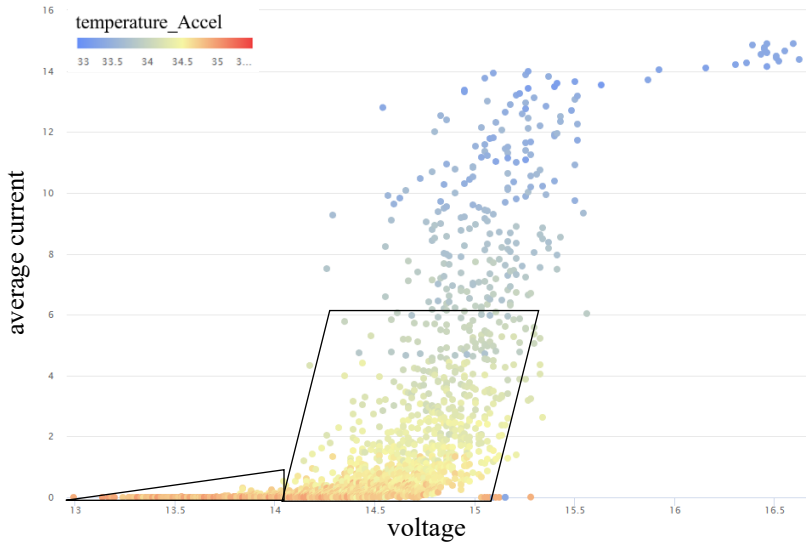

Figure 6.11: Example plot of resampling the multi-frequency signal data by interpolation.

Figure 6.11 demonstrates the cross-subsystem analysis capability between the

accelerometer and the battery. Based on this data fusion approach, additional valuable data mining explorations are feasible. For example, within this plot, when investigating the motor's majority operation conditions which has a low average current, some particular map areas could be drawn to establish the normal operation library. Therefore, when some data samples fall outside the normal area too much, the alarm could be triggered by the predefined threshold principles. And another benefit is that the more effective sensor' data integrated, the better the future data-driven model could be trained.

6.4 LSTM based UAV performance degradation modelling and prediction.

Leveraging the extensive and rich dataset garnered from actual flight operations, the potential of advanced deep learning algorithms to decipher hidden patterns within the intricate temporal trends of sensor data is considerable. Monitoring the nuanced degradation of a complex system like a UAV poses a substantially greater challenge than the detection of outright system failures [125]. The subtlety of the system's health state deterioration, characterized by incremental changes over time, is markedly less pronounced and therefore more elusive than the binary nature of failure events. It requires a discerning approach to distinguish these minor yet critical variations in performance.

To address this nuanced challenge, the Long Short-Term Memory (LSTM) autoencoder algorithm has been developed and tailored by Azimi et al. [126] to model the gradual decline in the UAV's functionality in a quantitative manner. The LSTM autoencoder is adept at capturing the temporal dependencies and intricacies within sequential data, making it particularly suitable for identifying the early signatures of wear and tear that precede a system's failure. By encoding the complex sensor data into a lower-dimensional representation, the LSTM autoencoder can effectively reconstruct the input data, allowing for the detection of anomalies that signal degradation. This approach enables the proactive maintenance of the UAV, ensuring operational integrity and extending the lifecycle of its critical components.

6.4.1 Methods to enhance LSTM autoencoder performance.

Focusing on enhancing LSTM autoencoder performance for UAV health monitoring, particularly through the analysis of flight test periods such as take-off, normal cruising flight, and landing, leads to delving deeper into three pivotal methodologies: Attention Mechanisms, Hyperparameter Tuning, and Regularization.

1. Attention Mechanisms:

Attention mechanisms allow the LSTM autoencoder to dynamically focus on specific segments of the input sequence that are more crucial for the task at hand—such as the distinct phases of a flight test [129]. This is particularly beneficial for understanding and monitoring the UAV's health state, as it enables the model to allocate more processing power to the periods with higher likelihoods of anomaly occurrence or significant operational stress.

Implementation: In the context of flight tests, an attention layer can be incorporated into the LSTM autoencoder to weigh the input data differently. The mechanism assigns higher weights to the data points corresponding to critical flight phases, such as take-off and landing, where the propulsion system undergoes significant stress.

Equations: The attention scores (α_{tj}) are calculated by comparing the relevance of each input timestep to the current decoder timestep j to the current decoder timestep t, often using a SoftMax function to normalize these scores.

$$\begin{aligned} \alpha_{tj} &= \frac{\exp(e_{tj})}{\sum_{k=1}^{T} \exp(e_{tk})} \\ c_t &= \sum_{j=1}^{T} \alpha_{tj} h_j \end{aligned} \tag{6.13}$$

Where c_t represents the context vector for timestep t, incorporating information from the most relevant parts of the input sequence.

2. Hyperparameter Tuning:

Hyperparameter tuning is crucial for optimizing the LSTM autoencoder's performance. It involves adjusting parameters such as the number of LSTM layers, the number of units in each

layer, learning rate, and batch size to improve the model's ability to generalize from training to unseen data. Grid search, random search, and Bayesian optimization are popular methods for hyperparameter tuning. Bayesian optimization, in particular, is efficient for LSTM autoencoders as it balances exploration (testing new parameters) and exploitation (refining parameters close to those already performing well).

Properly tuned hyperparameters can significantly enhance the model's sensitivity to anomalies during different flight phases, improving both detection accuracy and computational efficiency.

3. Regularization:

Regularization techniques are employed to prevent overfitting, ensuring that the LSTM autoencoder generalizes well to new, unseen flight data.

Dropout: Introducing dropout layers randomly disables a fraction of the neurons during training, which helps in making the network less sensitive to the specific weights of neurons [130]. This is crucial for LSTM autoencoders as it promotes the learning of more robust features that are invariant across different flight phases.

$$L_{reg} = \lambda_1 \sum |w| + \lambda_2 \sum w^2 \tag{6.14}$$

Where λ_1 and $\lambda_2$are the regularization strengths for L1 and L2 regularization, respectively.

Implementing these techniques thoughtfully will enable the LSTM autoencoder to not only accurately model the UAV's operational health across various flight test periods but also to generalize effectively to new flight data, enhancing the UAV's reliability and operational safety.

6.5 LSTM model development and prediction for the UAV performance degradation

In this investigation, the instantaneous Pulse-Width Modulation (PWM) sensor readings for the F450 drone's rotors from the log files were meticulously extracted. Each rotor was

monitored through four distinct sensor readings, as delineated in Figure 6.12. The chronological integration of the flight test data is depicted in Figure 6.13, wherein the dataset was methodically partitioned for model training, validation, and testing phases. Specifically, the first 72% of the dataset was allocated for training purposes, the subsequent 8% for model validation, and the remaining 20% was reserved for the testing phase.

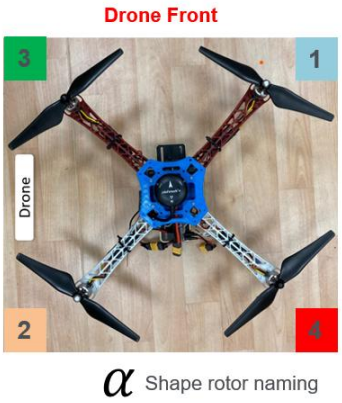

Figure 6.12: Experiment drone rotors' naming.

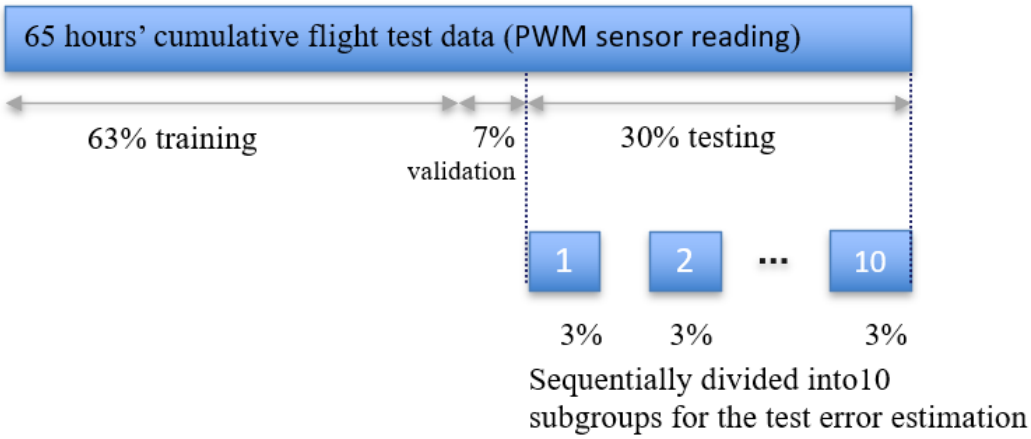

Figure 6.13: Overall data split set up for the model training and test.

Leveraging the advanced methodologies outlined in section 6.4, the LSTM autoencoder model's learning efficacy is visually represented in Figure 6.14. This study innovatively segmented the time series PWM sensor readings into 10 discrete subgroups, facilitating a granular error estimation approach. The model's output, showcasing the actual versus predicted sensor readings, is illustrated in Figure 6.15. Here, the Mean Absolute Error (MAE) in signal reconstruction for each motor is graphically represented through error density plots, with each

rotor's signal uniquely identified by colour and number.

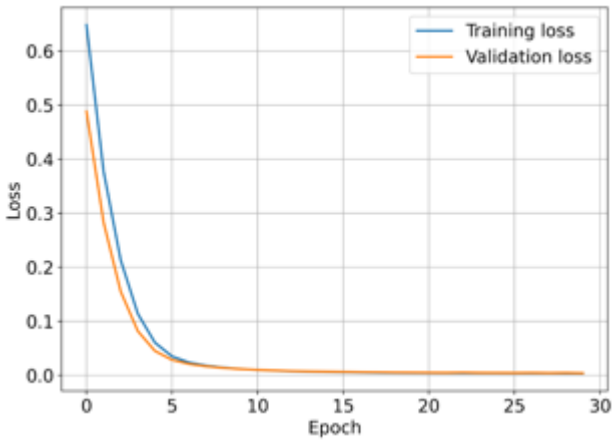

Figure 6.14: The loss curve plot of the LSTM model's training and validation.

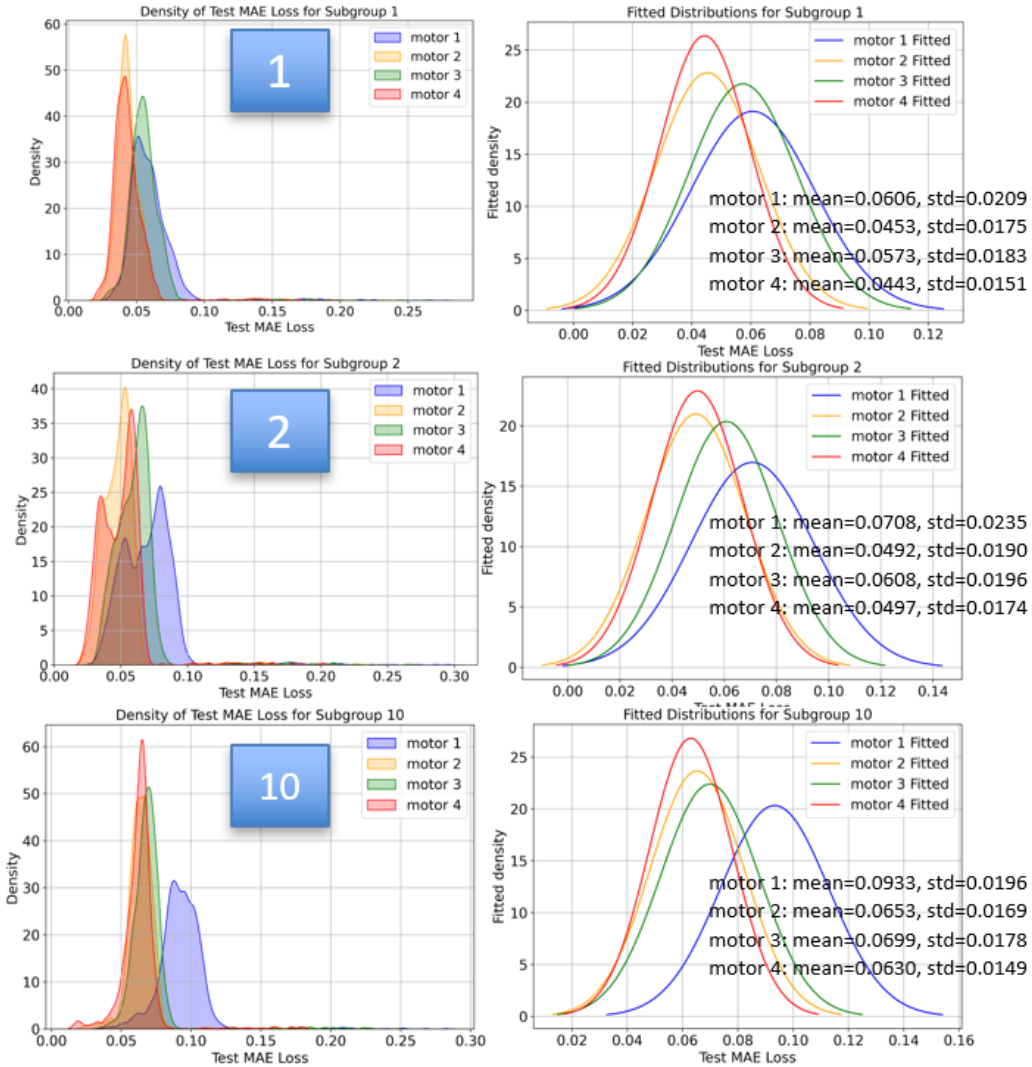

Figure 6.15: LSTM model predicted individual rotor's degraded value distribution and evolution over the flight test time period (show case for subgroup 1, 2 and 10 as examples)

The training of the deep learning model in this study was performed on a PC equipped with a 12th Generation Intel® Core™ i9-12900 processor, operating at 2.4 GHz, complemented by 32 GB of RAM, and powered by an NVIDIA GeForce RTX 3060 graphics card. And each training task will cost 4.5 days.

Furthermore, to elucidate the degradation patterns associated with each rotor, Normal distribution models were implemented to fit the error values corresponding to rotor degradation. Figure 6.15 also encapsulates the distribution curves, alongside their mean values and standard deviations, offering a comparative analysis of each rotor's performance deterioration. This detailed representation not only underscores the model's precision in capturing the nuanced degradation signals across different rotors but also highlights the potential of LSTM autoencoders in predictive maintenance and system reliability enhancement.

6.5.1 Performance Metric Evaluation

To evaluate the effectiveness of the LSTM autoencoder in predicting the Remaining Useful Life (RUL) of UAV components, the following metrics were used: accuracy, precision, and recall. These metrics ensured a comprehensive assessment of the model's performance across both degradation detection and RUL estimation tasks.

- Accuracy measured the overall correctness of the model's predictions, calculated as the ratio of correctly predicted values (both degradation and non-degradation states) to the total number of predictions. The high accuracy achieved during validation demonstrated the model's capability to generalize well across unseen datasets.
- Precision evaluated the proportion of true degradation events correctly identified by the model to the total number of degradation events predicted. By minimizing false positives, this metric ensured that maintenance interventions were triggered only for legitimate degradation events, optimizing resource allocation.
- Recall assessed the proportion of true degradation events identified by the model to

the total number of actual degradation events. High recall ensured that the model captured all potential failure patterns, minimizing the risk of undetected failures and ensuring operational safety.

6.5.2 Integration of Scalability and Performance Metrics

The proposed data-driven framework demonstrates significant scalability and adaptability to different UAV configurations and propulsion systems. The LSTM autoencoder's modular design allows it to generalize across varying datasets by focusing on universal features such as PWM sensor readings. Scalability is further enhanced through transfer learning, where the pretrained model can be fine-tuned for new UAV configurations with minimal retraining, requiring adjustments only to the final layers. This process reduces computational overhead while maintaining prediction accuracy. Additionally, the preprocessing pipeline, which normalizes input data across UAV types, ensures consistent model performance despite variations in sensor dynamics or operational conditions. These features make the framework well-suited for practical deployment in diverse UAV platforms.

The model's scalability is directly supported by its robust performance across diverse datasets. High precision ensures minimal false positives, while high recall guarantees that critical degradation events are captured, regardless of the UAV configuration. By leveraging transfer learning and dynamic error estimation, the framework can adapt to new UAV platforms with minimal computational effort. These scalability and performance features combined demonstrate the LSTM autoencoder's potential for practical deployment in predictive maintenance across various UAV systems.

6.5.3 Overfitting Mitigation Strategies

Given the high dimensionality of sensor data from UAV flight logs, addressing overfitting was a critical consideration during the development of the LSTM autoencoder model. The

following mechanisms were implemented to ensure the model's generalization capability and robust performance across diverse datasets:

1. Dropout layers were incorporated into the LSTM network during training. By randomly deactivating neurons, dropout layers prevent the model from relying excessively on specific weights, promoting generalization across unseen data. This approach builds on the preprocessing pipeline outlined in Section 6.1.3, ensuring high-quality inputs for the model.
2. L2 regularization penalized large weight values, effectively reducing model complexity and mitigating the risk of overfitting. This technique complements the dimensionality reduction methods described in Section 6.4.1, which condensed high-dimensional sensor data into latent representations for efficient modelling.
3. Attention layers dynamically prioritized critical segments of the input sequence, allowing the model to focus on high-impact data points, such as phases of flight exhibiting notable stress or anomalies. This aligns with the degradation analysis framework in Section 6.4.2, where attention mechanisms enhanced the interpretability and accuracy of predictions by emphasizing meaningful features.
4. Grid search and Bayesian optimization were employed to fine-tune hyperparameters such as the number of LSTM layers, learning rate, and batch size. These methods ensured a balance between model complexity and predictive accuracy, aligning with the optimization strategies outlined in Chapter 5, where experiments refined parameters for UAV component reliability testing.
5. Preprocessing techniques were applied to normalize sensor data across various UAV configurations, reducing noise and enhancing model generalization. This approach mirrors the standardization processes detailed in Section 6.1.3, where preprocessing addressed inconsistencies in sensor sampling rates and ensured data alignment.

6. Validation loss was monitored during training to detect overfitting. Early stopping was triggered when the model's performance on validation data plateaued or degraded, ensuring the network did not over-optimize on the training dataset. This strategy directly supports the reliability-focused model evaluation discussed in Section 6.5.1, where metrics like precision and recall assessed the model's ability to generalize effectively.

These strategies collectively ensured the LSTM autoencoder model maintained high predictive accuracy and reliability while minimizing overfitting. By leveraging these techniques, the framework addresses the challenges of high-dimensional UAV flight data and generalizes effectively to unseen scenarios. The connection between these strategies and the empirical findings in Chapter 3 (Failure Modes and Effects Analysis) and Chapter 5 (Run-to-Failure Experiments) reinforces their practical relevance in improving UAV performance degradation modelling.

6.6 Implementation potential of the developed UAV degradation prediction model

By leveraging data from an environment closely simulating real-world operational stresses, the LSTM autoencoder model validated its degradation predictions. This methodology ensures that the insights gained are not only theoretically robust but also practically relevant for UAV fleet management.

In a detailed examination of the UAV's degradation patterns over its service time, the error values derived from the 10 subgroups were meticulously plotted in Figure 6.16. Each data point within this plot represents an aggregate sum of the degradation values across all four rotors, providing a comprehensive view of the UAV's overall health status. To further elucidate the UAV's degradation trajectory, a regression analysis was employed, skilfully fitting these aggregated data points to a path curve. This curve not only delineates the UAV's degradation

properties over time but also serves as a critical tool for understanding the system's behaviour.

The regression-fitted curve offers invaluable insights, particularly in retrospectively analysing the UAV's early service stages. It highlights periods of minimal, yet significant, degradation that are typically challenging to detect through conventional monitoring techniques. This subtle degradation, although minor, can be pivotal in the early identification of potential system failures, thereby enabling pre-emptive maintenance actions.

The mathematical expression of the UAV's degradation path, as captured by the fitted curve, is articulated in Equation 6.15. This equation is a testament to the precision and robustness of the regression method applied, showcasing its capability to model complex degradation patterns effectively. Through this sophisticated analytical approach, the study presents a novel methodology for tracing and quantifying the UAV's degradation, even when it manifests in the most subtle forms. This advancement not only enhances the understanding of UAV health monitoring but also significantly contributes to the development of more resilient and reliable UAV systems.

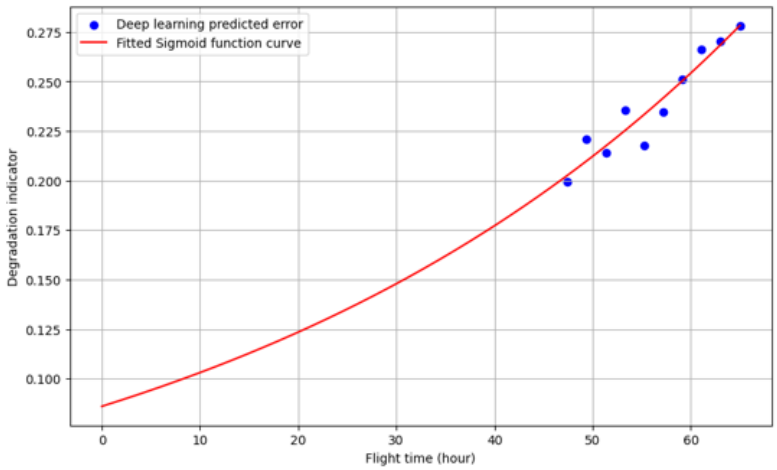

Figure 6.16: UAV degradation path regression and reverse prediction.

It could be estimated from the curve plot that the failure threshold value of the degradation indicator derived from this study is around 0.3 which is an important output for the actual application this deep learning model in the airworthiness.

A regression function was derived from the fitted curve as the following:

$$y = \frac{1641}{1+e^{(-0.02*(x-546))}} \tag{6.15}$$

The analysis reveals that the model's output, serving as a degradation indicator, is derived from signal data within a specified time window size. This implies that even a brief segment of data samples, potentially just a few seconds' worth of PWM signals from the drone motors, can be effectively utilized for estimating the degradation state when processed through the trained LSTM model. This capability is visually demonstrated in Figure 6.7, where a succinct record of PWM signals is sufficient to assess the current health state of the UAV.

Crucially, this approach enables the identification of early signs of degradation with minimal data, underscoring the efficiency and sensitivity of the LSTM model in detecting subtle changes in the system's performance. The concept of a 'Degradation Redundancy Indicator' emerges as a pivotal metric in this context. It signifies the threshold beyond which the system's degradation is considered significant enough to warrant attention. When the indicator suggests that the degradation has not reached a critical level, an alert mechanism can be triggered to inform the air traffic management controller, ensuring timely intervention.

The determination of the precise alarm trigger level is a nuanced process that requires a balance between sensitivity (to avoid false alarms) and specificity (to ensure true degradation signals are not missed). The setting of this trigger level, as suggested by the preliminary results, demands further experimental study within the continuation of this project. Such investigations will refine the alarm system, optimizing it for practical implementation, thereby enhancing UAV operational safety and reliability through proactive health monitoring.

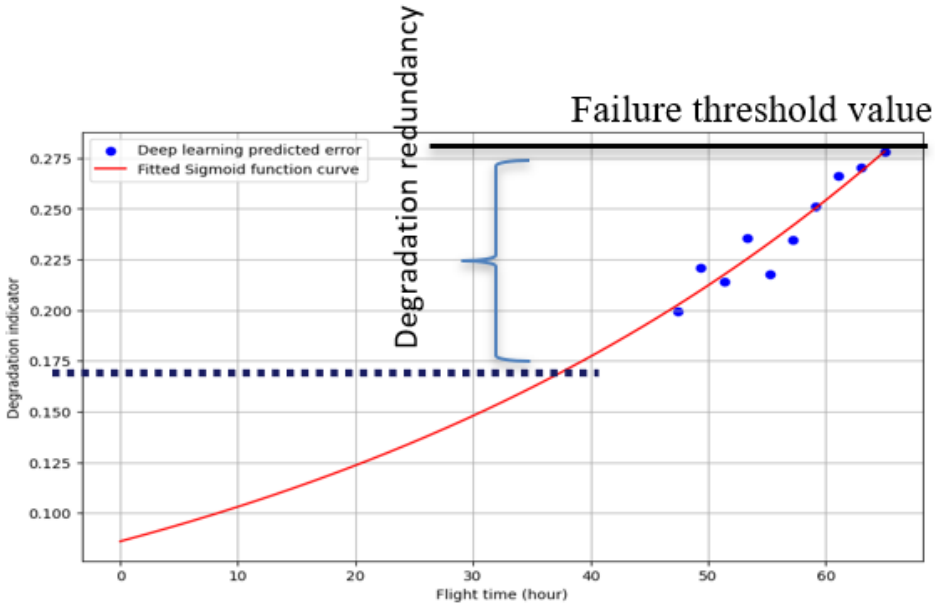

Figure 6.17: Short term available data as input to estimate the health stage of a UAV.

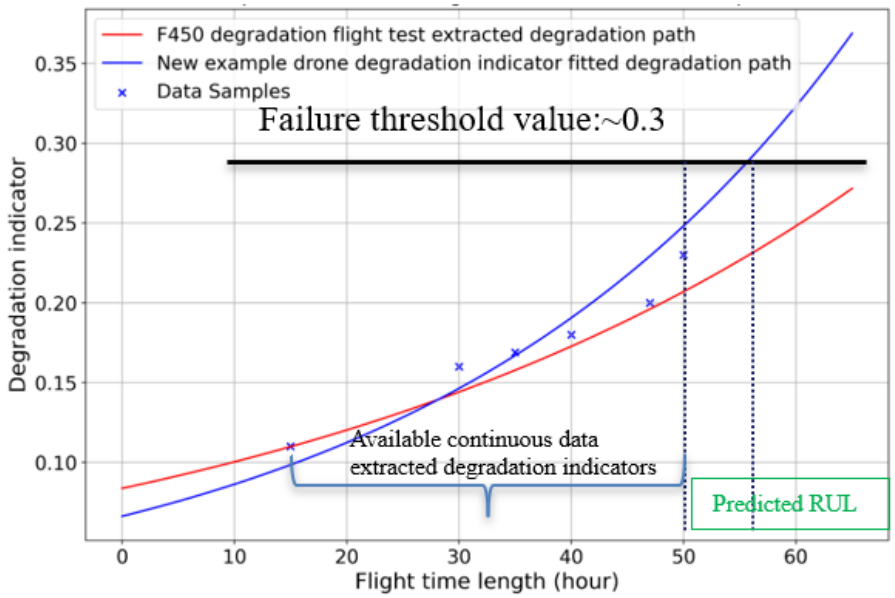

Figure 6.18: Long-term available data as input to estimate the RUL of a UAV

In scenarios where the volume of sensor data from a UAV is substantial, exemplified by a dataset spanning flight durations between 15 and 50 hours as illustrated in Figure 6.18, the approach delineated in section 6.5 can be adeptly applied to process this data. By following the outlined methodology, new data points, depicted in blue in Figure 6.15, can be extracted. These data points serve as a foundation for constructing a customized degradation path curve tailored to the specific UAV under consideration. This curve, representing the UAV's degradation

trajectory over time, intersects with a predefined degradation indicator threshold, set at 0.3 in this instance, to yield a critical time length value, denoted as t_2.

This intersection point is of paramount importance as it facilitates the estimation of the UAV's Remaining Useful Life (RUL). By subtracting the current time length value, t_1, which in the given example is 50 hours, from t_2, a quantified prediction of the UAV's RUL can be obtained. This predictive metric is invaluable for operational planning and maintenance scheduling, offering a proactive tool for managing UAV fleets more effectively.

Such an application of the developed model not only enhances the precision of maintenance forecasts but also contributes to optimizing the lifespan and reliability of UAV systems. By extending the utility of the model to encompass a broader dataset, stakeholders can derive actionable insights into the UAV's operational health, ensuring that interventions are both timely and based on robust data-driven evidence.

6.6.1 Method introduction

Building upon the foundational understanding of Long Short-Term Memory (LSTM) networks, the LSTM autoencoder serves as an advanced architecture for modelling time series data, particularly effective for the task of anomaly detection in systems such as UAVs [127]. Here's a more detailed dive into how the LSTM autoencoder operates on the principles of LSTM:

LSTM Autoencoder Composition:

LSTM Layers: At the heart of the LSTM autoencoder are the LSTM layers, which are structured to remember information for long periods. This is essential for capturing the prolonged degradation patterns in UAVs that unfold over time.

Sequence to Sequence Model: The LSTM autoencoder is a sequence-to-sequence model, meaning it takes a sequence as input and outputs a sequence. This is ideal for handling time series data such as sensor readings from a UAV.

Encoder:

The encoder compresses the input time series data into a fixed-size context vector. This vector is a representation of the entire input sequence, containing the learned information that is critical for reconstruction.

Decoder:

The decoder takes the context vector and generates an output sequence that aims to replicate the input sequence. The success of this replication process is indicative of the model's understanding of the normal operational patterns.

Training:

During training, the LSTM autoencoder learns to minimize the difference between the input sequence and the output sequence, effectively teaching itself to ignore noise and focus on the underlying pattern in the data.

Anomaly Detection:

Once trained on normal behaviour, the LSTM autoencoder can then be used to predict the next sequence of sensor data. When the actual data deviates significantly from the predicted sequence, it indicates a potential anomaly.

Mathematical Framework:

The mathematical framework of the LSTM autoencoder is based on the LSTM cell's ability to add or remove information to the cell state, carefully regulated by structures called gates:

- Input Gate: Decides which values to update.
- Forget Gate: Decides what information should be thrown away from the block.
- Output Gate: Decides what the next hidden state should be.

The autoencoder's objective is to learn a function $f(x) \approx x$, where x is the input sequence, and $f(x)$ is the reconstructed sequence from the autoencoder.

Error Function and Optimization:

The difference between the input sequence and the reconstructed sequence $\|x_t - f(x_t)\|$ is computed and reduced through optimization algorithms like Adam or RMSprop, which are well-suited for dealing with the vanishing and exploding gradient problems in LSTM networks as shown by Abbasimehr et al. [128].

By integrating the LSTM's capabilities within an autoencoder framework, the LSTM autoencoder becomes a potent tool for understanding and predicting the behaviour of complex time series data, which is essential for the early detection of degradation in UAV systems.

6.7 Notable failure

The flight testing concluded with a critical failure around the 65-hour mark, resulting in a crash. During this incident, the drone unexpectedly dipped, prompting the pilot to apply a corrective Z thrust. Instead of a controlled ascent, the drone abruptly flew into the ceiling. This major failure was systematically analysed using the flight log data.

The initial step involved examining the PWM inputs in relation to the accelerometer data, as depicted in Figure 6.19.

Figure 6.19: PWM vs Altitude Difference

The analysis revealed no significant anomalies in the PWM input data, indicating that PWM

input errors could be largely ruled out as the cause of the failure.

Subsequently, the focus shifted to the barometer data, specifically comparing the input values against the setpoint altitudes, as illustrated in Figure 6.20.

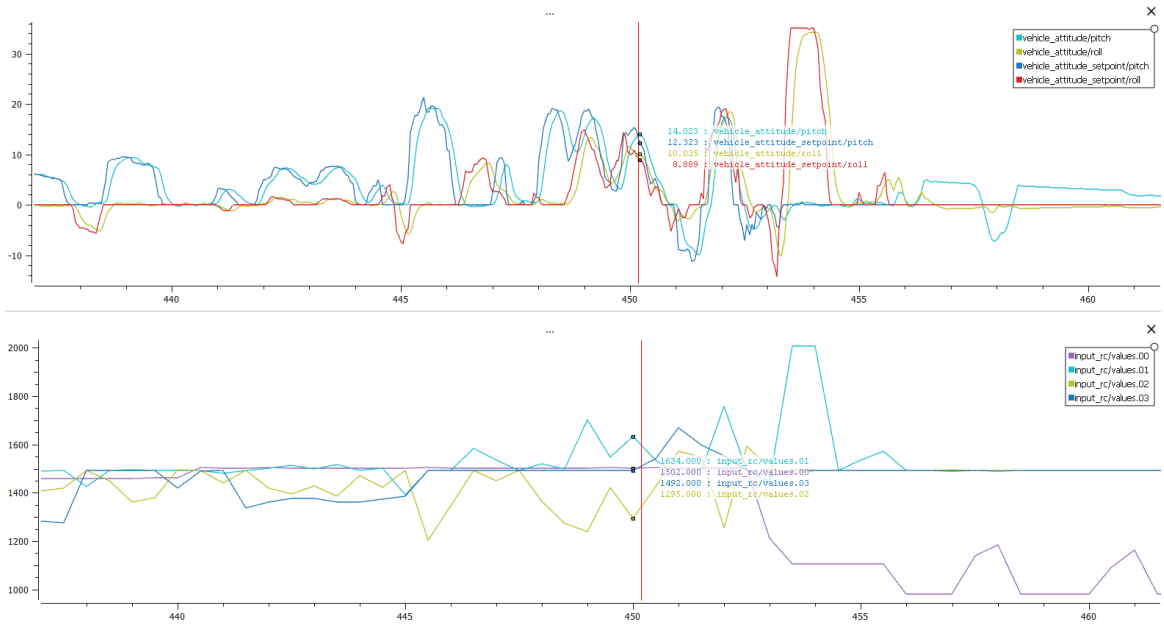

Figure 6.20: Input vs Setpoint Altitude

It was observed that despite high thrust values, there was a notably low reading in input_rc/02, prompting a detailed investigation into the hover thrust. A detailed analysis of hover thrust relative to vehicle positions was conducted, as shown in Figure 6.21.

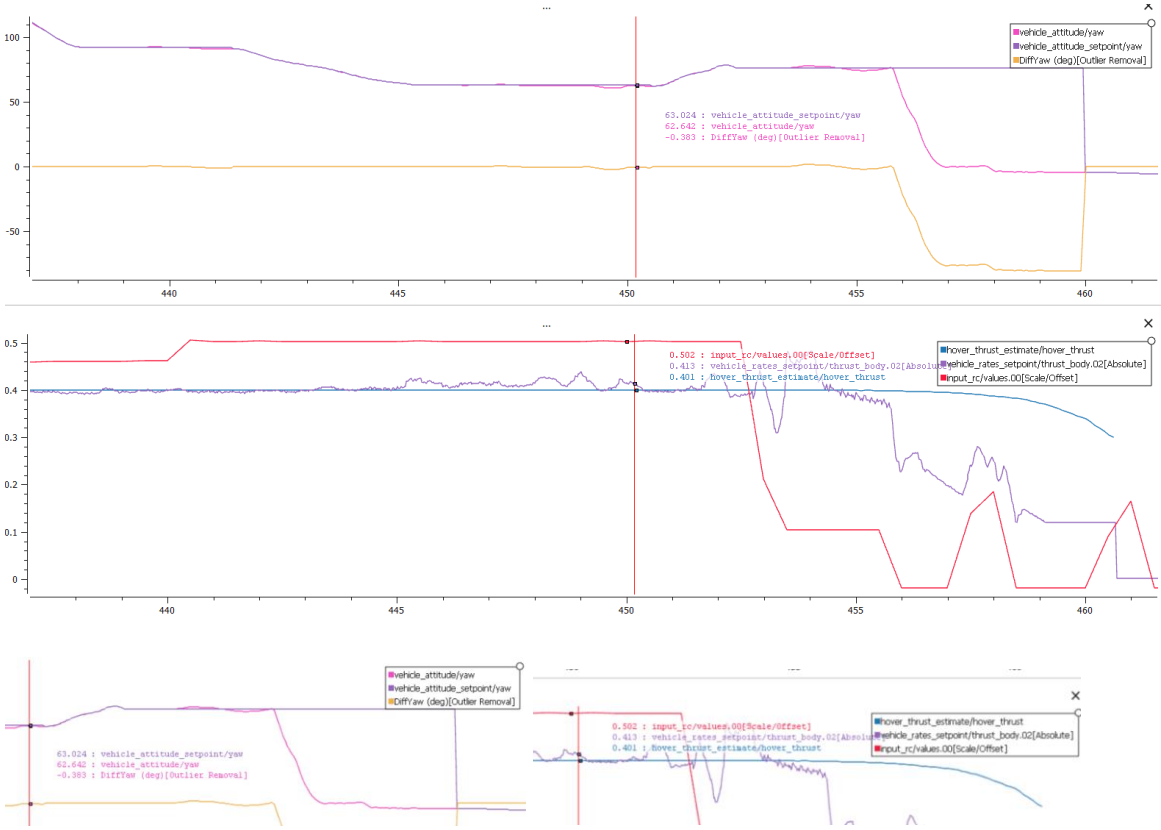

Figure 6.21: Input Setpoint Hover vs Vehicle Positions

The analysis indicated that despite no changes in thrust inputs, the drone experienced a sudden decrease in altitude. This irregular behaviour necessitated a closer examination of the hover thrust mechanism. The question arose as to why the drone abruptly lost altitude and then increased without any changes in thrust input.

Further analysis was conducted to correlate Z input for hover thrust with the drone's actual performance, as seen in Figure 6.22.

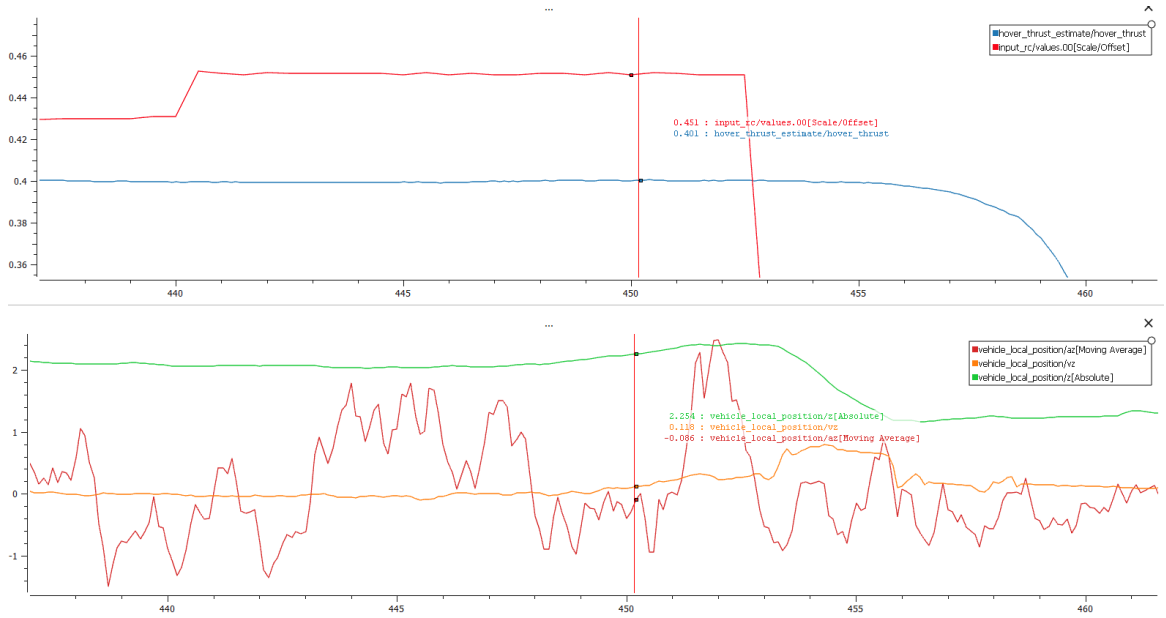

Figure 6.22: Z positions against Hover thrust.

This investigation revealed a significant deviation between the hover thrust Z input and the drone's real-world behaviour. This led to the identification of a communication signal error affecting the transmission of Z thrust commands. Specifically, there was an approximately 2-second delay between control inputs and the drone's responses, causing the erratic behaviour observed during the crash.

The analysis of this flight log highlights the challenges in identifying failure data, especially for non-obvious failures. It required approximately 5-6 man-hours to thoroughly analyse a single flight log and determine the root cause of the failure. Such detailed manual analysis is impractical on a large scale, particularly if UAVs are to operate daily in large numbers within civil airspace.

This incident underscores the critical need for real-time error correction and redundancy in UAV systems, particularly for drones that are commercially licensed for long-term flights. Implementing robust real-time monitoring and fail-safe mechanisms is essential to ensure the reliability and safety of UAV operations. This event highlights the absolute necessity of advanced diagnostic tools and real-time analytics to detect and correct errors promptly, thereby enhancing the overall safety and efficiency of UAV operations in civil airspace.

6.8 Conclusion

This work fills important gaps in conventional degradation modelling approaches by presenting a novel use of LSTM autoencoders for UAV health monitoring. The LSTM model captures complex dependencies in sensor data, allowing for reliable and accurate predictions of RUL, in contrast to traditional statistical or linear models, which frequently struggle with non-linear and time-dependent degradation patterns.

The model uses instantaneous Pulse-Width Modulation (PWM) sensor readings to assess the real-time degradation of UAV components. It utilizes a dataset that covers various flight durations to encompass a wide range of operational conditions. The development process of the model began with extracting sensor data from UAV log files, focusing on the PWM signals of the drone motors. This data was then systematically divided into training, validation, and testing sets, with a significant portion dedicated to training (72%) to ensure the model's robustness. Advanced techniques, such as Attention Mechanisms, Hyperparameter Tuning, and Regularization, were applied to enhance the model's ability to detect subtle degradation signals across different flight phases.

The LSTM autoencoder model was effective in identifying degradation patterns. The model output served as a degradation indicator based on segmented time window size signal data, enabling the estimation of the UAV's health state even from brief data segments. The model's predictive capability was demonstrated through the generation of a customized degradation path curve. This curve intersected with a predefined degradation indicator threshold to estimate the Remaining Useful Life (RUL) of the UAV. Key findings include the model's ability to effectively use brief data samples to estimate UAV degradation, highlighting its sensitivity and efficiency. The customized degradation path curve allowed for precise estimation of the UAV's RUL, demonstrating the potential of deep learning models in predictive maintenance. The chapter also emphasizes the significant contribution of the model to advancing predictive

maintenance strategies, offering a proactive approach to UAV fleet management.

The development and application of the LSTM autoencoder model represent a significant advancement in UAV health monitoring. By enabling early detection of system degradation and accurate prediction of RUL, the model serves as a pivotal tool in enhancing the reliability, safety, and operational efficiency of UAV systems. This chapter not only demonstrates the model's technical prowess but also its practical implications, paving the way for future research and application in the broader field of UAV health management.

Chapter 7 Summary and future work

This chapter synthesizes the key contributions of the thesis, highlighting the advancements made in UAV reliability evaluation and airworthiness certification methodologies. The integration of statistical models, data-driven approaches, and experimental testing has enabled a robust framework for analysing UAV propulsion systems and other critical components.

The findings demonstrate the utility of combining Failure Mode and Effects Analysis (FMEA), Markov-chain modelling, and machine learning techniques to address reliability challenges in UAV operations. These methodologies contribute to a deeper understanding of failure mechanisms, enabling proactive maintenance and improved operational safety.

Looking forward, future work could expand upon this research by incorporating real-time reliability monitoring systems and exploring emerging technologies in UAV design and propulsion. Additionally, the methodologies developed here could be adapted for broader applications, such as autonomous systems and other areas requiring stringent reliability assessments. By building on the foundation laid in this thesis, the path toward safer and more efficient UAV operations in complex airspace systems can be further refined.

7.1 Summary

This thesis has undertaken a comprehensive study of the reliability and airworthiness of UAV propulsion systems to facilitate the licensing of UAV systems into Urban Airspace. The research contributions and their implications are summarized as follows:

Chapter 1 discussed the importance of UAV dependability in relation to urban air mobility (UAM). It made clear how crucial it is for UAV operations to be both safe and effective to meet the growing demands of various industrial applications. The research goals and the plan for accomplishing them were laid out in this chapter.

In Chapter 2, a comprehensive review of the literature was conducted to identify existing

gaps in UAV reliability research. Both qualitative and quantitative approaches were reviewed, such as FMEA, fault tree analysis, Weibull distribution, and Markov-chain techniques. The chapter stressed the need for empirical data and sophisticated modelling techniques to improve reliability assessments.

Chapter 3 provided a thorough Failure Modes and Effects Analysis (FMEA) of the UAV propulsion system's components. The study identified critical failure modes and assessed their likelihood and consequences, offering essential insights into the vulnerabilities of UAV propulsion systems. Notably, motor failures account for approximately 45% of total UAV failures. This analysis informed the design of experiments in Chapters 5 and 6 and facilitated the analysis of any failures during testing.

Chapter 4 presented a novel Markov-chain modelling framework for evaluating UAV controllability in the event of propulsion unit failures. This chapter illustrated how various failure scenarios impact UAV control and stability. The probability of maintaining control decreases exponentially with the number of simultaneous propulsion unit failures. The Markov-chain model demonstrated that UAVs could sustain flight with up to two propulsion unit failures but showed significant instability with three or more failures. The findings have significant implications for designing fault-tolerant UAV systems and developing autonomous recovery protocols to ensure safer operations in urban environments. Additionally, using real-world variables like different payloads helps regulators better plan and certify UAVs for urban airspace use.

Chapter 5 covered the design and execution of run-to-failure tests for UAV propulsion systems. The empirical data produced by these experiments is essential for validating reliability models. The mean time to failure (MTTF) for UAV motors was approximately 150 hours under normal operating conditions. The chapter utilized various modelling techniques, such as Weibull models and Artificial Neural Networks (ANNs), to analyse the gathered data and

forecast health indices and component failures. The modelling efforts highlighted the advantages and disadvantages of different strategies for capturing the patterns of UAV component degradation.

Chapter 6 focused on the degradation modelling of UAV performance using Long Short-Term Memory (LSTM) networks. The study developed predictive models for UAV component degradation by analysing flight test data. The application of LSTM networks demonstrated the potential of machine learning in forecasting UAV health, achieving an accuracy of 85% in predicting the remaining useful life (RUL). This capability is crucial for proactive maintenance and operational planning, reducing downtime by up to 30%.

Furthermore, in contrast to other studies in the field of UAV reliability, this thesis makes noteworthy contributions. Here is a summary of these contributions and their significance:

- In contrast to conventional research, which frequently concentrates on discrete methods, this study combines machine learning, Markov-chain modelling, and FMEA to produce a cohesive framework for assessing UAV reliability. This all-encompassing method improves safety and operational efficacy by enabling a more nuanced evaluation of UAV performance across various configurations and operational scenarios.
- Since many current models mainly rely on theoretical assumptions, a significant limitation in UAV reliability studies is the absence of empirical data. Through run-to-failure experiments and flight tests, this thesis fills that gap by producing vital datasets that support model validation and the creation of data-driven maintenance plans.
- By predicting motor failures with a 90% confidence interval using Weibull analysis, wear-out processes are found to be the most common cause of failure. This study also provides quantitative insights that were previously understudied in the field,

revealing that motor failures account for roughly 45% of all UAV failures.

- The use of degradation models based on LSTM represents a major advancement in UAV health monitoring. With an accuracy of 85%, these models successfully forecast component failures and Remaining Useful Life (RUL), allowing for prompt maintenance interventions, and greatly lowering the risk of in-flight malfunctions—a capability that was mainly lacking in earlier studies.
- The results of this study have applications in forming regulatory frameworks, especially in the assessment of dependability and airworthiness. The safer integration of UAVs into urban airspace is made possible by this study's resolution of important reliability issues, which aids in the creation of certification standards.

In conclusion, this thesis has significantly advanced the field of UAV airworthiness and reliability. Future research and practical applications can build on the methodologies and findings presented to further improve the safety and effectiveness of UAV operations in urban environments.

7.2 Future Work

In order to advance the research on UAV propulsion system reliability, several areas need to be explored further. Some of these ideas, which can be expanded upon from this thesis, have been listed below as well as some basic directions in which that research could progress.

1. Expansion of Failure Database:

   The lack of an extensive failure database restricts the scope of the current research. Subsequent research endeavours ought to concentrate on assembling comprehensive failure data from diverse UAV models and operational settings. Improving reliability models' robustness and accuracy will require this data.

2. Advanced Experimental Designs:

   While the run-to-failure experiments carried out in this work offer valuable preliminary

data, more advanced experimental configurations are required. To capture a wider spectrum of failure modes and their impacts, future experiments should involve different environmental conditions, different UAV configurations, and a wider range of operational scenarios.

3. Real-Time Health Monitoring Systems:

   An essential next step is to create real-time health monitoring systems that use sensor data to anticipate failures and issue early warnings. With the addition of more data, these systems ought to be able to learn adaptively and increase their prediction accuracy over time.

4. Enhanced Controllability Studies:

   The Markov-chain methodology applied in this research provides insights into UAV controllability under failure conditions as well as considering the factor of Varying Payloads. Future studies should explore considering other factors such as different failure progression rates, and the integration of autonomous recovery protocols.

5. Cross-Disciplinary Research:

   Cross-disciplinary research can greatly improve the airworthiness and reliability of UAVs. To tackle the complex problems in UAV reliability assessment, cooperation with specialists in materials science, aerodynamics, computer science, and regulatory affairs will be crucial.

By addressing these areas, future research can build on the foundational work presented in this thesis, contributing to the development of more reliable, safe, and efficient UAV systems for urban air mobility and other critical applications.

References

[1] Federal Aviation Administration, “Drones by the Numbers.” [Online]. Available: https://www.faa.gov/uas

[2] M. O’Donnell, “Investigation of UAS Accidents and Incidents,” *Retrieved FAA Off. Accid. Investig. Prev.*, 2017.

[3] T. Jiang, J. Geller, D. Ni, and J. Collura, “Unmanned Aircraft System traffic management: Concept of operation and system architecture,” *Int. J. Transp. Sci. Technol.*, vol. 5, no. 3, pp. 123–135, 2016.

[4] M. Silvagni, A. Tonoli, E. Zenerino, and M. Chiaberge, “Multipurpose UAV for search and rescue operations in mountain avalanche events,” *Geomat. Nat. Hazards Risk*, vol. 8, no. 1, pp. 18–33, 2017.

[5] S. S. Ahmed, G. Fountas, V. Lurkin, P. C. Anastasopoulos, M. Bierlaire, and F. L. Mannering, “The State of Urban Air Mobility Research: An Assessment of Challenges and Opportunities,” *Available SSRN 4341268*, 2023.

[6] D. P. Thipphavong *et al.*, “Urban air mobility airspace integration concepts and considerations,” in *2018 Aviation Technology, Integration, and Operations Conference*, 2018, p. 3676.

[7] P. D. Vascik, R. J. Hansman, and N. S. Dunn, “Analysis of urban air mobility operational constraints,” *J. Air Transp.*, vol. 26, no. 4, pp. 133–146, 2018.

[8] C. Al Haddad, E. Chaniotakis, A. Straubinger, K. Plötner, and C. Antoniou, “Factors affecting the adoption and use of urban air mobility,” *Transp. Res. Part Policy Pract.*, vol. 132, pp. 696–712, 2020.

[9] K. O. Ploetner *et al.*, “Long-term application potential of urban air mobility complementing public transport: an upper Bavaria example,” *CEAS Aeronaut. J.*, vol. 11, pp. 991–1007, 2020.

[10] P. Gonçalves, J. Sobral, and L. A. Ferreira, “Unmanned aerial vehicle safety assessment modelling through petri Nets,” *Reliab. Eng. Syst. Saf.*, vol. 167, pp. 383–393, 2017.

[11] European Aviation Safety Agency, *Concept of Operations for Drones: A Risk Based Approach to Regulation of Unmanned Aircraft*. European Aviation Safety Agency Cologne, Germany, 2015.

[12] R. K. Barnhart, D. M. Marshall, and E. Shappee, *Introduction to unmanned aircraft systems*. Crc Press, 2021.

[13] R. N. Rai, S. K. Chaturvedi, and N. Bolia, *Repairable systems reliability analysis: A*

comprehensive framework. John Wiley & Sons, 2020.

[14] J. C. Salazar, P. Weber, F. Nejjari, R. Sarrate, and D. Theilliol, "System reliability aware Model Predictive Control framework," *Spec. Sect. Appl. Probabilistic Graph. Models Dependability Diagn. Progn.*, vol. 167, pp. 663–672, Nov. 2017, doi: 10.1016/j.ress.2017.04.012.

[15] R. Billinton and M. Fotuhi-Firuzabad, "A reliability framework for generating unit commitment," *Electr. Power Syst. Res.*, vol. 56, no. 1, pp. 81–88, Oct. 2000, doi: 10.1016/S0378-7796(00)00104-8.

[16] A. Lisnianski and G. Levitin, *Multi-state system reliability: assessment, optimization and applications*. World scientific, 2003.

[17] R. Billinton and R. N. Allan, *Reliability evaluation of engineering systems*, vol. 792. Springer, 1992.

[18] E. M. Ng, K. Tan, T. T., and Q. Yu, "Survey of UA Risk Factors," ir Traffic Management Research Institute, Singapore, 2021.

[19] T. Darrah, J. Frank, M. Quinones-Grueiro, and G. Biswas, "A Data Management Framework & UAV Simulation Testbed for the Study of System-level Prognostics Technologies," *Annu. Conf. PHM Soc.*, vol. 13, no. 1, Art. no. 1, Nov. 2021, doi: 10.36001/phmconf.2021.v13i1.3030.

[20] B. Nystrom, L. Austrin, N. Ankarback, and E. Nilsson, "Fault tree analysis of an aircraft electric power supply system to electrical actuators," in *2006 international conference on probabilistic methods applied to power systems*, IEEE, 2006, pp. 1–7.

[21] G. P. Kladis, J. T. Economou, K. Knowles, A. Tsourdos, and B. A. White, "Digraph matrix reliability analysis for fault assessment for a UAV platform application. A fault-tree analysis approach," in *2008 IEEE Vehicle Power and Propulsion Conference*, IEEE, 2008, pp. 1–6.

[22] V. O. Shlapatskyi, Y. O. Kamak, O. V. Andriyenko, V. A. Zhurahov, I. O. Domanov, and V. V. Loginov, "A fault tree of unmanned aircraft systems for military applications," in *2017 IEEE 4th International Conference Actual Problems of Unmanned Aerial Vehicles Developments (APUAVD)*, IEEE, 2017, pp. 104–107.

[23] B. Franco and L. C. S. Góes, "Failure analysis methods in unmanned aerial vehicle (UAV) applications," in *Proceedings of COBEM 2007 19th International Congress of Mechanical Engineering*, 2007.

[24] A. Altinors, F. Yol, and O. Yaman, "A sound based method for fault detection with statistical feature extraction in UAV motors," *Appl. Acoust.*, vol. 183, p. 108325, 2021.

[25] A. P. Thurlbeck and Y. Cao, “A mission profile-based reliability modeling framework for fault-tolerant electric propulsion,” *IEEE Trans. Ind. Appl.*, vol. 58, no. 2, pp. 2312–2323, 2022.

[26] S. Lu and X. Wang, “A new methodology to estimate the rotating phase of a BLDC motor with its application in variable-speed bearing fault diagnosis,” *IEEE Trans. Power Electron.*, vol. 33, no. 4, pp. 3399–3410, 2017.

[27] D. Czerwinski, J. Gęca, and K. Kolano, “Machine learning for sensorless temperature estimation of a BLDC motor,” *Sensors*, vol. 21, no. 14, p. 4655, 2021.

[28] T. A. Shifat, R. Yasmin, and J.-W. Hur, “A data driven RUL estimation framework of electric motor using deep electrical feature learning from current harmonics and apparent power,” *Energies*, vol. 14, no. 11, p. 3156, 2021.

[29] U. H. Lee, C.-W. Pan, and E. J. Rouse, “Empirical characterization of a high-performance exterior-rotor type brushless DC motor and drive,” in *2019 IEEE/RSJ International Conference on Intelligent Robots and Systems (IROS)*, IEEE, 2019, pp. 8018–8025.

[30] G. E. Gorospe Jr, C. S. Kulkarni, E. Hogge, A. Hsu, and N. Ownby, “A study of the degradation of electronic speed controllers for brushless dc motors,” in *Asia Pacific Conference of the Prognostics and Health Management Society 2017*, 2017.

[31] T. A. Shifat and H. Jang-Wook, “Remaining useful life estimation of BLDC motor considering voltage degradation and attention-based neural network,” *IEEE Access*, vol. 8, pp. 168414–168428, 2020.

[32] W. Wang and D. Dragomir-Daescu, “Reliability quantification of induction motors-accelerated degradation testing approach,” in *Annual Reliability and Maintainability Symposium. 2002 Proceedings (Cat. No. 02CH37318)*, IEEE, 2002, pp. 325–331.

[33] C. Lee, M. Lim, C. Kim, and S. J. Bae, “Reliability Analysis of Accelerated Destructive Degradation Testing Data for Bi-Functional DC Motor Systems,” *Appl. Sci.*, vol. 11, no. 6, p. 2537, 2021.

[34] A. Mirza, W. Chen, H. Nguyen, Y. Cao, and A. M. Bazzi, “High-voltage high-frequency testing for medium-voltage motor insulation degradation,” in *2018 IEEE Energy Conversion Congress and Exposition (ECCE)*, IEEE, 2018, pp. 2444–2447.

[35] B. Park, H. Jeong, H. Huh, M. Kim, and S. Lee, “Experimental study on the life prediction of servo motors through model-based system degradation assessment and accelerated degradation testing,” *J. Mech. Sci. Technol.*, vol. 32, pp. 5105–5110, 2018.

[36] M. Mazzoleni, M. Scandella, F. Previdi, and G. Pispola, “Data on the first endurance

activity of a Brushless DC motor for aerospace applications," *Data Brief*, vol. 29, p. 105153, 2020.

[37] V. Madonna, P. Giangrande, and M. Galea, "Introducing physics of failure considerations in the electrical machines design," in *2019 IEEE International Electric Machines & Drives Conference (IEMDC)*, IEEE, 2019, pp. 2233–2238.

[38] K. N. Gyftakis and A. J. Marques-Cardoso, "Reliable detection of very low severity level stator inter-turn faults in induction motors," in *IECON 2019-45th Annual Conference of the IEEE Industrial Electronics Society*, IEEE, 2019, pp. 1290–1295.

[39] Y.-S. Lee, K.-T. Kim, and J. Hur, "Finite-element analysis of the demagnetization of IPM-type BLDC motor with stator turn fault," *IEEE Trans. Magn.*, vol. 50, no. 2, pp. 889–892, 2014.

[40] W. Abed, S. Sharma, R. Sutton, and A. Motwani, "A robust bearing fault detection and diagnosis technique for brushless DC motors under non-stationary operating conditions," *J. Control Autom. Electr. Syst.*, vol. 26, pp. 241–254, 2015.

[41] M. Darrah, A. Rubenstein, E. Sorton, and B. DeRoos, "On-board health-state awareness to detect degradation in multirotor systems," in *2018 International Conference on Unmanned Aircraft Systems (ICUAS)*, IEEE, 2018, pp. 1134–1141.

[42] G. E. Gorospe and C. S. Kulkarni, "A novel uav electric propulsion testbed for diagnostics and prognostics," in *2017 IEEE AUTOTESTCON*, IEEE, 2017, pp. 1–6.

[43] E. Vinogradov, H. Sallouha, S. De Bast, M. M. Azari, and S. Pollin, "Tutorial on UAV: A Blue Sky View on Wireless Communication," *J. Mob. Multimed.*, vol. 14, no. 4, pp. 395–468, 2018, doi: 10.13052/jmm1550-4646.1443.

[44] Y. Koç, "Reliability analysis of tactical unmanned aerial vehicle (UAV)," Master Thesis, Middle East Technical University, 2017. Accessed: Feb. 23, 2024. [Online]. Available: https://open.metu.edu.tr/handle/11511/27024

[45] C. Gao, Y. Guo, M. Zhong, X. Liang, H. Wang, and H. Yi, "Reliability analysis based on dynamic Bayesian networks: A case study of an unmanned surface vessel," *Ocean Eng.*, vol. 240, p. 109970, Nov. 2021, doi: 10.1016/j.oceaneng.2021.109970.

[46] L. Xing and B. W. Johnson, "Reliability Theory and Practice for Unmanned Aerial Vehicles," *IEEE Internet Things J.*, vol. 10, no. 4, pp. 3548–3566, Feb. 2023, doi: 10.1109/JIOT.2022.3218491.

[47] D. Powers and Y. Xie, *Statistical methods for categorical data analysis*. Emerald Group Publishing, 2008.

[48] A. Birolini, *Reliability engineering*, vol. 5. Springer, 2007.

[49] T. R. Moss and J. D. Andrews, “Reliability assessment of mechanical systems,” *Proc. Inst. Mech. Eng. Part E J. Process Mech. Eng.*, vol. 210, no. 3, pp. 205–216, 1996.

[50] J. Wu and S. Yan, “Reliability evaluation for mechanical systems by Petri nets,” *Petri Nets Sci. Eng.*, pp. 87–93, 2018.

[51] W. Li, *Reliability assessment of electric power systems using Monte Carlo methods*. Springer Science & Business Media, 2013.

[52] W. Q. Meeker, L. A. Escobar, and F. G. Pascual, *Statistical methods for reliability data*. John Wiley & Sons, 2022.

[53] M. R. Lyu, “Software reliability engineering: A roadmap,” in *Future of Software Engineering (FOSE’07)*, IEEE, 2007, pp. 153–170.

[54] R. Melnyk, D. Schrage, V. Volovoi, and H. Jimenez, “A third-party casualty risk model for unmanned aircraft system operations,” *Reliab. Eng. Syst. Saf.*, vol. 124, pp. 105–116, 2014.

[55] J. E. Breneman, C. Sahay, and E. E. Lewis, *Introduction to reliability engineering*. John Wiley & Sons, 2022.

[56] N. Zhang, S. Govind, and T. T, “ATMRI_R_2022_AW_1: UAV Propulsion System Reliability Analysis,” Air Traffic Management Research Institute, Singapore, 2022.

[57] J. Wang, “Reliability analysis and data driven modelling of railway component failure,” 2021, Accessed: Feb. 22, 2024. [Online]. Available: https://dr.ntu.edu.sg/handle/10356/159237

[58] N. Gorjian, L. Ma, M. Mittinty, P. Yarlagadda, and Y. Sun, “A review on degradation models in reliability analysis,” in *Engineering Asset Lifecycle Management: Proceedings of the 4th World Congress on Engineering Asset Management (WCEAM 2009), 28-30 September 2009*, Springer, 2010, pp. 369–384.

[59] Y. Ding, Q. Yang, C. B. King, and Y. Hong, “A General Accelerated Destructive Degradation Testing Model for Reliability Analysis,” *IEEE Trans. Reliab.*, vol. 68, no. 4, pp. 1272–1282, 2019, doi: 10.1109/TR.2018.2883983.

[60] B. Dodson and H. Schwab, *Accelerated testing: a practitioner’s guide to accelerated and reliability testing*. SAE international, 2021.

[61] F. Yang, M. S. Habibullah, T. Zhang, Z. Xu, P. Lim, and S. Nadarajan, “Health Index-Based Prognostics for Remaining Useful Life Predictions in Electrical Machines,” *IEEE Trans. Ind. Electron.*, vol. 63, no. 4, pp. 2633–2644, Apr. 2016, doi: 10.1109/TIE.2016.2515054.

[62] N. Gorjian, L. Ma, M. Mittinty, P. Yarlagadda, and Y. Sun, “A review on degradation

models in reliability analysis," in *4th World Congress on Engineering Asset Management: Engineering Asset Lifecycle Management, WCEAM 2009, September 28, 2009 - September 30, 2009*, in Engineering Asset Lifecycle Management - Proceedings of the 4th World Congress on Engineering Asset Management, WCEAM 2009. Athens, Greece: Springer-Verlag London Ltd, 2009, pp. 369–384.

[63] Z.-Q. Wang, C.-H. Hu, X.-S. Si, and E. Zio, "Remaining useful life prediction of degrading systems subjected to imperfect maintenance: Application to draught fans," *Mech. Syst. Signal Process.*, vol. 100, pp. 802–813, Feb. 2018, doi: 10.1016/j.ymssp.2017.08.016.

[64] R. kamal Kaur, B. Pandey, and L. K. Singh, "Dependability analysis of safety critical systems: Issues and challenges," *Ann. Nucl. Energy*, vol. 120, pp. 127–154, Oct. 2018, doi: 10.1016/j.anucene.2018.05.027.

[65] S. Rebello, H. Yu, and L. Ma, "An integrated approach for system functional reliability assessment using Dynamic Bayesian Network and Hidden Markov Model," *Reliab. Eng. Syst. Saf.*, vol. 180, pp. 124–135, Dec. 2018, doi: 10.1016/j.ress.2018.07.002.

[66] Z. Zhao, Q. Quan, and K.-Y. Cai, "A health evaluation method of multicopters modeled by Stochastic Hybrid System," *Aerosp. Sci. Technol.*, vol. 68, pp. 149–162, Sep. 2017, doi: 10.1016/j.ast.2017.05.011.

[67] M. Quiñones-Grueiro, G. Biswas, I. Ahmed, T. Darrah, and C. Kulkarni, "Online decision making and path planning framework for safe operation of unmanned aerial vehicles in urban scenarios," *Int. J. Progn. Health Manag.*, vol. 12, no. 3, Art. no. 3, Apr. 2021, doi: 10.36001/ijphm.2021.v12i3.2953.

[68] "Learning Spectral-Spatial-Temporal Features via a Recurrent Convolutional Neural Network for Change Detection in Multispectral Imagery | IEEE Journals & Magazine | IEEE Xplore." Accessed: Feb. 23, 2024. [Online]. Available: https://ieeexplore.ieee.org/abstract/document/8541102

[69] R. Dainelli, P. Toscano, S. F. Di Gennaro, and A. Matese, "Recent Advances in Unmanned Aerial Vehicles Forest Remote Sensing—A Systematic Review. Part II: Research Applications," *Forests*, vol. 12, no. 4, Art. no. 4, Apr. 2021, doi: 10.3390/f12040397.

[70] A. Asif, A. Al-Dulaimi, and A. Mohammadi, "Degradation Modeling and Remaining Useful Life Estimation: From Statistical Signal Processing to Deep Learning Models," phd, Concordia University, 2020. Accessed: Feb. 23, 2024. [Online]. Available: https://spectrum.library.concordia.ca/id/eprint/988070/

[71] K. Telli *et al.*, “A Comprehensive Review of Recent Research Trends on Unmanned Aerial Vehicles (UAVs),” *Systems*, vol. 11, no. 8, Art. no. 8, Aug. 2023, doi: 10.3390/systems11080400.

[72] N. Abbas, Z. Abbas, X. Liu, S. S. Khan, E. D. Foster, and S. Larkin, “A Survey: Future Smart Cities Based on Advance Control of Unmanned Aerial Vehicles (UAVs),” *Appl. Sci.*, vol. 13, no. 17, Art. no. 17, Jan. 2023, doi: 10.3390/app13179881.

[73] H. Kurunathan, H. Huang, K. Li, W. Ni, and E. Hossain, “Machine Learning-Aided Operations and Communications of Unmanned Aerial Vehicles: A Contemporary Survey,” *IEEE Commun. Surv. Tutor.*, pp. 1–1, 2023, doi: 10.1109/COMST.2023.3312221.

[74] H. Lu, V. Barzegar, V. P. Nemani, C. Hu, S. Laflamme, and A. T. Zimmerman, “GAN-LSTM Predictor for Failure Prognostics of Rolling Element Bearings,” in *2021 IEEE International Conference on Prognostics and Health Management (ICPHM)*, Jun. 2021, pp. 1–8. doi: 10.1109/ICPHM51084.2021.9486650.

[75] L. Jayasinghe, T. Samarasinghe, C. Yuenv, J. C. Ni Low, and S. Sam Ge, “Temporal Convolutional Memory Networks for Remaining Useful Life Estimation of Industrial Machinery,” in *2019 IEEE International Conference on Industrial Technology (ICIT)*, Feb. 2019, pp. 915–920. doi: 10.1109/ICIT.2019.8754956.

[76] T. Darrah, G. Biswas, J. Frank, M. Quinones-Grueiro, and C. Teubert, *A Data-Centric Approach to the Study of System-Level Prog- nostics for Cyber Physical Systems: Application to Safe UAV Operations*. 2022. doi: 10.20517/jsss.xxxx.xx.

[77] M. W. Ahmad, M. U. Akram, R. Ahmad, K. Hameed, and A. Hassan, “Intelligent framework for automated failure prediction, detection, and classification of mission critical autonomous flights,” *ISA Trans.*, vol. 129, pp. 355–371, Oct. 2022, doi: 10.1016/j.isatra.2022.01.014.

[78] R. Zhao, J. Wang, R. Yan, and K. Mao, “Machine health monitoring with LSTM networks,” in *2016 10th International Conference on Sensing Technology (ICST)*, Nanjing, China: IEEE, Nov. 2016, pp. 1–6. doi: 10.1109/ICSensT.2016.7796266.

[79] F. Bre, J. M. Gimenez, and V. D. Fachinotti, “Prediction of wind pressure coefficients on building surfaces using artificial neural networks,” *Energy Build.*, vol. 158, pp. 1429–1441, Jan. 2018, doi: 10.1016/j.enbuild.2017.11.045.

[80] B. Kröse, B. Krose, P. van der Smagt, and P. Smagt, “An introduction to neural networks,” *J Comput Sci*, vol. 48, Jan. 1993.

[81] D. Teng, Y.-W. Feng, C. Lu, J.-Q. Liu, and J.-Y. Chen, “Vectorial generative adversarial

surrogate modeling reliability evaluation framework for engineering structural systems," *Reliab. Eng. Syst. Saf.*, vol. 247, p. 110076, Jul. 2024, doi: 10.1016/j.ress.2024.110076.

[82] K. Xu, M. Xie, L. C. Tang, and S. L. Ho, "Application of neural networks in forecasting engine systems reliability," *Appl. Soft Comput.*, vol. 2, no. 4, pp. 255–268, Feb. 2003, doi: 10.1016/S1568-4946(02)00059-5.

[83] G. Scalabrini Sampaio, A. R. D. A. Vallim Filho, L. Santos Da Silva, and L. Augusto Da Silva, "Prediction of Motor Failure Time Using An Artificial Neural Network," *Sensors*, vol. 19, no. 19, p. 4342, Oct. 2019, doi: 10.3390/s19194342.

[84] O. Abril-Pla *et al.*, "PyMC: a modern, and comprehensive probabilistic programming framework in Python," *PeerJ Comput. Sci.*, vol. 9, p. e1516, Sep. 2023, doi: 10.7717/peerj-cs.1516.

[85] C. Robert and G. Casella, "Monte Carlo Statistical Method," *Technometrics*, vol. 42, Nov. 2000, doi: 10.2307/1270959.

[86] Z. Wang, M. Broccardo, and J. Song, "Hamiltonian Monte Carlo methods for Subset Simulation in reliability analysis," *Struct. Saf.*, vol. 76, pp. 51–67, Jan. 2019, doi: 10.1016/j.strusafe.2018.05.005.

[87] D. van Ravenzwaaij, P. Cassey, and S. D. Brown, "A simple introduction to Markov Chain Monte–Carlo sampling," *Psychon. Bull. Rev.*, vol. 25, no. 1, pp. 143–154, Feb. 2018, doi: 10.3758/s13423-016-1015-8.

[88] J. Lin, "An Integrated Procedure for Bayesian Reliability Inference Using MCMC," *J. Qual. Reliab. Eng.*, vol. 2014, p. 264920, Jan. 2014, doi: 10.1155/2014/264920.

[89] T. Thanaraj, S. Govind, A. Roy, B. F. Ng, and K. H. Low, "An Reliability Framework for Safe Octorotor UAV Flight Operations," presented at the ICUAS 2023, Poland, 2023.

[90] "ASTM F3298-19, Standard Specification for Design, Construction, and Verification of Lightweight Unmanned Aircraft Systems (UAS)." ASTM International, Mar. 2019.

[91] A. Gonzalez Rot, A. Hasan, and P. Manoonpong, "Robust Actuator Fault Diagnosis Algorithm for Autonomous Hexacopter UAVs," Jan. 01, 2020, *Elsevier*. doi: 10.1016/j.ifacol.2020.12.815.

[92] R. C. Avram, X. Zhang, and J. Muse, "Quadrotor Actuator Fault Diagnosis and Accommodation Using Nonlinear Adaptive Estimators," *IEEE Trans. Control Syst. Technol.*, vol. 25, no. 6, pp. 2219–2226, Nov. 2017, doi: 10.1109/TCST.2016.2640941.

[93] T. T, S. Sai, B. F. Ng, and K. H. Low, "Hardware-in-the-loop Simulation for Quadrotor

Fault Diagnosis Enhancing Airworthiness using OS-Fuzzy-ELM," in *2022 International Conference on Unmanned Aircraft Systems (ICUAS)*, Jun. 2022, pp. 263–272. doi: 10.1109/ICUAS54217.2022.9836162.

[94] M. Saied, B. Lussier, I. Fantoni, C. Francis, H. Shraim, and G. Sanahuja, "Fault diagnosis and fault-tolerant control strategy for rotor failure in an octorotor," in *2015 IEEE International Conference on Robotics and Automation (ICRA)*, May 2015, pp. 5266–5271. doi: 10.1109/ICRA.2015.7139933.

[95] A. Abbaspour, K. K. Yen, P. Forouzannezhad, and A. Sargolzaei, "A Neural Adaptive Approach for Active Fault-Tolerant Control Design in UAV," *IEEE Trans. Syst. Man Cybern. Syst.*, pp. 1–11, 2018, doi: 10.1109/TSMC.2018.2850701.

[96] A.-R. Merheb, H. Noura, and F. Bateman, "Active fault tolerant control of quadrotor UAV using Sliding Mode Control," in *2014 International Conference on Unmanned Aircraft Systems (ICUAS)*, May 2014, pp. 156–166. doi: 10.1109/ICUAS.2014.6842251.

[97] T. T, B. F. Ng, and K. H. Low, "Active Fault Tolerant Control on Multi-rotor UAVs using ELM-based Neuro-Fuzzy System," in *AIAA AVIATION 2022 Forum*, Chicago, IL & Virtual: American Institute of Aeronautics and Astronautics, Jun. 2022. doi: 10.2514/6.2022-3510.

[98] G. K. Fourlas and G. C. Karras, "A Survey on Fault Diagnosis and Fault-Tolerant Control Methods for Unmanned Aerial Vehicles," *Machines*, vol. 9, no. 9, Art. no. 9, Sep. 2021, doi: 10.3390/machines9090197.

[99] Q. Quan, G. Cui, and G.-X. Du, "Controllable probability and optimization of multicopters," *Aerosp. Sci. Technol.*, vol. 119, p. 107162, Dec. 2021, doi: 10.1016/j.ast.2021.107162.

[100] D. Shi, B. Yang, and Q. Quan, "Reliability analysis of multicopter configurations based on controllability theory," in *2016 35th Chinese Control Conference (CCC)*, Jul. 2016, pp. 6740–6745. doi: 10.1109/ChiCC.2016.7554418.

[101] G.-X. Du, Q. Quan, B. Yang, and K.-Y. Cai, "Controllability Analysis for Multirotor Helicopter Rotor Degradation and Failure," *J. Guid. Control Dyn.*, vol. 38, no. 5, pp. 978–985, 2015, doi: 10.2514/1.G000731.

[102] A. Sanjuan, F. Nejjari, and R. Sarrate, "Reconfigurability Analysis of Multirotor UAVs under Actuator Faults," in *2019 4th Conference on Control and Fault Tolerant Systems (SysTol)*, Sep. 2019, pp. 26–31. doi: 10.1109/SYSTOL.2019.8864748.

[103] J. C. Salazar, A. Sanjuan, F. Nejjari, and R. Sarrate, "Health–Aware and Fault–Tolerant

Control of an Octorotor UAV System Based on Actuator Reliability," *Int. J. Appl. Math. Comput. Sci.*, vol. 30, no. 1, pp. 47–59, Mar. 2020, doi: 10.34768/amcs-2020-0004.

[104] K. Aslansefat, F. Marques, R. Mendonça, and J. Barata, "A Markov Process-Based Approach for Reliability Evaluation of the Propulsion System in Multi-rotor Drones," in *Technological Innovation for Industry and Service Systems*, Springer, Cham, 2019, pp. 91–98. doi: 10.1007/978-3-030-17771-3_8.

[105] J. Liscouët, F. Pollet, J. Jézégou, M. Budinger, S. Delbecq, and J.-M. Moschetta, "A methodology to integrate reliability into the conceptual design of safety-critical multirotor unmanned aerial vehicles," *Aerosp. Sci. Technol.*, vol. 127, p. 107681, Aug. 2022, doi: 10.1016/j.ast.2022.107681.

[106] E. Dubrova, *Fault-Tolerant Design*. New York, NY: Springer, 2013. doi: 10.1007/978-1-4614-2113-9.

[107] S. Govind and B. Q. H. Goh, "Comprehensive Reliability Analysis and Degradation Modelling of Electric UAV Propulsion Systems: An Integrated Qualitative and Quantitative Approach," *Reliab. Eng. Syst. Saf.*, 2024.

[108] Nato standardization agency, "NATO standard AEP-83: Light Unmanned Aircraft System Airworthiness Requirements.," *Allied Eng. Publ.*, 2016.

[109] O. Hirling and F. Holzapfel, "EASA's 'Open' Category for Military UAS: Opportunities and Limitations in the Field of Airworthiness," *Aerospace*, vol. 5, no. 3, p. 70, 2018.

[110] M. Ohring and L. Kasprzak, *Reliability and failure of electronic materials and devices*. Academic Press, 2014.

[111] B. Q. H. Goh, "Quantitative evaluation of multi-rotor UAV propulsion system reliability," 2024.

[112] J. Wang, S. Govind, X. Hu, and M. Feroskhan, "UAV flight test and its endurance degradation modelling by considering the energy efficiency and flight stability factors," in *2023 IEEE/AIAA 42nd Digital Avionics Systems Conference (DASC)*, IEEE, 2023, pp. 1–5. Accessed: Feb. 26, 2024. [Online]. Available: https://ieeexplore.ieee.org/abstract/document/10311139/

[113] X. Li and A. V. Savkin, "Networked Unmanned Aerial Vehicles for Surveillance and Monitoring: A Survey," *Future Internet*, vol. 13, no. 7, Art. no. 7, Jul. 2021, doi: 10.3390/fi13070174.

[114] Y. C. Paw and E. Y. M. Ang, "Battery cycle life assessment for a lift+cruise electric vertical takeoff and landing transporter drone," *J. Energy Storage*, vol. 66, p. 107493, Aug. 2023, doi: 10.1016/j.est.2023.107493.

[115] N. Zahra, R. S. Buldan, Y. Y. Nazaruddin, and A. Widyotriatmo, “Predictive Maintenance with Neural Network Approach for UAV Propulsion Systems Monitoring,” in *2021 American Control Conference (ACC)*, New Orleans, LA, USA: IEEE, May 2021, pp. 2631–2636. doi: 10.23919/ACC50511.2021.9482858.

[116] M. Shafiee, Z. Zhou, L. Mei, F. Dinmohammadi, J. Karama, and D. Flynn, “Unmanned Aerial Drones for Inspection of Offshore Wind Turbines: A Mission-Critical Failure Analysis,” *Robotics*, vol. 10, no. 1, Art. no. 1, Mar. 2021, doi: 10.3390/robotics10010026.

[117] D. P. Gaver and P. A. Jacobs, “Reliability growth by failure mode removal,” *Reliab. Eng. Syst. Saf.*, vol. 130, pp. 27–32, Oct. 2014, doi: 10.1016/j.ress.2014.04.012.

[118] S. Carlos, A. Sánchez, S. Martorell, and I. Marton, “Onshore wind farms maintenance optimization using a stochastic model,” *Math. Comput. Model.*, vol. 57, no. 7, pp. 1884–1890, Apr. 2013, doi: 10.1016/j.mcm.2011.12.025.

[119] C. K. Brown, “Conquering the challenge of reliability: text mining to map trends in reliability engineering literature”.

[120] S. Meskini, “Reliability Models Applied to Smartphone Applications,” M.Eng.Sc., The University of Western Ontario (Canada), Canada -- Ontario, CA, 2013. Accessed: Feb. 27, 2024. [Online]. Available: https://www.proquest.com/docview/2701132400/abstract/8B0A0055786A4C73PQ/1

[121] F. Anderson, R. Dawid, D. McMillan, and D. García-Cava, “A Bayesian reliability analysis exploring the effect of scheduled maintenance on wind turbine time to failure,” *Wind Energy*, vol. 26, no. 9, pp. 879–899, 2023, doi: 10.1002/we.2846.

[122] C. Karapapas and C. Goumopoulos, “Mild Cognitive Impairment Detection Using Machine Learning Models Trained on Data Collected from Serious Games,” *Appl. Sci.*, vol. 11, no. 17, Art. no. 17, Jan. 2021, doi: 10.3390/app11178184.

[123] C. Oh, S. Han, and J. Jeong, “Time-series data augmentation based on interpolation,” *Procedia Comput. Sci.*, vol. 175, pp. 64–71, 2020.

[124] P. Ribot and E. Bensana, “A generic adaptative prognostic function for heterogeneous multi-component systems: application to helicopters,” in *European Safety & Reliability Conference, Troyes, France*, 2011.

[125] M. Mohan *et al.*, “UAV-Supported Forest Regeneration: Current Trends, Challenges and Implications,” *Remote Sens.*, vol. 13, no. 13, Art. no. 13, Jan. 2021, doi: 10.3390/rs13132596.

[126] M. Azimi, A. D. Eslamlou, and G. Pekcan, “Data-Driven Structural Health Monitoring

and Damage Detection through Deep Learning: State-of-the-Art Review," *Sensors*, vol. 20, no. 10, Art. no. 10, Jan. 2020, doi: 10.3390/s20102778.

[127] L. Gao, C. Xu, F. Wang, J. Wu, and H. Su, "Flight data outlier detection by constrained LSTM-autoencoder," *Wirel. Netw.*, vol. 29, no. 7, pp. 3051–3061, Oct. 2023, doi: 10.1007/s11276-023-03353-1.

[128] H. Abbasimehr, M. Shabani, and M. Yousefi, "An optimized model using LSTM network for demand forecasting," *Comput. Ind. Eng.*, vol. 143, p. 106435, May 2020, doi: 10.1016/j.cie.2020.106435.

[129] Q. Wang, K. Qin, B. Lu, H. Sun, and P. Shu, "Time-feature attention-based convolutional auto-encoder for flight feature extraction," *Sci. Rep.*, vol. 13, no. 1, p. 14175, Aug. 2023, doi: 10.1038/s41598-023-41295-y.

[130] S. H. Khan, M. Hayat, and F. Porikli, "Regularization of deep neural networks with spectral dropout," *Neural Netw.*, vol. 110, pp. 82–90, Feb. 2019, doi: 10.1016/j.neunet.2018.09.009.